Author:
Czapnik, Paulina J

Title:
Investigation into the expression of cardiomyocyte specific genes in cardiac macrophages after injury.

Investigation into the expression of cardiomyocyte specific genes in cardiac macrophages after injury.

Paulina Julia Czapnik

A dissertation submitted to the University of Bristol in accordance with the requirements for award of the degree of MSc by Research in Physiology and Pharmacology in the Faculty of Biomedical Science and School of Physiology, Pharmacology and Neuroscience (September 2021).

Word count: 24412

Abstract

Cardiovascular disease, encompassing coronary heart disease and myocardial infarction, remains the biggest killer worldwide. Coronary heart disease can result in blockage of a coronary artery resulting in a robust inflammatory response, severe cardiomyocyte necrosis, adverse tissue remodelling and scarring with direct consequences of permanently diminished heart function and, ultimately, heart failure. Large amounts of work has concentrated on cell replacement therapies for lost cardiomyocytes, but recent studies are demonstrating the importance of other cell types in the heart during the response to injury. Macrophages, representing a heterogeneous immune cell population, are predominant players in the post infarcted cardiac microenvironment where they are responsible for clearance of necrotic cells, tissue repair and driving fibrosis in mammals. However, recent studies have demonstrated their roles in successful regeneration of damaged heart muscle and an unexpected role in conduction of electric potential. An unbiased proteomic study performed in the Richardson Lab revealed expression of nine cardiac and muscle-specific proteins in cardiac macrophages within regenerative adult zebrafish post myocardial infarction. This study confirms expression of six genes in cardiac macrophages of the post infarcted heart, but also within resident cells obtained from healthy hearts, suggesting that macrophages might play another unexpected role in heart homeostasis. Use of a double transgenic line fluorescently labelling macrophages and cardiac myosin light chain 7 (*myl7)* expressing cells, along with flow cytometry and high-resolution confocal imaging, allowed investigation of cardiac (*myl7)* positive macrophages in the response to injury and their *in situ* characterisation. In this study, it was observed that *myl7* expressing cardiac macrophages comprise up to 48% of the total cardiac macrophage population and these cells respond to injury in a similar way to other macrophages. Three possible mechanisms likely contributing to this phenomenon are proposed.

.

Acknowledgements

Foremost, I would like to express my heartfelt appreciation to my supervisor Dr. Rebecca Richardson for her continuous support, enthusiasm, and motivation during my MRes study. This thesis would not be possible without her valuable guidance and feedback, which I am truly grateful for.

Secondly, I would like to thank Laura Bevan, for training and advice on the technical aspects of this project. Laura was a vital member of the Richardson lab, always there to help and share her experience. I would like to acknowledge other lab members, who keenly shared their knowledge in aspects of molecular biology – Dr. Rebecca Ryan, Flow Cytometry – Bethany Moyse and image analysis – Aaron Scott.

This work would also not be possible without my progress panel: Dr. Chrissy Hammond and Dr Borko Amulic, who were there to support me in initial stages of my research work.

I am truly grateful for the opportunity to be part of zebrafish community established by Dr Richardson, Dr. Hammond and the Prof. Martin lab. It was a pleasure to work alongside such a passionate and dedicated researcher team.

I would like to thank the British Heart Foundation and the Oxbridge Centre of Regenerative Medicine for funding this study.

Lastly, but not least I would like to thank University of Bristol facilities for the technical support and expertise they provided: Dr Andy Herman and Helen Rice from Biomedical Sciences Flow Cytometry Facility; Dr. Stephen Cross from The Wolfson Bioimaging Facility for custom plugin design and advice in image analysis; Matthew Green and other members from Zebrafish facility for taking great care of my transgenic zebrafish lines.

I declare that the work in this dissertation was carried out in accordance with the requirements of the University's *Regulations and Code of Practice for Research Degree Programmes* and that it has not been submitted for any other academic award. Except where indicated by specific reference in the text, the work is the candidate's own work. Work done in collaboration with, or with the assistance of, others, is indicated as such. Any views expressed in the dissertation are those of the author.

SIGNED: ..... DATE: .....

Table of Content

List of Figures

List of Tables

List of Abbreviations

A – Apex

AVC – Atrio-ventricular canal

AVN – Atrio-ventricular node

BA – Bulbus Arteriosus

CHD– Coronary Heart Disease

CM – Cardiomyocyte

cMP – Cardiac macrophages

CPCs – Cardiac progenitor cells

CPM – copy per million

csf1ra – colony stimulating factor 1 receptor a

CT – Cycle threshold

CVD – cardiovascular disease

DAMPs - damage associated pattern molecules

dpa – days post amputation

dpi – days post injury

E – efficiency

ECM –extracellular matrix

ERS – Expressed Repetitive Element

FACS – Fluorescence-activated cell sorting

FC – non-fluorescent (FACS sorted background) fin cells

fMP – macrophages derived (FACS sorted) from fins

FRP – fluorescence reporter proteins

FSC – forward scatter

GFP – Green Fluorescent Protein

GOI – Gene of interest

HR – Heart rate

IFC – Imaging Flow Cytometry

IL – Interleukin

INF – Interferon

IS – Injury site

LAD – Left anterior descending

mef2a – myocyte enhancer factor 2A

mfap – microfibril-associated glycoprotein

MI – myocardial infarction

MIA – Modular Image Analysis

MMP – matrix metalloprotease

MP – macrophages

mpeg1 – macrophage-expressed gene, tandem duplicate 1

NER1 – growth factor neuregulin 1

nkx2.5 – NK2 homeobox 5

O/N – Overnight

PBS – Phosphate Buffered Saline

PCR – Polymerase Chain Reaction

PFA – Paraformaldehyde

RIN – RNA integrity number

RQ – Relative quantification

RT – room temperature

SAN – sino-atrial node

SSC – side scatter

SV – sinus venous

TGF – Transforming Growth Factor

Tnfα – Tumour Necrosis Factor alpha

tv – transcript variant

Un – uninjured

UR – Unaffected region

V – Ventricle

VEGF – Vascular Endothelial Growth Factor

WT – Wild type

Chapter 1: Introduction

1.1. Background

Cardiovascular disease (CVD), as a whole, remains the leading cause of mortality worldwide, claiming 17.9 million lives each year with myocardial infarction (MI), often as a result of coronary heart disease (CHD), accounting for one third of deaths (WHO, 2016). MI is caused by occlusion of the blood flow in one of the coronary arteries, which results in necrosis of cardiomyocytes in the apex part of the ventricle due to prolonged hypoxia and ischemia (Mann, 1999). Necrosis triggers acute injury responses including an immune response, which resolves over time, however, with excessive tissue remodelling and fibrous scar formation as direct consequences (Prabhu and Frangogiannis, 2016; Talman and Ruskoaho, 2016). The stiffened scar diminishes heart contraction, restricts blood flow and can result in serious arrythmias or tachycardia, which can ultimately lead to heart failure (Richardson *et al.*, 2015; Azevedo *et al.*, 2016). Changes to medical practice and public understanding have improved prevention and early intervention of MI, but heart transplant remains the only effective method to fully restore the function of a permanently damaged heart. However, a limited number of donors are available and complications from graft rejection does not make this option viable for most patients (Prabhu and Frangogiannis, 2016; Spath, Mills and Cruden, 2016). Therefore, there is a real clinical need to identify new therapeutic strategies to improve treatments for patients suffering from heart failure.

1.2. Traditional and emerging cardiovascular therapies

1.2.1. Guideline-indicated therapies

MI can be prevented and/or the extent of damage resulting from an MI minimized by early recognition, diagnosis and immediate treatment and this has led to a reduction in the number of people suffering from permanent cardiac damage after MI in recent years. However, MI can still occur and treatments need to be available in these cases. The main symptoms of an acute MI include pressure and pain in the chest, which radiates to the left arm and neck, shortness of breath, dizziness and nausea

(Kosuge *et al.*, 2006). Patients showing symptoms require emergency hospital admission. MI is confirmed by the presence of abnormalities in the heart rhythm and blood supply via electrocardiogram (ECG) and the detection of cardiac tissue injury markers (troponin and creatine kinase) via a blood test (Ibanez *et al.*, 2018). Post-MI treatment is focused on re-establishing the correct vascularisation to reduce cardiomyocyte loss and limit reperfusion damage and is usually achieved by pharmacological treatment and surgical repair. Treatment options include antiplatelet drugs to prevent blood clotting, thrombolytic drugs to dissolve arterial plaque, vasodilators to decrease blood pressure and antihypertensive drugs to reduce muscle contraction, therefore reducing oxygen demand (Lu *et al.*, 2015; Alabas *et al.*, 2020). The surgical repair depends on the severity of the damage, but may involve an angioplasty or coronary bypass surgery to improve heart function (Lu *et al.*, 2015; Ibanez *et al.*, 2018). Although guideline-indicated therapies have been developed and an increased survival rate of affected individuals is observed, the mortality rate from severe MI remains high. For example, in the UK between 30-40% patients die in the first two years post-MI (Alabas *et al.*, 2020), unless a heart transplant is received. To improve outcomes for more patients and to prolong patient lives new effective and safe treatments still need to be developed.

1.2.2. Innovative therapies for heart tissue renewal

Due to the poor survival rate following a severe MI and the limited therapeutic interventions available, novel strategies are currently being tested and introduced into clinical trials to improve patient recovery following cardiovascular disease. The majority of guideline indicated therapies have been developed to limit damage to the myocardium following an MI and to reduce the burden on an infarcted heart in the longer term. Recently proposed potential therapies, however, are more focussed on the potential restoration of cardiac function following acute MI. Following a severe MI 1 billion cardiomyocytes can be lost resulting in serious detrimental effects on cardiac function (Laflamme and Murry, 2005). New innovative therapies, therefore, concentrate on finding ways to replace these lost cardiomyocytes and can be divided broadly into three main areas of interest: cell replacement therapies, restoration of regenerative potential and manipulation of the infarcted heart's microenvironment.

Cell replacement therapies focus on delivery of exogenous stem cells or progenitor cells, which are differentiated *ex-vivo* into cardiomyocytes and delivered to the site of injury (Liew, Ho and Soh, 2020). Regenerative potential is restored mainly by attempts to stimulate myocyte progenitor cells or pre-existing endogenous cardiomyocytes to de-differentiate and re-enter the cell cycle via delivery of growth factors (Bersell *et al.*, 2009; Liew, Ho and Soh, 2020). The healing process after MI involves dynamic and complex interactions between cardiomyocytes and surrounding cells in the microenvironment, especially immune cells. Various techniques of immunomodulation have been explored with the hope to improve cardiac recovery after injury (Zlatanova, Pinto and Silvestre, 2016). For example, cytokines and biomolecules are used to target macrophages, as they are the predominant immune cells in the process of inflammation, alter ECM remodelling and activate cardiac fibroblast transition to myofibroblasts (Valentin *et al.*, 2009; Kain *et al.*, 2015). Unfortunately, however, even though these strategies have shown promising results in animal models, these innovate treatments have resulted in contradictory results or have been shown to be ineffective in clinical trials. These unfavourable outcomes are thought to be mostly due to short term effectiveness by targeting only the acute immune response and via activation of apoptotic, necrotic or autophagy pathways which lead to degeneration of surviving cardiomyocytes (Spath, Mills and Cruden, 2016; Zlatanova, Pinto and Silvestre, 2016; Khodayari *et al.*, 2019). The observed limitations of these new approaches are associated primarily with unstandardized procedures and currently insufficient understanding of the molecular basis of regeneration.

1.3. Animal models to study repair and regeneration

In contrast to poor repair outcomes and minimal cardiomyocyte renewal in humans (e.g. adult mammals) (Bergmann *et al.*, 2009), some animals can regenerate their heart after injury involving cardiomyocyte restoration and scar resolution. These animals include: at neonatal stages - mice (Porrello *et al.*, 2011) and pigs (Ye *et al.*, 2018); or at any stage of their lives - zebrafish (Poss, Wilson and Keating, 2002), axolotls (Cano-Martínez *et al.*, 2010) and newts (Witman *et al.*, 2011). Over the past few years, these models have provided important resources to reveal evolutionary

conserved processes of regeneration, dissecting the molecular mechanisms of cardiovascular disease and developing innovative therapeutic approaches for effective heart repair and functional recovery that can be translated in humans. Neonatal mice and zebrafish are at the forefront of these efforts due to their genome similarity to human and the molecular toolboxes available and will be discussed further here.

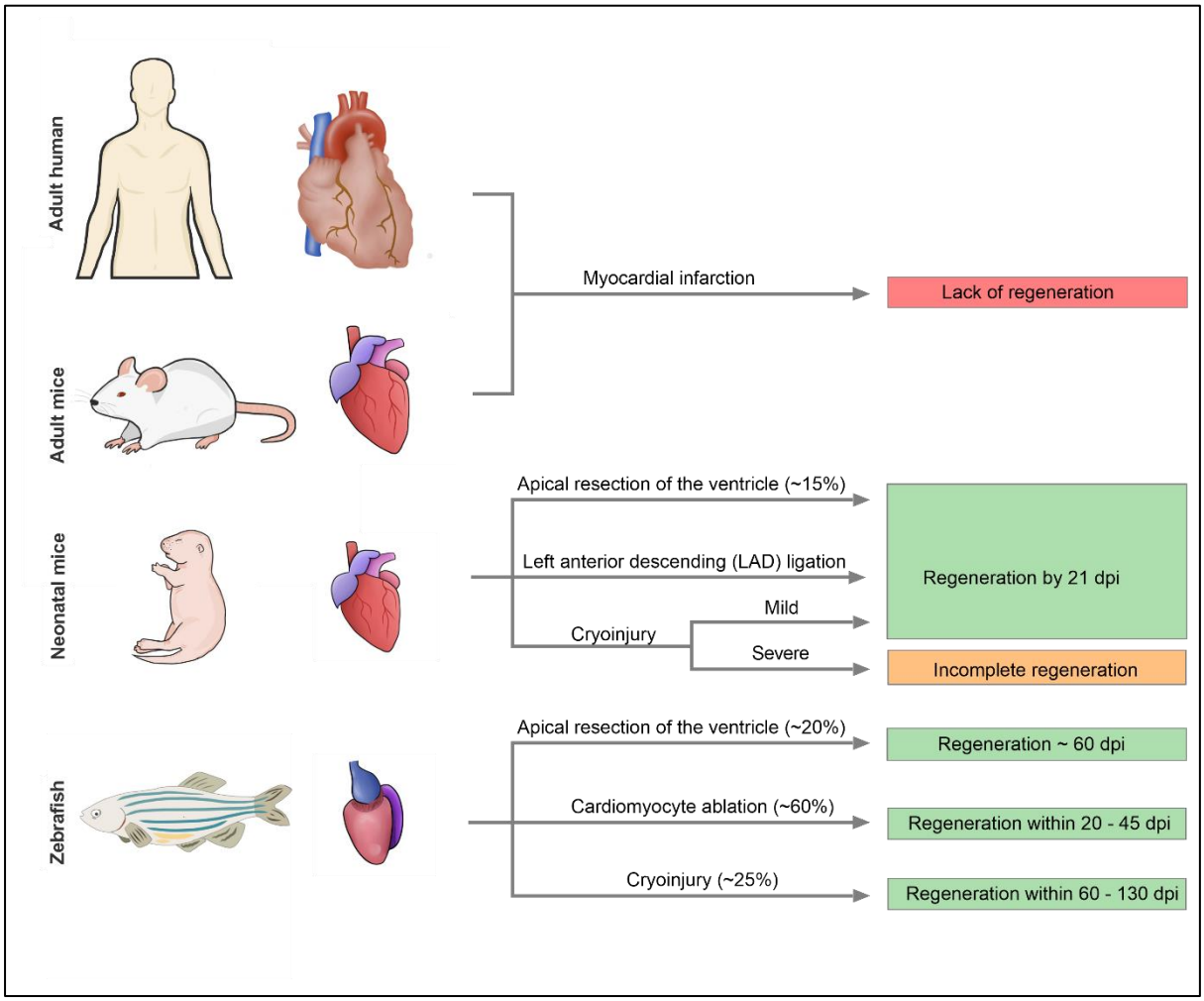

Figure 1.1. Summary of cardiac regenerative models in mice and zebrafish. Left anterior descending (LAD) ligation (mice) and cryoinjury (zebrafish) are the most accurate cardiac injury models in terms of pathophysiology features of MI; dpi – days post injury.

1.3.1. Neonatal mice

In contrast to adult human or mice, neonatal mice are capable of efficiently regenerating up to 15% of their resected heart. It has been demonstrated that, when the surgery is performed on the first day of postnatal life (P1), the lost myocardium

can be replaced with new cardiomyocytes within 21 days post amputation (dpa) and the systolic function of a healthy heart is recovered at 60 dpa (***Figure 1.1***) (Porrello *et al.*, 2011). However, this regenerative ability is lost when the injury occurs at or after day 7 of post-natal life (P7) (Porrello *et al.*, 2011).

Although apical resection of the heart is a useful tool to investigate cardiac regenerative potential and its limitations in mammals and zebrafish, it does not reflect the ischaemia-induced injury observed in human MI. An alternative model of injury using left anterior descending (LAD) ligation, where a surgical suture is applied to cut off the arterial blood circulation in the ventricle, more closely recapitulates clinical hallmarks of MI and has been used extensively in rodent models (Porrello *et al.*, 2013; Mahmoud *et al.*, 2014). The LAD model is commonly used in adult mice to mimic MI, causing extensive ischaemia-induced cell death of cardiomyocytes and irreversible fibrosis, however, studies using this model in neonatal mice also reveal a robust regenerative response featuring cardiomyocyte hypertrophy and scar resolution (***Figure 1.1***) (Porrello *et al.*, 2013). Although LAD ligation is the most reliable model for MI in rodents, it is technically challenging to perform (especially in neonatal mice) and can result in variable injury size, which makes comparing repair responses between experimental groups difficult (Strungs *et al.*, 2013). Consequently, cryoinjury (developed in zebrafish and described below) was adapted for use in mice to overcome this caveat (Strungs *et al.*, 2013). The effectiveness of the neonatal mouse response to cryoinjury, however, depends on the severity of the injury. Full regeneration (with minimal or no scarring) is retained following mild (partial myocardial wall damage), but regeneration is incomplete following severe (full thickness myocardial wall) cryoinjury (***Figure 1.1***) (Darehzereshki *et al.*, 2015).

Use of all of these different injury models has revealed the ability of neonatal mice to successfully regenerate the myocardium and restore heart function by 21 days post injury (dpi) via proliferation of pre-existing cardiomyocytes (Porrello *et al.*, 2011, 2013; Darehzereshki *et al.*, 2015). Later studies have shown that cardiac regenerative capacity drops after 2 days of post-natal life, suggesting only a very narrow regenerative window. P2 mice retain full capacity for myocardial regeneration, but the injury response is accompanied by fibrosis and scar formation from P2 onwards (Notari *et al.*, 2018). The neonatal mouse is an important, relatively recent, addition to the regenerative model repertoire, however, this narrow window of

available study and lack of mature cellular processes (e.g. immune system) limits their usability.

1.3.2. Zebrafish

Zebrafish, a non-mammalian vertebrate, has been widely used in many research fields due to advantages such as rapid external development, transparency, ease of genetic manipulation, as well as regenerative capabilities in many organs (Beffagna, 2019; Giardoglou and Beis, 2019). The anatomy of the zebrafish heart differs somewhat from mammals. The adult zebrafish heart consists of only two chambers, one atrium and one ventricle, which are connected to the blood circulation via the sinus venous (SA) and bulbus arteriosus (BA) (***Figure 1.2***) (Hu *et al.*, 2000). Despite the reduced number of chambers, the developmental programmes, architecture and cellular composition are similar to humans (Hu *et al.*, 2000; Bakkers, 2011). In addition, zebrafish more closely resemble human cardiovascular electrophysiology (Nemtsas *et al.*, 2010) and heart rate (HR = ~120) (Tsai *et al.*, 2011) than mice (van Opbergen *et al.*, 2018). Despite a lack of an atrio-ventricular node (AVN) and His-Purkinje system, key structures of mammalian electrical conduction, the contraction pattern is maintained in adult zebrafish (Sedmera *et al.*, 2003). An electrical impulse is generated in pacemaker cells in the sino-atrial node (SAN) and atrio-ventricular canal (AVC) and electrical conduction is propagated from the SAN to the ACV to maintain rhythmic contraction of the zebrafish heart (Sedmera *et al.*, 2003; Poon *et al.*, 2016).

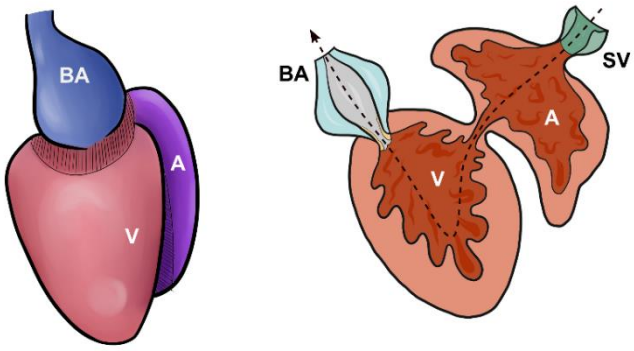

Figure 1.2. Structure of the zebrafish heart. Zebrafish hearts contain only two chambers: atrium (A) and ventricle (V). Zebrafish have systematic blood circulation: deoxygenated

venous blood flows in via the sinus venous (SV) and is pumped out via the bulbus arteriosus (BA) to be re-oxygenated in the gills then distributed around the body.

Following resection of ~20% of the apex of the ventricle, zebrafish exhibit robust regenerative responses allowing complete recovery of the myocardium within 60 dpa, without residual scarring (***Figure 1.1***) (Poss, Wilson and Keating, 2002; Raya *et al.*, 2003), with later studies confirming that the myocardium regenerates via proliferation of existing cardiomyocytes (discussed more in ***section 1.5.2***) (Jopling *et al.*, 2010; Kikuchi *et al.*, 2010). However, similar to what has already been discussed for neonatal mice, although the apical resection model has contributed to discoveries of major mechanisms involved in successful regeneration of the heart, it lacks the clinical features of MI.

A now well established cryoinjury model in adult zebrafish, where a liquid nitrogen cooled probe is applied to the ventricular wall to induce local cardiomyocyte death, triggering adverse cellular responses and subsequent scarring, recapitulates the pathophysiological features of ischemic injury in the human heart (Chablais *et al.*, 2011; Schnabel *et al.*, 2011; González-Rosa and Mercader, 2012). Regeneration of the heart following cryoinjury, which usually leads to loss of ~20(+5)% of the myocardium, involves clearance of necrotic tissue and removal of deposited scar tissue which are progressively replaced by new cardiomyocytes (Chablais *et al.*, 2011; Schnabel *et al.*, 2011; Chablais and Jaźwińska, 2012a; González-Rosa and Mercader, 2012; Bevan *et al.*, 2020). Full recovery is delayed and can take 60 -180 dpi depending on the lesion size (González-Rosa and Mercader, 2012; Hein *et al.*, 2015; Bevan *et al.*, 2020).

As an alternative to mechanical injury, genetic cardiomyocyte ablation via diphtheria toxin A expression has been developed, with the aim to examine muscle-specific regeneration (Wang *et al.*, 2011). This model results in non-selective and dispersed cardiomyocyte death (~60%) within a week from 4-hydroxytamoxifen treatment, resulting in signs of cardiac failure (Wang *et al.*, 2011). Complete myocardial regrowth is achieved within 45 days after ablation with only sparse collagen deposition (***Figure 1.1***) (Wang *et al.*, 2011). This innovative approach provides a useful model for investigating cardiomyocyte renewal but fails to recapitulate the localised ischaemia and cell death associated with acute MI.

It is not only the similarity of biological features which make the zebrafish a powerful tool to study cardiovascular diseases, advances in genome sequencing and genetic manipulation techniques as CRISR-Cas9 and morpholinos (gene specific antisense oligomers that, by complementary binding, prevent mRNA translation or splicing) also contribute to their importance (reviewed in Koster and Sassen, 2015). Zebrafish were the first vertebrate species to have their full genome sequenced. This has revealed that zebrafish have 70% orthologous genes with humans, from which 82% overlap with genes causing human disease (Howe *et al.*, 2013).

1.4. The homeostatic heart

A great deal of emphasis has been placed on developing therapies to replace lost cardiomyocytes and to discover the endogenous mechanisms that allow regenerative models to naturally recover these cells after injury, however, in recent years studies have started to reveal the importance of other cell types present in the heart for successful repair and regeneration. For this reason, a number of recent studies have sought to fully characterise the heterogenous cell populations present in the homeostatic heart.

1.4.1. Cellular composition of the heart

The heart, the first organ developed during embryogenesis, is the centre of the cardiovascular system, responsible for pumping blood around the body. The adult murine heart contains heterogenous cell populations, including cardiomyocytes, endocardial, epicardial, fibroblasts, immune and vascular cells, which provide structure and the distinct physiological functions of the heart (Pinto *et al.*, 2016; Talman and Ruskoaho, 2016). Cardiomyocytes are responsible for generating and maintaining the contractile forces of the heart. Cardiomyocytes form the myocardium which constitutes 75-85 % of the heart by mass, but cardiomyocytes themselves constitute only ~20 % of the total cell count (Pinto *et al.*, 2016; Zhou and Pu, 2016). The remaining cells represent the non-excitable cell populations of the heart. Endothelial cells, encompassing the innermost endocardial lining and the vasculature throughout the heart, are the most abundant by cell count (~45%). Epicardial cells cover the outermost surface of the myocardium. Fibroblasts make up

~13% of the cell population, provide a structural framework for the heart via extracellular matrix synthesis (ECM) and take a role in cell-to-cell communication via release of signalling molecules (Krenning, Zeisberg and Kalluri, 2010; Pinto *et al.*, 2016; Zhou and Pu, 2016). Leukocytes, mainly resident macrophages, make up ~6% of total heart cells (Pinto *et al.*, 2016; Talman and Ruskoaho, 2016). Direct and indirect interaction between cardiomyocytes and non-contractile cells not only maintains cardiac physiological function in the homeostatic state, but also coordinate tissue healing and regeneration after injury (O'Rourke, Dunne and Monaghan, 2019).

1.4.2. Cardiomyocytes – the functional drivers of the heart

Cardiomyocytes are large contractile cells contributing to the majority of the mass of the heart. The contractile forces of cardiomyocytes arise from functional units called sarcomeres, which are organised in rows, and then bundle to form tubular myofibrils (***Figure 1.3A-C***) (Rassier, 2017). Sarcomeres are composed of thick and thin filament sets (***Figure 1.3B***) (Rassier, 2017). Thin filaments are constructed of two actin polymers stabilised with two entwining tropomyosin molecules bound to troponin protein complexes (integrated Troponin T, C and I proteins), whereas thick filaments are bundles of two of each: myosin hexamers, myosin heavy chains and their regulatory and essential light chains (***Figure 1.3C***) (Rassier, 2017). Electric impulses generated in the pacemaker and passed through the myocardium cause an influx of calcium ions into cardiomyocytes. Troponin binds to these calcium ions and a conformational change exposes myosin binding sites usually covered by tropomyosin (Rassier, 2017). This allows the myosin heads to bind actin and pull these towards the centre causing sarcomere contraction (Squire, 2016; Rassier, 2017). When calcium ion concentration decreases and ATP binds to myosin head, tropomyosin covers the myosin binding site releasing the myosin heads leading to sarcomere relaxation (Squire, 2016; Rassier, 2017). This rhythmical contraction allows blood circulation around the body to deliver oxygen and nutrients, which maintain functions of vital organs.

Therefore, it is not surprising that massive cardiomyocyte death and subsequent tissue replacement with fibrous scarring leads to the poor outcome following MI in mammals. During embryogenesis, cardiomyocytes are capable of cell division to allow for heart growth. Following embryogenesis, cardiomyocyte turnover decreases

drastically and is estimated to be ≤ 1.5% per year in adult mammals (Bergmann *et al.*, 2009, 2015) and is clearly not sufficient to recompensate the loss of cardiac muscle after acute injury (~25%). By contrast, cardiomyocyte turnover of healthy adult zebrafish is 3% higher during homeostasis (Poss, Wilson and Keating, 2002; Sallin *et al.*, 2015).

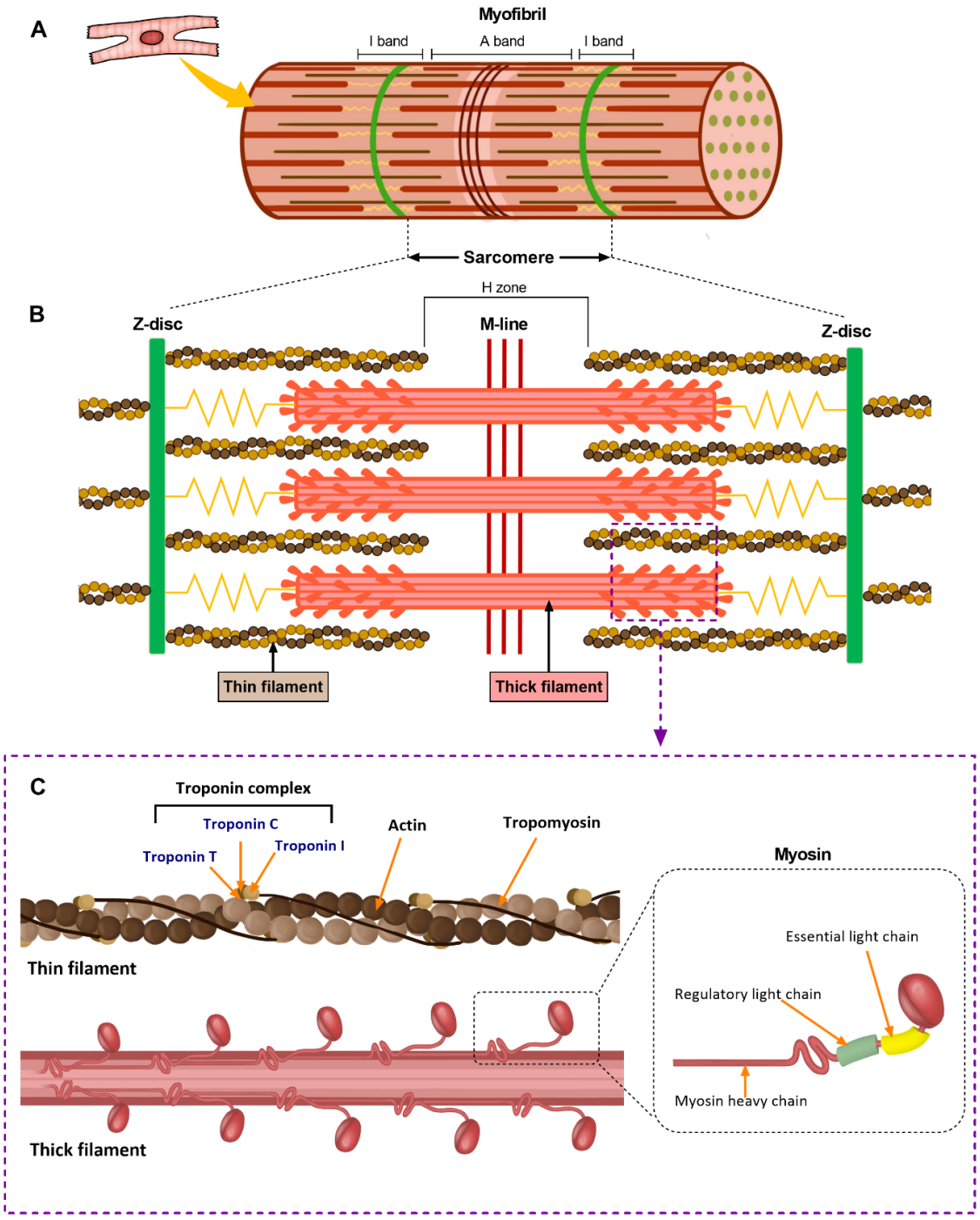

Figure 1.3. Contractile units of heart muscles. Cardiomyocytes are composed of many myofibers (A), which are formed from organised rows of functional units called sarcomeres

(B). Each sarcomere is composed of arranged contractile proteins: Actins, Tropomyosin and Troponins forming thin filaments and bundles of myosin hexamers (consisting of myosin heavy chain and regulatory and essential light chains). In the presence of calcium and ATP, myosin heads bind to the actin, resulting in shortening of the sarcomere length (contraction). When calcium concentration drops and ATP increases, myosin heads are released, thus the sarcomere relaxes.

1.5. The cellular response to cardiac injury

1.5.1. Important repair and regeneration phases

Acute cardiac injuries, such as cryoinjury or MI, cause massive cardiac tissue necrosis and fibrous scar formation. This occurs during two repair phases, which are conserved across species – **the inflammatory** and **reparative phases.** Maturation of the scar tissue is a final phase of the healing process in adult mammals resulting in permanent fibrosis, which changes tissue architecture and stiffens the ventricular wall. In zebrafish, the transition from the reparative to a **regenerative phase** is observed, which is an interplay between pro-fibrotic vs a pro-regenerative environment, resulting in collagen remodelling and cardiomyocyte replacement (Ryan, Moyse and Richardson, 2020).

Inflammatory phase (~1-7 dpi): Acute cardiac injury and subsequent local hypoxia, results in damaged and programmed cell death (apoptosis and necrosis) of surrounding cells in the first hours after injury (Chablais *et al.*, 2011; González-Rosa *et al.*, 2011; Schnabel *et al.*, 2011). Cardiomyocyte death, characterised by the loss of striation, and nuclear and mitochondrial damage peak at 3-4 dpi (González-Rosa *et al.*, 2011; Schnabel *et al.*, 2011). Necrosis is followed by an acute immune response with neutrophils and macrophages clearing and degrading cellular remnants, extracellular matrix (ECM) and fibrin (in later days) to prepare the injury site for repair (***Figure 1.4B***) (Chablais *et al.*, 2011; González-Rosa *et al.*, 2011; Schnabel *et al.*, 2011; Lai *et al.*, 2017).

Reparative phase (~3 – 14 dpi): Fibrin formation, preventing excessive bleeding, on the marginal zone of the injury is integral part of the reparative phase (but is typically removed by 14 dpi) (Chablais *et al.*, 2011; Schnabel *et al.*, 2011). Apoptotic cell

numbers, mainly present in the outer layer and border zones, peak at 4 dpi and subsequently decrease to homeostatic levels at the end of the reparative process (Chablais *et al.*, 2011; González-Rosa *et al.*, 2011; Schnabel *et al.*, 2011). A continued pro-inflammatory environment, maintained by cytokine production from damaged cells and activated immune cells, directly stimulates local vascular cells and promotes fibroblast activation and differentiation to myofibroblasts (González-Rosa, Peralta and Mercader, 2012; Turner, 2016). Myofibroblasts and, to some extent epi- and endocardial cells, synthesise collagen and ECM, which initially strengthens the infarcted ventricular wall to secure it against future rupture, but later contributes to fibrous scar formation (***Figure 1.4C***) (González-Rosa *et al.*, 2011; Chablais and Jaźwińska, 2012b; Saxena *et al.*, 2013; Sánchez-Iranzo *et al.*, 2018).

Regenerative phase (in adult zebrafish): Cardiomyocytes start to regenerate from 4 dpi onwards with proliferation peaking at 7 dpi but then dramatically decreasing by 14 dpi (Chablais *et al.*, 2011; González-Rosa *et al.*, 2011; Bednarek *et al.*, 2015; Bertozzi *et al.*, 2021). New cardiomyocytes invade from the border zone and slowly penetrate the injury site (González-Rosa *et al.*, 2011; Schnabel *et al.*, 2011). By 21 dpi almost full recovery of the myocardium is observed, the fibrotic tissue is largely replaced by cardiomyocytes and only small areas of remaining injury and collagen deposition are present (***Figure 1.4D***) (Chablais *et al.*, 2011; González-Rosa *et al.*, 2011). Collagen is gradually eliminated and almost fully removed by the time regeneration is completed at 60 – 130 dpi (Chablais *et al.*, 2011; González-Rosa *et al.*, 2011; Schnabel *et al.*, 2011) and studies suggest that anti-inflammatory macrophages are important in this process (Bevan *et al.*, 2020). Indeed, resolution of the inflammatory response has been shown to be vital for regeneration in adult zebrafish (De Preux Charles *et al.*, 2016; Lai *et al.*, 2017; Bevan *et al.*, 2020).

Revascularisation of the injured area spans across all phases and is crucial for effective regeneration (***Figure 1.4A-C**).* New coronary vasculature sprouting from pre-existing vessels starts from ~1 dpi, with the process largely complete by 21 dpi (González-Rosa *et al.*, 2011; Marín-Juez *et al.*, 2016). Epicardial and endocardial cells also respond to injury. Epicardial cells proliferate to form a thickened multi-layered epicardium, which fully covers the injured area by 7 dpi and later compacts (Lepilina *et al.*, 2006; González-Rosa *et al.*, 2011; Schnabel *et al.*, 2011). Endocardial cells rapidly expand and their proliferation peaks at 5 dpi (González-

Rosa *et al.*, 2011; Kikuchi *et al.*, 2011; Münch *et al.*, 2017). Both cell linages show an organ-wide activation pattern, but epicardial cell activation is restricted to the injury site at later stages (Lepilina *et al.*, 2006; Schnabel *et al.*, 2011). Epicardial and endocardial cells temporarily alter their morphology while migrating towards the injury (Lepilina *et al.*, 2006; González-Rosa, Peralta and Mercader, 2012; Münch *et al.*, 2017).

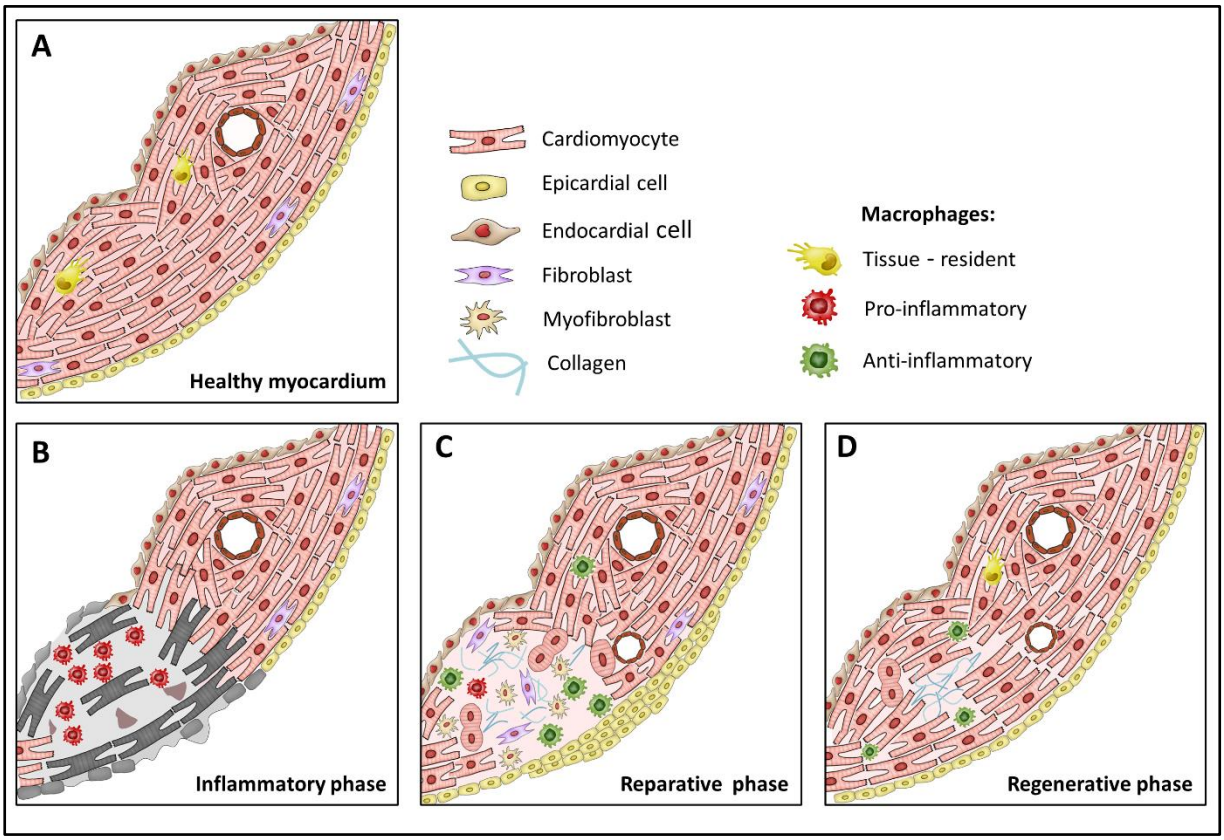

Figure 1.4. Cardiac repair and regeneration in zebrafish. (A) Cardiac cell populations in the homeostatic state. (B) Inflammatory phase: Massive cardiac cell necrosis is followed by infiltration of phagocytic cells, which clear cellular remnants. (C) Reparative phase: Fibrin forms at the injury site and pro-inflammatory cytokines and growth factors secreted from recruited immune cells promote activation of vascular cells and fibroblast transdifferentiation to myofibroblasts. Myofibroblasts synthesise and deposit ECM and collagen, which form transient fibrotic scarring. (D) Regenerative phase: Cardiomyocytes proliferate and penetrate the injury area. Fibrotic tissue is slowly replaced by cardiomyocytes. Neovascularization, and epithelial and endothelial cell renewal all contribute to both reparative and regenerative phases.

It is becoming increasingly clear, particularly from studies in adult zebrafish, that multiple different cell types are required for regeneration to occur. Two of these cell types, which are relevant to this study, are cardiomyocytes and macrophages and these will be discussed in more detail here.

1.5.2. Cardiomyocytes in regeneration

The first studies undertaken in zebrafish showed that following apical resection the heart successfully regenerates by 60 dpa (Poss, Wilson and Keating, 2002; Raya *et al.*, 2003). However, the phenomenon of cardiomyocyte regeneration remained unclear. Initially it was suggested that cardiac progenitor cells (CPCs) are the main source of new cardiomyocytes during cardiac regeneration (Raya *et al.*, 2003; Lepilina *et al.*, 2006). In zebrafish, CPCs are identified by the very first cardiac lineage markers expressed during embryogenesis - *nkx2.5, hand2*, and *tbx20* – transcription factors responsible for myocyte differentiation (Lepilina *et al.*, 2006). The regenerating regions of amputated zebrafish hearts were investigated for presence of CPCs and low expression of these markers was observed, suggesting the presence of CPCs in the regenerating myocardium (Raya *et al.*, 2003; Lepilina *et al.*, 2006). Interestingly, CPCs residing in human and mouse myocardium (defined as cKit+ expressing cells) predominantly give rise to cardiac endothelial cells not cardiomyocytes (Van Berlo *et al.*, 2014; Sultana *et al.*, 2015).

However, two studies published in 2010 disputed this theory of new cardiomyocytes being derived from undifferentiated progenitor cells (Jopling *et al.*, 2010; Kikuchi *et al.*, 2010). Through lineage tracing approaches, both groups presented that new cardiomyocytes repopulating the injury originate from proliferation of pre-existing cardiomyocytes (Jopling *et al.*, 2010; Kikuchi *et al.*, 2010). Mitotic activity of zebrafish cardiomyocytes was reported in earlier studies (Poss, Wilson and Keating, 2002; Ahuja, Sdek and MacLellan, 2007) but these later studies demonstrated that existing mature zebrafish cardiomyocytes synthesise DNA and re-enter the cell cycle to undergo mitosis (Jopling *et al.*, 2010). Interestingly, the proliferative activity of cardiomyocytes is not only observed at the border zone of the injury but also in distinct areas of heart (Jopling *et al.*, 2010; Sallin *et al.*, 2015). Later, this mechanism was also shown to underlie the origin of regenerating cardiomyocytes in neonatal

mice (Porrello *et al.*, 2011, 2013; Senyo *et al.*, 2013). A further study revealed that the mouse cardiomyocyte proliferative window is transient and is lost between 5 – 7 days of post-natal life (Zebrowski and Engel, 2013). Despite some mitotic activity and DNA synthesis after this time, as in adult humans, adult mouse cardiomyocyte loss is recompensated only partially by hypertrophy of remaining cells (Soonpaa *et al.*, 1996; Bersell *et al.*, 2009; Senyo *et al.*, 2013).

Proliferating cardiomyocytes undergo partial dedifferentiation manifesting as morphological and transcriptomic changes. During cell division, zebrafish cardiomyocytes disassemble their sarcomeres in the midzone, which is evident by a loss of striation and the presence of disorganised myofibrils (Jopling *et al.*, 2010; Kikuchi *et al.*, 2010) similar to what has been described for post-injury proliferating cardiomyocytes in newts and mice (Oberpriller *et al.*, 1995; Bersell *et al.*, 2009). Furthermore, transcriptional profiling of cardiomyocytes after injury revealed changes in expression of sarcomere proteins and repression of embryonic myomesin in zebrafish (Wu *et al.*, 2016).

During mammalian (human and mice) embryonic heart development, almost all cardiomyocytes are mononucleated and diploid, but undergo transduction to binucleated and polyploid during post-natal stages (Brodsky, Chernyaev and Vasilyeva, 1992; Adler *et al.*, 1996; Soonpaa *et al.*, 1996; Senyo *et al.*, 2013). Conversely, the majority of cardiomyocytes in zebrafish are mononucleated and diploid throughout their lifetime (Kikuchi *et al.*, 2010; Patterson *et al.*, 2017). Therefore, the difference in the ‘’ploidy’’ nature of cardiomyocytes across regenerative models has drawn attention and has been suggested to be a limiting factor of mammalian cardiomyocyte proliferation (Gan, Patterson and Sucov, 2020; Hesse *et al.*, 2021). The significance of this observation was confirmed by two independent experimental studies inducing cardiomyocyte polyploidisation in zebrafish, which led to inhibition of proliferation and diminished heart regeneration (Patterson *et al.*, 2017; González-Rosa *et al.*, 2018). In addition, an earlier study investigating the molecular mechanism of NRG1 (growth factor neuregulin 1) action in proliferation and regeneration of cardiac muscles, showed that injection of NRG1 *in-vivo* induced cell cycle activity in adult mice after LAD ligation. Interestingly, only mononucleated cardiomyocytes complete cell division fully, whereas binucleated cardiomyocytes undergo hypertrophy and polyploidisation (Bersell *et al.*, 2009).

Interestingly, one recent study demonstrates that multiple cryoinjuries exhaust heart regeneration capacity in adult zebrafish. After more than three injuries, the ability to resolve scar is reduced and not fully complete at 60 dpi. Cardiomyocytes re-enter the cell cycle rapidly for a short time, but overall proliferation is reduced compared to following only one injury (Bise *et al.*, 2020). This suggests that adult zebrafish do not have limitless regeneration although the mechanisms underlying this are yet to be determined. Indeed, although many comprehensive studies have investigated the specifics of the regenerative process in adult zebrafish, our current understanding remains incomplete and new and unexpected findings, particularly related to the importance of the inflammatory response, are still being revealed (Ryan, Moyse and Richardson, 2020).

1.5.3. Cardiac macrophages

1.5.3.1. Origin, types and activation state of macrophages.

Macrophages of the innate immune system are mononuclear phagocytes which play crucial roles in maintaining immunity and homeostatic function. Tissue resident macrophage populations in mammals are established during embryogenesis (Epelman *et al.*, 2014). In the first wave, yolk-sack derived embryonic progenitors populate the heart where they maintain their local pools by self-renewal throughout life. In the second wave, yolk-sack derived erythro-myeloid precursor cells (EMP) populate the foetal liver, where they transdifferentiate into monocyte progenitors able to differentiate to monocytes before the bone marrow develops (Epelman *et al.*, 2014). Progenitors derived from the foetal liver are the major source of tissue resident macrophages (Epelman *et al.*, 2014). Later, a small percentage of macrophages residing in the myocardium are replaced with circulating monocyte-derived macrophages, where their numbers rise during cardiac stress (Yona *et al.*, 2013; Epelman *et al.*, 2014; Gentek, Molawi and Sieweke, 2014). Despite their origin, macrophages can exhibit similar functions and phenotypes in response to microenvironmental stimuli (Murray and Wynn, 2011; Frodermann and Nahrendorf, 2018) and can be broadly classified as pro-inflammatory: activated by IFN-y (Interferon gamma), TNF (Tumour Necrosis Factor) and DAMP (Damage-associated molecular patterns) signalling and secreting i.e. TNFα, IL-1β, IL6 (Interleukins 1β and 6), or anti-inflammatory: activated by IL-6, IL-10 and TGF-β signalling and secreting

i.e. IL-10, VEGF (Vascular endothelial growth factor) (***Figure 1.5***) (Nahrendorf *et al.*, 2007; Kain, Prabhu and Halade, 2014). Anti-inflammatory macrophages exhibit pro-reparative functions (Kain, Prabhu and Halade, 2014; Frodermann and Nahrendorf, 2018). In zebrafish less is known about these different activation states although, similar to mammalian macrophages, they are often distinguished via *mpeg1* (*macrophage-specific marker 1*) expression (Ellett *et al.*, 2011) and can be further differentiated via their expression of pro-inflammatory cytokines, such as *tnfα*, *il8* and *il1β* (Nguyen-Chi *et al.*, 2015; Simões *et al.*, 2020) and anti-inflammatory (pro-resolving) markers, such as transforming growth factor (*tgfβ*) (Simões *et al.*, 2020). Recently, expression of Wilms tumour suppressor protein 1b (wt1b) has been characterised as a hallmark of a pro-regenerative macrophage phenotype in the regenerative tissues of zebrafish (Sanz-Morejón *et al.*, 2019). In the homeostatic state, *wtb1*$^{+}$ macrophages population are negligible in number, however, after injury their numbers expand rapidly and migrate to the injury site, where they constitute up to 40-70% of the total macrophage population in cryoinjured heart (Sanz-Morejón *et al.*, 2019).

1.5.3.2. Macrophage response following acute injury

Macrophages are abundant cell players in the post-MI microenvironment. After acute injury, absolute numbers of cardiac macrophage dramatically decrease (Epelman *et al.*, 2014; Lavine *et al.*, 2014; Dick *et al.*, 2019). In the ischemic zone, 60-70% of both resident and recruited cardiac macrophages are lost, presumably via cell death (Dick *et al.*, 2019). Whereas the loss of cardiac macrophages is mainly recompensated by the influx of monocyte-derived macrophages, peaking at 2 dpi (which gradually decrease), resident macrophages, whose total numbers account for 3-5% of total cardiac macrophages, self-renew their pools independently (between 2 – 7dpi) (Dick *et al.*, 2019). Macrophages arising from monocytes express pro-inflammatory gene signatures and phenotype (Epelman *et al.*, 2014; Lavine *et al.*, 2014; Dick *et al.*, 2019; Simões *et al.*, 2020) (***Figure 1.5***). Pro-inflammatory macrophages together with neutrophils (peaking at 1 dpi) clear necrotic tissue and secrete matrix metalloproteases (MMPs) to digest the ECM and aid repair (Nahrendorf *et al.*, 2007; Yan *et al.*, 2013; Lai *et al.*, 2017; Thackeray and Bengel, 2018; Bevan *et al.*, 2020) (***Figure 1.5***). In addition, pro-inflammatory macrophages secrete cytokines and growth factors to attract other immune cells, stimulate local

vascular cells and promote fibroblast to myofibroblast differentiation (Turner *et al.*, 2009; Frangogiannis, 2015; Turner, 2016; Frodermann and Nahrendorf, 2018) (***Figure 1.5***). Changes in macrophage phenotype from proinflammatory to anti-inflammatory (pro-resolving/pro-regenerative) is seen during the early-mid inflammatory phase (Jung *et al.*, 2013; Heidt *et al.*, 2014; Thackeray and Bengel, 2018; Bevan *et al.*, 2020; Simões *et al.*, 2020) (***Figure 1.5***). Indeed, a recent thorough evaluation of macrophage dynamics and inflammatory markers in the response to cardiac injury in adult zebrafish revealed dynamic expression of the pro-resolving factor, *tgfβ*, within the first 24 hours which then stayed elevated until 14 dpi (Simões *et al.*, 2020). Another population of recently identified pro-regenerative macrophages in zebrafish cryoinjured heart, defined by endogenous expression *wt1b*, peaks at 4 dpi after cryoinjury constituting approximately 50-70% of the total macrophage population, which then drops to ~40% at 21 dpi (Sanz-Morejón *et al.*, 2019). Interestingly, using both a cardiac cryoinjury and a fin amputation model, *wt1b*$^{+}$ macrophages migrate towards and accumulate at the site of the injury for a prolonged time (Sanz-Morejón *et al.*, 2019). Reduction of the number of these *wt1b*$^{+}$ macrophages resulted in a decrease in cardiomyocyte proliferation (Sanz-Morejón *et al.*, 2019). Anti-inflammatory macrophages exhibit pro-reparative and tissue healing functions, silence inflammation, stimulate cardiomyocyte proliferation and angiogenesis, (Van Amerongen *et al.*, 2007; Shiraishi *et al.*, 2016), and, in adult zebrafish, contribute to both scar formation and scar resolution in later phase (Sanz-Morejón *et al.*, 2019; Bevan *et al.*, 2020; Simões *et al.*, 2020) (***Figure 1.5***). This macrophage response is also accompanied by other innate and adaptive immune cells, but their numbers are lower and their functions in regeneration are yet to be fully evaluated (reviewed in Dittrich and Lauridsen, 2019 and Ryan, Moyse and Richardson, 2020).

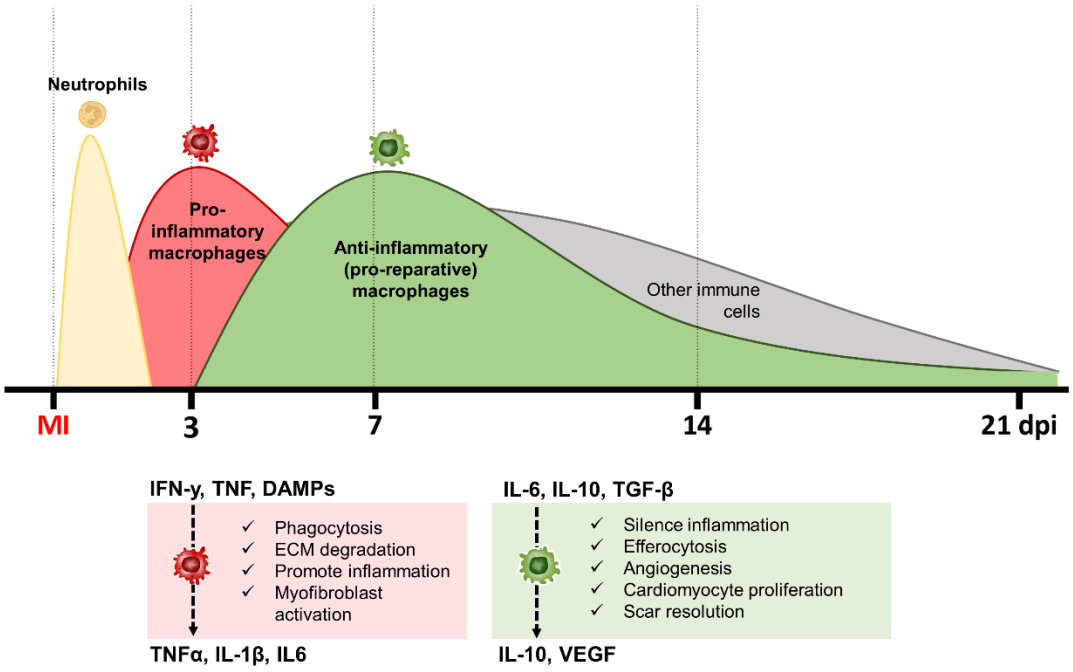

Figure 1.5. Cardiac immune cell dynamics. Infiltration of neutrophils and different macrophages and their relative timing during the pathophysiological phases of MI. The innate immune response is accompanied by lymphocytes of the adaptive immune system, although less is known about their function. Pro-inflammatory macrophages prepare tissue for repair, whereas anti-inflammatory macrophage aid repair and regeneration.

1.5.3.3. Reparative and regenerative functions of macrophages

A comparative study on cardiac mononuclear phagocytes of neonatal and adult mice has shown that cardiac repair depends on differences in the magnitude and activation of macrophages. Macrophages are more abundant in healthy and post-MI neonatal hearts and their response is quicker and global whereas this response is delayed and injury restricted in adult mice (Aurora *et al.*, 2014). Moreover, differs in transcriptional profile, neonatal macrophages express more pro-regenerative (anti-inflammatory) phenotype, whereas adult macrophages more pro-inflammatory and pro-fibrotic phenotype after injury (Aurora *et al.*, 2014). Their role in successful regeneration was further highlighted by macrophage depletion experiments, which resulted in defective and incomplete angiogenesis in post MI neonatal hearts, a crucial step in successful regeneration (Aurora *et al.*, 2014; Simões *et al.*, 2020).

An initial attempt to investigate the difference in cardiac macrophage plasticity between regenerative neonatal and non-regenerative adult mice using a

cardiomyocyte ablation model revealed a difference in the origin and response of cardiac macrophages (Lavine *et al.*, 2014). In this study, macrophage subsets were distinguished by expression of major histocompatibility complex II (MHC-II) and chemokine (C–C motif) receptor 2 (CCR2), specific to monocyte-derived macrophages. The adult mouse heart consists of macrophages of three distinct origins: embryonic (yolk sac and foetal liver) and hematopoietic (bone marrow), which can be differentiated using specific markers (MHC-2^{lo} CCR2^{-} and MHC-2^{hi} CCR2^{-}, respectively) and monocyte-derived (MHC-2^{hi} CCR2^{+}), as well as monocytes (MHC-2^{lo}CCR2^{+}) (Lavine *et al.*, 2014).Cardiac macrophages of neonatal mice are almost entirely populated from embryonic-derived resident macrophages (MHC-2^{lo} CCR2^{-}) and monocytes (MHC-2^{lo} CCR2^{+}) (Lavine *et al.*, 2014). A recent transcriptomic study has improved our understanding of cardiac macrophage heterogeneity in adult mice (Dick *et al.*, 2019). Four different macrophages (*Timd4* cluster, *Mhc-II* cluster, *Ccr2* cluster, *Isg* cluster) and one monocyte cluster has been identified based on their gene signature (Dick *et al.*, 2019). This result aided in the characterisation of TIMD4 as a novel and exclusive marker of cardiac resident macrophages, which further distinguishes MHC-2$^{lo/hi}$ CCR2^{-} from recruited/replaced macrophages residing in the murine myocardium (Dick *et al.*, 2019).

The earlier study has shown that despite monocyte infiltration after cardiomyocyte ablation, neonatal mice retain and expand this embryonic-derived resident macrophage population (MHC-2^{lo} CCR2^{-}), which were shown to generate a minimal inflammatory response but promote cardiac recovery and cardiomyocyte proliferation and angiogenesis (Lavine *et al.*, 2014). In adult mice, however, loss of cardiac macrophages was recompensated by a monocyte-derived subtype (MHC-2^{hi} CCR2^{+}) of highly pro-inflammatory macrophages which results in tissue architecture remodelling and interstitial scarring (Lavine *et al.*, 2014). Depletion of resident macrophages in neonatal hearts significantly affected regeneration processes and resulted in pathological changes, whereas depletion of monocyte-derived macrophages in adult hearts improved post-MI outcome (Lavine *et al.*, 2014). Contrary to these findings which relies on limited macrophage markers, the Epelman's group has observed that 60% of absolute macrophages are lost at 2 days post infarction and this involved both resident (MHC-2^{lo} CCR2^{-} TIMD4^{+}) and (MHC-2^{hi} CCR2^{-} TIMD4^{-}) macrophages (Dick *et al.*, 2019). Yet, the MHC-2^{hi} CCR2^{-} TIMD4^{-} population account for the vast majority of the lost macrophages, where MHC-2^{lo}

CCR2^{-} TIMD4^{+} are depopulated to a lesser extent (Dick *et al.*, 2019). Overall, macrophage density increases over 28 dpi with MHC-2^{lo} CCR2^{-} TIMD4^{+} accumulating at the peri-infarct zone (Dick *et al.*, 2019). Interestingly, selective depletion of resident macrophages with diphtheria toxin receptor (DTR) leads to cardiomyocyte hypertrophy and excessive fibrosis, whilst the size of the infarct remained unaffected at 7dpi (Dick *et al.*, 2019).

Stainier and colleagues used comparative transcriptomics and functional studies on two teleost models, regenerative zebrafish and non-regenerative medaka, to reveal differences in the cardiac injury response and underline the role of immune cells in successful regeneration. In this study, cardiac macrophages were depleted in zebrafish via injection of clodronate liposomes (CL) 1 day before cryoinjury (Lai *et al.*, 2017). These liposomes are taken up by phagocytic cells and the cytotoxic clodronate is released during its intracellular degradation (Rooijen and Sanders, 1994). Accumulation of toxic concentrations of clodronate drives macrophages to apoptosis (Rooijen and Sanders, 1994). Consequently, reduced macrophage response resulted in defective neovascularization of the injured area, decreased cardiomyocyte proliferation, and excessive and persistent scarring in regenerative zebrafish (Lai *et al.*, 2017). Moreover, this led to reduced clearance of neutrophils emphasising the role of macrophages in orchestrating the inflammatory response (Lai *et al.*, 2017). It should to be noted, however, that CL treatment targets any activated phagocytes (Schmidt-Weber *et al.*, 1996) and its effect on other cell types are not fully explored. Therefore, genetic approaches such as *mpeg1.1* morpholino knock out (Benard *et al.*, 2015) or the diphtheria toxin depletion system under a *mpeg1.1* promoter (Goren *et al.*, 2009) would provide more specific macrophage depletion. By contrast, stimulation of the innate immune response in non-regenerative medaka via poly:1:C (Toll like receptor antagonist) injection, accelerated neutrophil and macrophage responses, similar to that observed in zebrafish, which resulted in improved re-vascularisation, increased cardiomyocyte proliferation and enhanced neutrophil clearance (Lai *et al.*, 2017).

It has become clear that macrophages are important players in repair and regenerative processes and their complex plethora of activation states and developmental origins is only beginning to be fully determined. Additionally, studies

are revealing new roles for macrophages beyond their classical phagocytic function suggesting that more needs to be uncovered about their precise roles in the heart.

1.6. Unexpected roles for cardiac macrophages

Recently, Nahrendof and colleagues revealed a novel function for macrophages in the healthy mouse heart (Hulsmans *et al.*, 2017). Their comprehensive study has demonstrated that cardiac resident macrophages are abundant in the AV node and communicate with cardiomyocytes through connexin 43 (Cx43) - containing gap junctions. Macrophages coupled with cardiomyocytes in this manner accelerate and enable electrical conduction (Hulsmans *et al.*, 2017). This was further confirmed by depletion of Cx43- containing or AV node macrophages leading to impaired conduction (Hulsmans *et al.*, 2017). Additionally, a recent transcriptomic study on zebrafish and neonatal mice has shown enrichment of collagen genes in cardiac macrophages following MI (Simões *et al.*, 2020). Their complementary experiments revealed that macrophages located near the injury site not only express collagen transcripts but contribute to scar formation via active collagen production and disposition in the border zone of the infarcted heart (Simões *et al.*, 2020). Interestingly, macrophage-derived collagen found in the infarcted heart accounts for 6.25% of total collagen deposited in scarring cardiac muscles (Simões *et al.*, 2020). Macrophages have been intensively explored over the past 20 years, but both of these studies reveal unexpected roles of cardiac macrophages and enrich our knowledge of non-canonical functions of these important cells.

1.6.1. Cardiomyocyte specific protein expression in cardiac macrophages.

Unpublished proteomic data from the Richardson Lab using TgBAC(*tnfα:GFP*); Tg(*mpeg1.1:mCherry*) double transgenic zebrafish, which aimed to investigate pro-inflammatory (*tnfa*+ *mpeg1.1*+) and anti-inflammatory (*mpeg1.1*+) macrophage specific markers, has revealed unexpectedly high expression of nine cardiomyocyte/muscle specific proteins in FACs sorted cardiac macrophages at 7 dpi. A full list of these genes along with their relative expression level in pro-inflammatory (*tnfα+)* and anti-inflammatory (*tnfα-)* immune cells is presented (***Figure 1.6A-B*****).** Interestingly, the proteins identified in the proteomics study are building

blocks of the sarcomere and are all involved in muscle function including roles in contraction or oxygen transport (Vlecken *et al.*, 2009; Yang, Shih and Xu, 2014). The exact roles and importance of this cardiac protein expression in the cardiac macrophages, and how their expression related to injury or homeostasis are yet to be elucidated. Taking into consideration these novel functions reported in cardiac macrophages, I hypothesised that specific cardiac macrophage subsets express cardiomyocyte proteins during, and this expression is altered after, acute injury to the heart.

A

Protein name	Protein symbol	Ortholog	
	Zebrafish	Human	Mice
Myosin heavy chain 7-like	Myh7l	-	-
Actin, alpha 1a, skeletal muscle	Acta1a	ACTA1	ACTA1
Tropomyosin 4a	Tpm4a	TPM4 *	TPM4 *
Myoglobin	Mb	MB	MB
Myosin, heavy chain 6, cardiac muscle, alpha	Myh6	MYH6	MYH6
Cardiac myosin light chain 2	Myl7	MYL7	MYL7
Cardiac myosin light chain-1	Cmlc1	MYL4	MYL4
Troponin T2, cardiac	Tnnt2a	TNNT	TNN2
Troponin C1, cardiac and skeletal	Tnnc1	TNNC	TNNC1

B

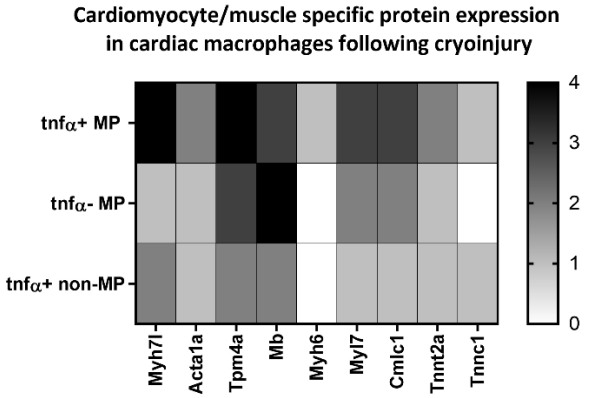

Figure 1.6. Proteomic data obtained from TgBAC(*tnfα:GFP*); Tg(*mpeg1.1:mCherry*) hearts at 7 dpi. This analysis demonstrates expression of cardiomyocyte specific proteins in cardiac macrophages. (A) Table of the proteins identified plus their human and mice orthologs. (B) Heat map of the relative expression level in different macrophage populations. (*) Mammalian TPM4 isoform is truncated in striated muscle (Zajdel *et al.*, 2013).

1.7. Aims and objectives:

The hypothesis of this thesis is:

“Cardiac macrophages express cardiomyocyte specific genes during homeostasis and this expression is altered after acute injury to the heart"

The main aim of this research was to validate the observed cardiomyocyte specific gene expression in cardiac macrophages and to determine if this expression was related to repair and regeneration. In order to test this hypothesis and address this aim the following objectives were proposed:

Objectives:

1. Confirm expression of nine genes encoding the proteins of interest in cardiac macrophages via RT-PCR/qPCR at different time points post-injury and in uninjured hearts.
2. Analysis of macrophages derived from the Tg*(myl7-GFP);* Tg*(mpeg1:mCherry)* double transgenic line via flow cytometry.
3. Characterisation of the localisation and phenotype of *myl7* expressing macrophages from Tg*(myl7-GFP);* Tg*(mpeg1:mCherry)* fish via high-power confocal microscopy.

Chapter 2. Materials and methods

2.1. Primer design

The Ensembl database was used to obtain sequences of the gene of interests (GOI), previously identified by proteomic data (***Figure 1.6.A***). Based on all obtained sequences the primers were designed using the PrimerBlast/PrimerOutput3 online tool, aiming to target across an exon-exon junction and producing an amplicon size ranging from 50 to 200 bp of coding sequence, with a melting temperature (Tm) of 60 °C +/-2 °C. Primers for *mb* (Roesner, Hankeln and Burmester, 2006), *myl7* (*cmlc2a*) (Sander *et al.*, 2013), *myh6* (Shih et al., 2015), *ef1a* (Moriarty *et al.*, 2012) and *loopern4* (Vanhauwaert *et al.*, 2014), were previously published. Please refer to full list of primers for specific sequences, amplicon size and references (***Table 2.1***).

2.2. Animal procedures

The following previously published zebrafish transgenic lines were used in the study: TgBAC*(tnfα:GFP)* (Marjoram *et al.*, 2015); Tg*(mpeg1.1:mCherry)* (Ellett *et al.*, 2011); Tg*(myl7:GFP)* (Geoffrey Burns *et al.*, 2005) and Tg*(mpeg1:GFP-CAAX)* (Villani *et al.*, 2019). For all experimental procedures fish aged 4-18 months were randomly assigned to control or test experimental groups and anaesthetised via immersion in 0.025% MS-222 (A5040; Sigma). Cardiac injuries on adult zebrafish were carried out as described previously (González-Rosa and Mercader, 2012). Briefly, fish were anaesthetised and placed ventral side up in a sponge soaked with anaesthesia. A small (approx. 4 mm) incision was made through the body wall above the beating heart with a scalpel, the ventricle was dried with a sterile cotton bud and a liquid nitrogen cooled probe was applied for 30 sec on the ventricular wall of the exposed heart. Fish were returned to fresh aquarium water and monitored after the procedure until fully recovered from general anaesthesia. At the required experimental time-point, animals were culled via an overdose of anaesthetic. All animal work was carried out in accordance with U.K. Home Office and local University of Bristol regulations.

2.3. Preparation of single cell suspensions and FAC sorting

A single cell suspension was prepared from harvested heart ventricles and fins (combined anal, dorsal, and caudal) following the protocol established by Sander et al. (2013) with minor modifications. For the hearts the atria and outflow tract were removed and ventricles were torn open to wash out the blood with PBS (D8662, Sigma). Fins were also washed in PBS and cut up. Tissue samples were placed in 250 µl of ice- cold perfusion buffer (10 mM HEPES, 30 mM taurine, and 5.5 mM glucose in PBS) per ventricle/fin. Perfusion buffer was replaced with an equal volume of digestion buffer - 0.25% trypsin (15090046; Sigma), 12.5 µM $CaCl_2$, and 5 mg/ml collagenase II (10738473; GIBCO) in perfusion buffer. Tissues were digested for 2 hours at 32 °C in a thermomixer at 800 rpm and frequently mixed by pipetting. Digestion was terminated by incubating on ice and addition of one volume of stopping buffer - 12.5 µM $CaCl_2$, 10% (v/v) FBS (11591821; Thermo Fisher Scientific) in perfusion buffer. The resulting cell suspension was filtered through a 40 µm sterile cell strainer (22363547; Thermo Fisher Scientific) into an Eppendorf tube, then cells were pelleted by centrifugation for 10 min at 4 °C at 300 g. Cells were resuspended in 300 µl of suspension buffer (50 U/mL, 0.05 mg/mL Pen-Strep, 0.8 µM CaCl2, 2% FBS in Sterile PBS) and stained with DRAQ7 (ab109202; Abcam) to determine dead cells prior to flow cytometry. Samples were sorted on a BD Influx Fluorescence Associated Cell Sorter in sterile conditions at 4 °C for mCherry and/or GFP positive cells from five different time points (uninjured (Un), 3, 7, 14 and 21 dpi). Non-fluorescent cells were also collected. Data was analysed in FlowJo_v10.6.2 software by the gating method. Please refer to ***section 4.2*** for gating strategy.

2.4. RNA isolation from whole zebrafish tissue

Ventricles and fins were prepared in the same manner as for dissociation, but placed directly into TRI reagent (T9424, Merck) (3 ventricles/ or 4 fins per 500 µl). The samples were homogenised by syringe and 22G sharp needle, then stored at -80 °C. Samples were thawed at room temperature (RT) for 5 min prior to RNA isolation, before proceeding with a standard chloroform-isopropanol method. Firstly, 100 µl of chloroform (10488400, Fisher Scientific) was added, vortexed immediately and centrifuged for 15 min at 4 °C at 12000 x g. The upper aqueous phase (approx. 180 µl) was transferred to new tube, 0.5 µl of 20 mg/mL glycogen added and the RNA was precipitated via addition of 250 µl isopropanol (I9516-500ML, Sigma). Samples

were incubated for 10 min at RT, then centrifuged for 15 min at 4 °C, at 12000 x g. Samples were washed with cold 75 % EtOH and an additional washing step was performed to enhance purity of the RNA material, centrifuging for 10 min and 5 min, respectively. To eliminate residual alcohol after removing the supernatant, samples were pulse centrifuged at low speed and allowed to air dry. Dried RNA was resuspended in 10 µl Nuclease Free Water (NF-H_2O) and quantified on a NanoDrop 2000 Spectrophotometer (Thermo Fisher Scientific).

2.5. Isolation of RNA from and FACS sorted cells

RNA was isolated using an RNeasy Micro Kit (74004, Qiagen). Fluorescent cells isolated by FACS were sorted directly into 500 µl of RTL Buffer containing Beta-mercaptoethanol (β-ME) (11426581, Fisher Scientific) when the cell count was ≤100000. Cell counts >100000 were collected into 100 µl of sterile PBS (D8662, Sigma) and centrifuged to pellet the cells (mainly fin cells). The supernatant was removed, leaving 100 µl of cell suspension, then 350 µl of RTL buffer were added. In all cases the volume of the RTL buffer to aqueous phase was adjusted to a 3.5–1 ratio, respectively. Cells were vortexed for 1 min and homogenised directly using a syringe and a 20G blunt needle, then frozen immediately at -80 °C. Samples were processed the following day according to the manufacturers RNA clean up and concentration protocol. The volume of the samples was measured prior to adding 100 % EtOH to maintain the correct volume. RNA was resuspended in the minimal volume of 14 µl of NF-H_2O. RNA obtained from each sample (cardiac macrophages, non-fluorescent cells, cardiomyocytes, and fin macrophages) from two sorts were pooled together for each time point in order to obtain enough cells. Samples were adjusted to 50 µl with NF-H_2O and sent to the Genomics Facility (University of Bristol) for precipitation using RNAClean XP beads (A66514, Beckman Coulter). Precipitation was performed following the manufacturer's protocol. RNA was retrieved with the minimal appropriate volume of 15 µl NF-H_2O, which could be used to fully cover the used beads and achieve the most concentrated samples. Additionally, the quality and quantity of RNA was measured using RNA ScreenTape Analysis and/or High Sensitivity RNA ScreenTape Analysis run on an Agilent Bioanalyzer 2200 and the data analysed using TapeStation Analysis Software v.A.02.02.

2.6. cDNA Synthesis

Each RNA sample isolated using the Trizol-Chloroform method described above was reverse transcribed to complementary DNA (cDNA) using the Maxima First strand Kit (K1671, Thermo Fisher Scientific) with dsDNase treatment, according to the manufacturer's instruction. A 20 µl reaction was set up containing 8 µl RNA template, 1 µl 10X dsDNase Buffer, 1 µl dsDNase, 5 µl 5x Reaction Mix, 2 µl Maxima enzyme and 4 µl NF-H_2O. The dsDNase treatment was carried out for 2 min at 37 °C and cDNA synthesis for 10 min at 25 °C followed by 15 or 30 min (depending on RNA concentration) at 50 °C and terminated by heating at 85 °C for 5 min on a Bio-Rad T100 Thermal Cycler machine.

2.7. Amplification of RNA from sorted cells

Purified RNA from sorted cells (cardiac macrophages and cardiomyocytes) from five different time-points (unwounded, 3, 7, 14, 21dpi) were amplified with a QuantiTect Whole transcriptome kit (207043, Qiagen) according to the manufacturer's instructions. Approximately 16.2 ng or 17.5 ng of total RNA of each sample were adjusted with NF-H_2O to a total volume of 5 µl and amplified for either 8 h for high cDNA yields or 2 h for standard cDNA yields. Reverse transcription, ligation and amplification mixes were prepared fresh prior to each step and incubations were performed in a Bio-Rad T100 Thermal Cycler machine. Briefly, 5 µl of RNA from each sample were reverse transcribed for 30 min at 37 °C, then the reaction was terminated for 5 min at 95 °C and samples were cooled to 22 °C. 10 µl of the ligation mix was added to each sample and incubated for 2 h at 22 °C. Lastly, amplification was completed by adding 30 µl of the amplification mix and incubating samples for 2 or 8 h.

2.8. Reverse Transcription PCR (RT-PCR)

RT-PCR was performed with a QIAGEN Fast Cycling PCR Kit (203745) accordingly to manufacturer's instructions using a Bio-Rad T100 Thermal Cycler machine. A 20 µl PCR reaction was set up containing 10 ng/µl forward and reverse primers and 1 µl of 25 ng cDNA template. The thermocycling condition were adjusted, as recommended, to expected amplicon size to establish best annealing temperature

(T_a) for amplification of GOI (95°C for 5 min, 35 cycles of 96°C for 5 sec, T_a for 5 sec, 72°C for 15 sec followed by 1 min at 72°C).

2.9. Primer validation and relative gene expression (qPCR)

Each qPCR reaction contained 2x PowerUp SYBR Green Master Mix (A25780; Thermo Fisher Scientific), 1 µl of cDNA, adequate concentration (in nM) of each forward and reverse primer, in a total of 10 µl made up with NF-H_2O. qPCR was preformed using three replicates for each cDNA concentration obtained from total heart RNA. For initial primer validation, cDNA was adjusted to 50 ng/µl before a 1:5 serial dilution was prepared and run to generate the standard curve. Water and cDNA-minus samples were run as a negative control for each assay. A QuantStudio™ Real-Time PCR machine and their Design & Analysis Software v.1.4.3 was used to perform each qPCR assay and perform initial analysis of the data. Thermocycling conditions were optimized at 95 °C for 2 min, followed by 40 cycles at 95 °C for 1 sec and 60 °C for 30 s. The specificity of all the reactions was determined by running a melting curve analysis at the end of the qPCR cycles and electrophoresis on 2% agarose gels at 100V for 30 min. Only primers with efficiency between 90 -110 % and $r^2 > 0.99$ were used. The steady state expression of various genes was normalised with *ef1α* and standard deviation (SD) calculated. Relative Quantification were measured using Pfaffl's correction equation (Pfaffl, 2001).

2.10. Heart imaging and analysis

Whole hearts were dissected from euthanised adult Tg*(myl7-GFP);* Tg*(mpeg-mCherry)* fish at five different time points (unwounded, 3, 7, and 14 dpi). Hearts were washed in PBS, then placed in 4 % paraformaldehyde (P6148; Sigma) and incubated at RT for 2 h on an orbital shaker. Hearts were washed five times in PBS before mounting in 1.5 % Low Melting Point Agarose (A9414; Sigma-Aldrich). Images were acquired on a Leica SP8 Multiphoton Microscope using a 10x HC APO L-U-V-I and 25×/0.95 HC Fluotar water dipping lens. Two channels were recorded: GFP (cardiomyocytes) and mCherry (macrophages). Each channel was recorded sequentially to limit crosstalk between fluorophore signals and detection wavelengths were set to avoid GFP/mCherry contamination. Images were processed and analysed in Fiji (Schindelin *et al.*, 2012). Intensity of green signal in macrophages

was measured using a Modular Image Analysis (MIA) custom plugin designed by Dr Stephen Cross (Wolfson Bioimaging Facility, University of Bristol). Briefly, the GFP+ signal was measured in a 3D volume projection of individual macrophages (mCherry+) across the Z-stacks at two areas of the heart: mid and apex from uninjured ventricles or the unaffected region of ventricle and injury site from injured ventricles as presented in ***Figure 5.1.***

2.11. Statistics

In all cases n value refers to number of biological replicates. GraphPad Prism6/7 was used for raw data recording and analysis. For imaging data sets, a Grubb's outlier test was performed, and any significant GFP signal outliers (alpha=0.05) were removed along with their corresponding volume and circularity. Data distribution were checked prior to statistical analysis. Statistical significance was determined via nonparametric Mann-Whitney or Kruskal-Wallis/Dunn's multiple comparison tests (details under figure description). Indicated significance= *P<0.05; **P< 0.01; ***P< 0.005; ****P< 0.001. In all cases error bars represent minimum and maximum values.

Gene	Forward	Reverse	Amplicon size	Exon-Exon junction	Slope	R^2	Efficiency (%)	Reference
mb	GAAGTTCTCAACCG TCTGTTCAA	GCTTCCCGCCAGATC ACCCT	93	Yes	-3.336	0.993	99.42	Roesner et al, 2006
cmlc1	ACGCCAACAGGAG AGATGAA	CTGGTCCTTGGCTCT TGAGA	192	No	-3.344	0.997	99.07	PrimerBLAST
myl7 (cmlc2a)	GGCTCTTCCAATGT CTTCTCC	GGACTCCAGCTCTTC ATCAC	168	Yes	-3.346	0.997	94.45	(Sander *et al.*, 2013)
tpm4a	GGTGTGACTTCTTT GGACGC	TCCTCCACCAGCTGA ATCC	185	Yes	-3.108	0.995	109.78	PimerOutput3
tnnt2a	CTTCGGCGGTTACA TGCAAA	CAATGTCCAGAGGTT TGCGT	106	Yes	-3.239	0.997	103.56	PimerOutput3
myh6	TGAAGACCTGAGAA GGCAAC	CAGTTCCTCGGTTCT CTGAA	223	No	-3.461	0.98	94.49	(Shih *et al.*, 2015)
acta1a	GACTCACGAGAAC GAGC AG	GGATTTTACCTGGTG AC GC	174	Yes	-3.583	0.992	90.14	PimerOutput3
tnnc1a	GCCAGAACCCTACC CCTGAA	CTGGCCTTCCTTTGC TGTCA	108	Yes	-3.486	0.995	93.58	PrimerBLAST
myh7l	TTCAGTGGAATGTG CGTGCA	CTACGTGCCTCAGAC TTCGC	169	No	-3.531	0.994	91.94	PrimerBLAST
nkx2.5	GTCTGGGAGACAC GTCCACT	ATGCTGGACATGCTC GACGG	145	No	-3.574	0.99	90.45	PrimerBLAST
mef2aa	ATGAACCCCACGAG AGCAGA	CCGAAACGGTCGTCC ATGAG	130	Yes	-3.542	0.993	91.56	PrimerBLAST
loopern4	TGAGCTGAAACTTT ACAGACACAT	AGACTTTGGTGTCTC CAGAATG	Repbase		-3.342	0.997	99.19	(Vanhauwaert *et al.*, 2014)
ef1a	CGTGGTATCACCAT TGACATTGC	TCAGCCTGAGAAGTA CCAGTGA	124	Yes	-3.214	0.999	98.00	(Moriarty *et al.*, 2012)

Table 2.1. Primer sets used for qPCR relative expression assay. Primer sequences and their resources are presented in the table, together with specificity of target amplicon size and the validation details.

Chapter 3: Expression of cardiomyocyte specific genes in cardiac macrophages in healthy and injured zebrafish hearts.

The aim of the work described in this chapter was to validate the expression of nine cardiomyocyte or muscle specific proteins that were found in a proteomics data set from sorted cardiac macrophage populations at 7 dpi. In order to assess active transcription of the genes encoding these proteins in cardiac macrophages, and due to limited antibodies being available to specifically detect zebrafish proteins, transcript levels of the corresponding genes were investigated by RT-qPCR. RT-qPCR is a powerful tool to investigate gene expression changes over a time course after injury or treatment. It allows rapid quantification of RNA in real time, converted to complementary cDNA (copy of RNA template) in a process of reverse transcription (RT), measuring amplification of the signal generated by a fluorescent probe (Adams, 2020). Minimum Information for Publication of *Q*uantitative (MIQE) guidelines have been published to standardise qPCR methodology in order to produce more reproducible and comparable data from experimental studies (Taylor *et al.*, 2010). According to the MIQE guidelines and to maximise the quality of the qPCR data analysis, the relative expression assay was planned to be performed using the Vandesompele method (Vandesompele *et al.*, 2002), where two reference genes are chosen to normalise data using their geometric mean value. This method is thought to minimise variation in reference gene expression observed between tissues, developmental stages and gender of the fish (McCurley and Callard, 2008). A recently validated reference gene in zebrafish (Gistelinck et al., 2016) and mice (Renard et al., 2018) is *loopern4,* an Expressed Repetitive Element (ERE) (Vanhauwaert et al., 2014). Additionally, ***ef1α, a*** widely used reference gene known for the stability of its expression, was chosen for this study (Tang *et al.*, 2007; Moriarty *et al.*, 2012). Prior to RT-qPCR relative gene expression analysis, all primer sets were validated to determine the efficiency and specificity of their target gene amplification as described in ***section 2.1.*** For a full list of primers and their specification please refer to ***Table 2.1***.

For RT-qPCR analysis of cardiomyocyte gene expression in cardiac macrophages, zebrafish ventricles and fins (as a tissue specific control) from two transgenic lines Tg(*myl7:GFP*); Tg(*mpeg1.1:mCherry*) and Tg(*mpeg1.1:mCherry*) were collected. These transgenic lines allow separation of macrophages via expression of *macrophage-expressed gene, tandem duplicate 1,* labelled with red fluorescence (*mpeg1.1:mCherry+),* from cardiomyocytes with *cardiac myosin, light chain 7* labelled with green fluorescence (*myl7:*GFP+) from ventricular tissue (non-fluorescence cells, mainly cardiomyocytes) (Geoffrey Burns *et al.*, 2005; Ellett *et al.*, 2011). For this study hearts from uninjured fish and different time points post-cryoinjury were collected. Three time points corresponding to important macrophage and cardiomyocyte responses during heart repair and regeneration (described in ***section 1.5.1***) along with 7 dpi (from which proteomic data was obtained) were selected.

Cardiomyocytes (*myl7*+ or background non-fluorescent cardiac cells), cardiac and fin macrophages (*mpeg1.1*+) and fin background cells (non-fluorescent) were sorted from 5 or 6 ventricles and 12 fins per time point via FACS (Schematic workflow ***Figure 3.1***). Details on the gating strategy and FACS plots of cell populations can be found in ***Figure 4.1 and 4.2***, respectively.

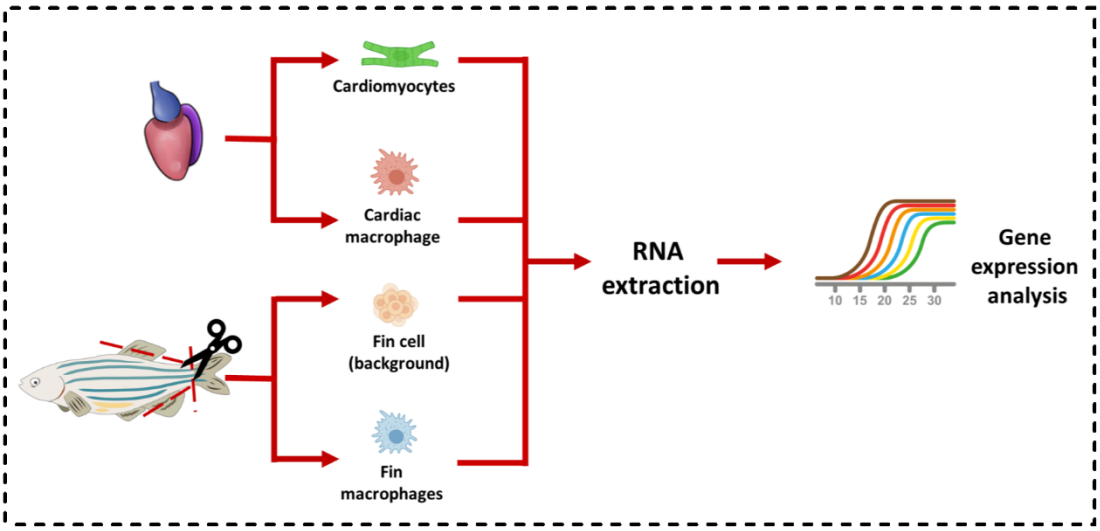

Figure 3.1. Schematic representation of experimental work flow. Five or six ventricles and 12 fins were collected from uninjured and post cryoinjury Tg(*myl7:GFP*); Tg(*mpeg1.1:mCherry*) or Tg(*mpeg1.1:mCherry*) fish and sorted via FACS for cardiac macrophages (mCherry+) and cardiomyocytes (GFP+) or non-fluorescent ventricular cells

(where single transgenic line Tg(*mpeg1.1:*mCherry) was used) and fin cells (tissue specific control). RNA was extracted from sorted cell populations and gene expression analysis performed.

3.1. Technique optimisation for RNA extraction and RT-qPCR

3.1.1. Optimisation of low RNA yield from sorted cells

Initial experiments using the TRIzol-Chloroform extraction method revealed that extraction of RNA from sorted zebrafish cells is a challenging process, manifested by low numbers of starting cells and extremely low and variable RNA yields. Yields as low as 3.9 - 64 ng (median = 16.55; n=8) of RNA per 20,000 cells was observed (***Table 3.1***). Along with unsatisfactory yields, the purity ratios obtained fell between 2.3 – 1.5 of the 280/260 ratio and 0.47- 0.03 of the 260/230 ratio, suggesting low purity and contamination of the samples by protein or organic compounds (***Table 3.1***). In previous studies a yield ranging from 14.5 ng - 41.11 ng (average median = 23.4 ng) of high quality intact RNA (tested by Fragment analyser described in more details below) from sorted cells has been estimated (Loontiens *et al.*, 2019). Therefore, considerable technique optimisation was required to obtain sufficient yields of high-quality RNA for downstream PCR analyses. To improve yields of RNA, the extraction method was changed to column based Micro RNeasy extraction (Qiagen) as this has been described to be the most efficient method for ultra-low cell counts (Mack, Neubauer and Brendel, 2007; Loontiens *et al.*, 2019; Wang *et al.*, 2019) and to eliminate possible downstream degradation of RNA, β-ME RNase inhibitor was introduced and the dissociation protocol was shortened (as described in ***section 2.1/2.4***). This change led to an improvement in the obtained quantities of RNA, resulting in 2.96 – 98.26 ng of total RNA per 20,000 cells (median = 22.26;) (***Table 3.1***)***.*** However, the absorbance ratios obtained with this new method were comparable to those of TRIzol-Chloroform extracted samples, suggesting purity was still an issue, however, this could also be due to a reduction in Nanodrop accuracy when assessing nucleic acid concentrations ≤20 ng/µl (Koetsier and Cantor, 2019).

Method	Sample	cell count	Conc. (ng /µl)	280/260	260/230	volume	Total RNA (ng)	Total RNA per 20k cells
TRIzol- Chloroform	CM 3dpi	127000	2.5	1.73	0.03	10	**25**	3.94
	cMP 3dpi	20000	1.9	2	0.03	10	**19**	19.00
	CM 7dpi	54297	7.5	1.54	0.23	10	**75**	27.63
	cMP 7dpi	19155	1.35	1.61	0.28	10	**13.5**	14.10
	cMP 3dpi	29293	9.3	1.62	0.36	10	**93**	63.5
	CM 3dpi	215178	10.2	1.86	0.5	10	**102**	9.48
	CM Un	200310	7.6	1.76	0.47	15	**114**	11.38
	cMP Un	10502	1.6	2.39	0.02	15	**24**	45.71
RNeasy Micro Kit	FC Un	300000	21.1	2.08	0.62	12	**253.2**	16.88
	fMP Un	87000	10.1	2.02	0.24	12	**121.2**	27.86
	fMP Un	92600	9.7	2.21	0.26	12	**116.4**	25.14
	CM Un	25140	5.8	2.4	0.41	12	**69.6**	55.37
	cMP 3dpi	30124	5.11	1.72	0.02	18	**91.98**	98.26
	cMP dpi	88345	5.8	1.53	0.39	18	**104.4**	16.24
	FC 3dpi	200000	3.5	1.69	0.14	18	**63**	12.96
	fMP 3dpi	49000	9.6	1.67	0.06	18	**172.8**	32.16

Table 3.1. Sample data from FACS sorted cells. Cell count varies between samples and time-point. cMP – cardiac macrophages; CM – cardiomyocytes; fMP – fin macrophages; FC – fin cells.

Consequently, the Nanodrop purity assessment method might not be reliable for estimating low RNA quantities from sorted cells. To address this issue, four samples extracted with the RNeasy Micro Kit were sent to the University of Bristol Genomics Facility for RNA ScreenTape Analysis (Fragment analyser - for results refer to ***Table 3.2***). The results of this assay indicated higher concentrations of the samples compared to Nanodrop readings, underlining its low sensitivity to small amounts of nucleic acid and inappropriate choice of quantification method for ultra-low RNA yield from zebrafish sorted cells, as suggested in other studies (Loontiens *et al.*, 2019). Additionally, the RNA quality was evaluated by generating RNA integrity number (RIN) and 28/18s ratios, which reflects degradation of RNA (lower value = more

degraded) (Schroeder *et al.*, 2006). Tested samples had RIN scores that ranged between 5.8 - 8.2 (***Table 3.2***). RIN scores of at least 7 or higher are generally considered as acceptable for successful downstream applications, however, RIN scores >8 are highly desirable to achieve the best quality, reproducible data (Schroeder *et al.*, 2006). Following this initial technique optimisation, the extraction with the RNeasy Micro Kit followed by the RNA ScreenTape Analysis was adopted for subsequent experiments.

		Nanodrop			*TapeStation assay*		
Sample	Cell count	Conc. (ng/µl)	Ratio 280/260	Ratio 260/230	Conc. (ng/µl)	RIN	Ratio 28/18s
cMP 3 dpi	25200	30.1	1.65	0.61	12.03	7.1	2.1
CM 3dpi	170328	27.9	1.67	0.56	13.3	5.8	2.2
fMP 3dpi	103528	18.7	1.89	0.9	28.3	8.4	2
FC 3dpi	400000	32.8	1.97	1.64	57.6	7	2.4

Table 3.2. Comparison of RNA quantity and quality measurements taken by Nanodrop vs RNA ScreenTape Analysis. Comparison of four samples demonstrates the variability of RNA yields across cell populations. TRIzol- Chloroform extraction resulted in low total RNA yield and purity (determined by nanodrop ratios); median = 16.55, n = 8. RNeasy Micro Kit extraction resulted in higher total RNA yields, but still low purity; median = 22.26. Yield per 20,000 cells were calculated for comparison. The Nanodrop overestimates concentration values when low yields are analysed. RNA ScreenTape Analysis is a more suitable technique due to its higher accuracy and generation of RIN (RNA integrity number) scores. RIN number assesses intact RNA, RIN > 8 should be used for qPCR. cMP – cardiac macrophages; CM – cardiomyocytes; fMP – fin macrophages; FC – fin cells.

3.1.2. RT-qPCR assay set up – purification of the samples

Although significant improvements in RNA yield were made using the described protocol it is also paramount for successful qPCR to eliminate any contamination in the RNA samples. Degradation of RNA and contamination by protein or organic compounds compromise downstream accuracy of gene quantification (Taylor *et al.*, 2010). Alternative methods of RNA purification were investigated and RNAClean XP

bead clean-up was chosen for this study. To test the recovery rate and efficiency of the RNAClean XP clean-up for low RNA concentration samples, four RNA samples extracted from sorted zebrafish cells with various RNA concentrations (measured by nanodrop) were sent to the Genomics Facility (***Table 3.3***). Preparation of samples and purification were performed as described in ***section 2.5***. Pre- and post-clean up RNA ScreenTape analyses were run to assess the concentration and quality of the samples (***Table 3.3***). Pre-purification fragment analysis again underlined incorrect nanodrop RNA quantification (***Table 3.3***). Furthermore, post-purification fragment analysis indicated a high recovery rate and increased purity of the samples compared with pre-purification results (***Table 3.3***). RIN scores (all ≥7) changed minimally after purification (***Table 3.3***), demonstrating the suitability of this method for low quantities of RNA and confirming that the Aligent ScreenTape Analysis is the most sensitive method for assessing RNA quality and quantity for downstream applications.

		Nanodrop					**Pre–Clean up TapeStation**					**Post–Clean up TapeStation**				
Sample	Cell count	Conc. (ng /µl)	280/260	260/230	volume	Total RNA (ng)	Conc. (ng /µl)	RIN	28/18s	volume	Total RNA (ng)	Conc. (ng /µl)	RIN	28/18s	volume	Total RNA (ng)
FC Un	300000	28.3	1.86	0.05	10	283	27.4	7	1.2	10	274	16.7	7	1.3	15	250.5
fMP Un	100000	3.6	1.78	0.05	11	39.6	4.6	9.1	1.5	11	50.6	3.45	9.8	1.6	15	51.75
FC 3dpi	300000	9	1.91	0.04	12	108	12.2	8.3	1.8	12	146.4	10.1	8.2	1.5	15	151.5
fMP 7dpi	100000	4.9	1.97	0.08	11	53.9	6.65	8.7	2	11	73.15	6.29	8.1	1.8	15	94.35

Table 3.3. Purification of low RNA concentrations. Four samples were sent to test the RNAClean XP bead clean up method. Nanodrop measurements were taken to adjust the concentration to the Aligent TapeStation assay detection range. Aligent TapeStation assays were performed pre- and post- RNAClean XP bead clean up to assess the suitability, effectiveness and recovery rate of the clean up protocol with low RNA quantities. RIN - RNA integrity number; FC – Fin cells; fMP – fin macrophages; Un – uninjured.

3.1.3. Amplification of low RNA quantities for robust RT-qPCR analysis

Once the extraction and purification workflow were established, samples were collected from sorted cells extracted from different time-points post-injury. Cells from heart and fins of Tg(*myl7*:GFP); Tg(*mpeg1*:mCherry) double transgenic fish were sorted for cardiac macrophages (mCherry+) and cardiomyocytes (GFP^+ cells), fin macrophages ($mCherry^+$ cells) and background (non-fluorescent) fin cells at five different time points – uninjured, 3, 7, 14 and 21 dpi as described in ***section 2.3.*** For full RNA sample concentrations and quantity please refer to ***Table 3.4.*** Overall, most samples had sufficient RNA of high purity (RIN 7.6 – 9.2) although some samples were shown to be degraded (RIN < 5.5 or undetermined).

			Nanodrop			Tape Station				
No	Sample	Total cell count	Conc. (ng/µl)	Volume	Total RNA (ng)	Conc. (ng)	Volume	RIN	28/18 s	Total RNA (ng/µl)
Un	cMP	34146	3.37	50	168.5	4.4	13	6.1	1.8	57.2
	CM	700310	6.33	50	316.5	16.1	13	5.7	1.7	209.3
	fMP	182908	7.29	50	364.5	8.51	13	8	2.1	110.63
3dpi	cMF	32614	2.0356	50	101.78	5.12	13	9.2	2	66.56
	CM	106754	3.712	50	185.6	5.05	13	8	1.9	65.65
	fMP	251234	5.46	50	273	26	13	8	1.8	338
7dpi	cMP	71200	7.906	50	395.3	7.61	11	8.5	1.8	83.71
	CM	126154	6.847	50	342.35	4.97	11	8.1	1.9	54.67
	fMP	182235	11.407	50	570.35	18.9	13	8.1	1.9	245.7
14dp..	cMP	13101	8.306	50	415.3	3.39	13	3.9	-	44.07
	CM	110427	5.638	50	281.9	5.68	13	5.5	2	73.84
	fMP	263444	9.61	50	480.5	29.3	13	7.6	-	380.9
21dp..	cMP	8775	1.768	50	88.4	2.66	11	8.7	-	29.26
	CM	84727	2.34	50	117	2.99	11	?	1.9	32.89
	fMP	16000	4.784	50	239.2	10.2	13	?	-	132.6

Table 3.4. Cell count, quantity and quality of fifteen samples from 5 different time points after pooling. Nanodrop and post-RNAClean XP clean-up Aligent TapeStation assay readings are presented. Colour coding of RIN scores highlights the quality of RNA – high (green), moderate (yellow) and poor (red). 28/18s RNA ratio was not obtained in 4 samples. cMP – cardiac macrophages; CM – cardiomyocytes; fMP – fin macrophages; FC – fin cells.

3.1.3.1. Pilot experiment for RNA amplification

Although the best protocol had been established to obtain the highest yield and quality of RNA, unfortunately, the final RNA quantities were still insufficient to test the full panel of nine cardiomyocyte/muscle genes plus two reference genes, together with two cardiac and two macrophage markers, which were chosen as cross contamination controls. To exclude contamination of cardiac macrophages with cardiomyocytes or cardiomyocyte remnants, two cardiac specific genes, which were not identified in the proteomic data were chosen: *NK2 homeobox 5* (*nkx2.5*), an important transcription factor involved in correct ventricle formation and heart function that is highly expressed in the adult myocardium (Targoff, Schell and Yelon, 2008; Targoff *et al.*, 2013; George, Colombo and Targoff, 2015) and *Myocyte specific enhancer factor 2a* (*mef2a*), which regulates cardiomyocyte differentiation and contractility and is expressed in the nucleus (Wang *et al.*, 2005; Desjardins and Naya, 2016). Conversely, to exclude contamination of background cardiomyocytes with macrophages, two alternative macrophage-specific markers used in zebrafish studies were chosen: *microfibrillar-associated protein 4* (*mfap4)* (Walton *et al.*, 2015) and *colony stimulating factor 1 receptor a* (*csf1ra*) (Gray *et al.*, 2011; Dee *et al.*, 2016) .

A literature review was undertaken to identify potential methods for maximising or amplifying small quantities of RNA. One method that showed promise was the QuantiTect Whole Transcriptome kit from Qiagen. According to the manufacturer the QuantiTect Whole Transcriptome kit produces cDNA from total RNA through whole transcriptome amplification and as little as ≥10 ng of good quality total RNA is needed to produce 10 µg or 40 µg of cDNA in a 2 hr standard or 8 hr high-yield reaction, respectively. The QuantiTect Whole Transcriptome kit is one of several amplification kits available and has been widely used in research and clinical settings when dealing with ultra-low yields of RNA (chemistry and application of RNA amplifications kits reviewed by Li and Eberwine, 2018) but mainly for RNA-Seq experiments (Shanker *et al.*, 2015). However, this kit has not been widely used for analysis of gene expression using qPCR.

Initially, therefore, a short pilot study was performed to assess whether the QuantiTect Whole Transcriptome kit would be suitable for downstream qPCR applications. Two samples with the lowest (FC Un; RIN = 7) and highest (fMP Un; RIN = 9.8) RIN value (presented in ***Table 3.3***) were used for an initial RNA amplification pilot study. These samples also provided examples of two different cell populations used in this study – fin cells (lowest RIN) and fin macrophages (highest RIN). The highest amount possible (17.5 ng) of total RNA of each sample was amplified using the 2 hr standard protocol. The amplified cDNA was assessed via qPCR at three cDNA dilutions: 1:15, 1:25 and 1:50 (recommended by the manufacturer) for *ef1α* and *loopern4* expression (reference genes). Each dilution of cDNA amplified *ef1α* in C_T < 22 cycles (***Figure 3.2A***). By comparison, *loopern4* amplification crossed the threshold at C_T <24 cycle and showed more distinct C_T values between dilutions compared to *ef1α,* but still maintaining good reproducibility between samples and their triplicates (***Figure 3.2B***). The melting curves were investigated to determine the specificity of the amplification. No secondary structures were present and both gene amplicon curves appeared at the expected temperatures (*ef1α* =80°C; *loopern4* = 73°C) and no primer dimer formation was observed in non-template controls (***Figure 3.2C-D***). This pilot study suggested that amplification of RNA using the QuantiTect Whole Transcriptome kit is a promising approach to increase cDNA yield and allow robust relative gene expression assays with multiple genes to be performed.

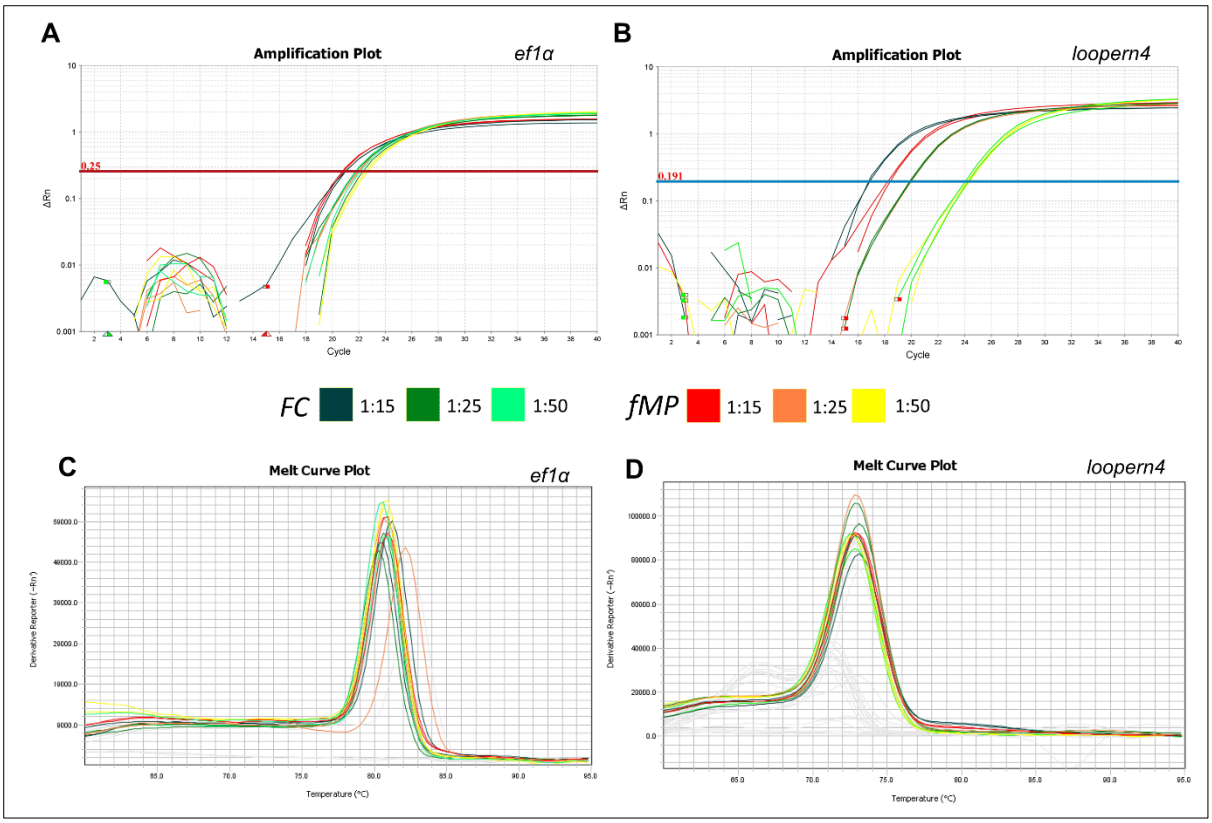

Figure 3.2. RT-qPCR amplification of cDNA samples made with the QuantiTech Whole Transcriptome kit in the initial pilot study. RNA from fin cells (FC Un; RIN = 7) and fin macrophages (fMP; RIN = 9.8) was used. Three dilutions (1:15, 1:25, 1:50) of each sample were tested for successful amplification with two reference genes – *ef1α* (A) and *loopern4* (B). Each cDNA dilution showed consistency in amplification across triplicates for both genes (A, B), except the 1:15 dilution of *loopern4* (B). Melting curve analysis confirmed specificity of the primers and excluded possible primer-dimer formation in amplified cDNA samples – *ef1α* (C) and *loopern4* (D).

3.1.3.2. Quantification of amplified cDNA with Standard Curve

Following this promising pilot study, ten samples from the injury time-course were amplified with the QuantiTect Whole Transcriptome kit using the longer 8 hr protocol to maximise yield (cMP and CM from each time point; see ***Table 3.4***) using 16.5 ng of total RNA from each sample as starting material. According to the Qiagen protocol the same amount of good quality starting RNA should yield the same concentration of cDNA although, as the RIN of purified RNA varied between the samples, the efficiency of amplification might differ somewhat. Therefore, samples could require further quantification in order to identify the optimal concentration for use in

downstream qPCR, however, quantification of resultant cDNA yield remains difficult. To address this problem, firstly, samples were quantified via a *loopern4* standard curve. Five dilutions of the 3 and 14 dpi amplified cDNA samples (1:150, 1:200, 1:250, 1:300, 1:350) were used to determine the best concentration and assess the reproducibility of the amplification across samples. However, this standard curve analysis demonstrated that the dilution series did not amplify as expected, with no clear separation in cycle number for each dilution, making it difficult to determine the correct concentration *(samples of cDNA from 3 dpi cardiomyocytes presented as an example* (***Figure 3.3A***)). Some variation between dilutions of different samples might be expected but the Cycle threshold (C_T) varied massively *(1:200 samples from 3 and 14 dpi as an example* (***Figure 3.3B***)). This deviation between sample concentration would make quantification of all samples (10 samples in 5 different dilutions) via this standard curve method time and consumable consuming. Therefore, the rest of the samples were matched by C_T value with the 3 and 14 dpi dilution series. Consequently, a 1:350 dilution for CM and cMP of Un, 3 and 21 dpi and a 1:250 dilution for 7 and 14 dpi were used for Relative Quantification (RQ) via RT-qPCR.

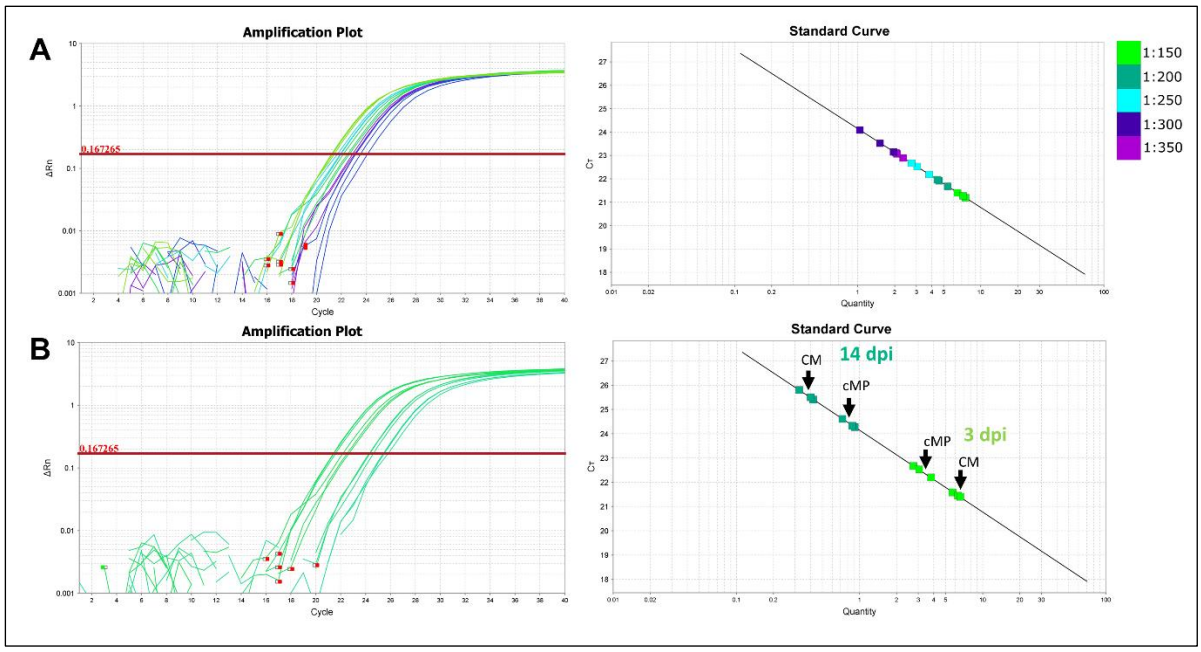

Figure 3.3. RT – qPCR of amplified cDNA with loopern4 for standard curve quantification. Five different dilutions of amplified cDNA from cardiomyocytes and cardiac macrophages from 3 dpi and 14 dpi samples were run (1:150, 1:200, 1: 250, 1:300, 1:350).

Amplification of cDNA from 3 dpi cardiomyocytes with loopern4 (A). Variation of C_T of the same cDNA concentration between samples and between replicates was observed. Samples from 3 and 14 dpi at 1:200 dilution provided as an example (B).

3.1.3.3. Relative gene expression using amplified cDNA

Initially, relative quantification (RQ) of *myl7* was performed with the chosen cDNA dilutions of cardiomyocytes and cardiac macrophages using two reference genes. Unfortunately, the chosen dilutions, which revealed expression of *loopern4* at between 19-29 CT cycle, only amplified ***ef1α*** at very late CT cycles (33-36) and no amplification of *myl7* was observed ***(Figure 3.4A***). Analysis of *nkx2.5* and ***ef1α*** provided similar results with few replicates amplifying the cardiomyocyte marker *nkx2.5* and continued ***ef1α*** expression only at very late CT cycles (***Figure 3.4B***). Furthermore, RT-PCR analysis of *myl7*, ***ef1α*** and *loopern4* expression in additional dilutions of cDNA (up to 1:20) failed to reveal better results with no amplification of *myl7* in any samples and negligible expression of ***ef1α*** (***Figure 3.4C***). Collectively, these results suggested unsuccessful amplification of cDNA from sorted cell samples, either due to RNA degradation or issues with kit efficiency.

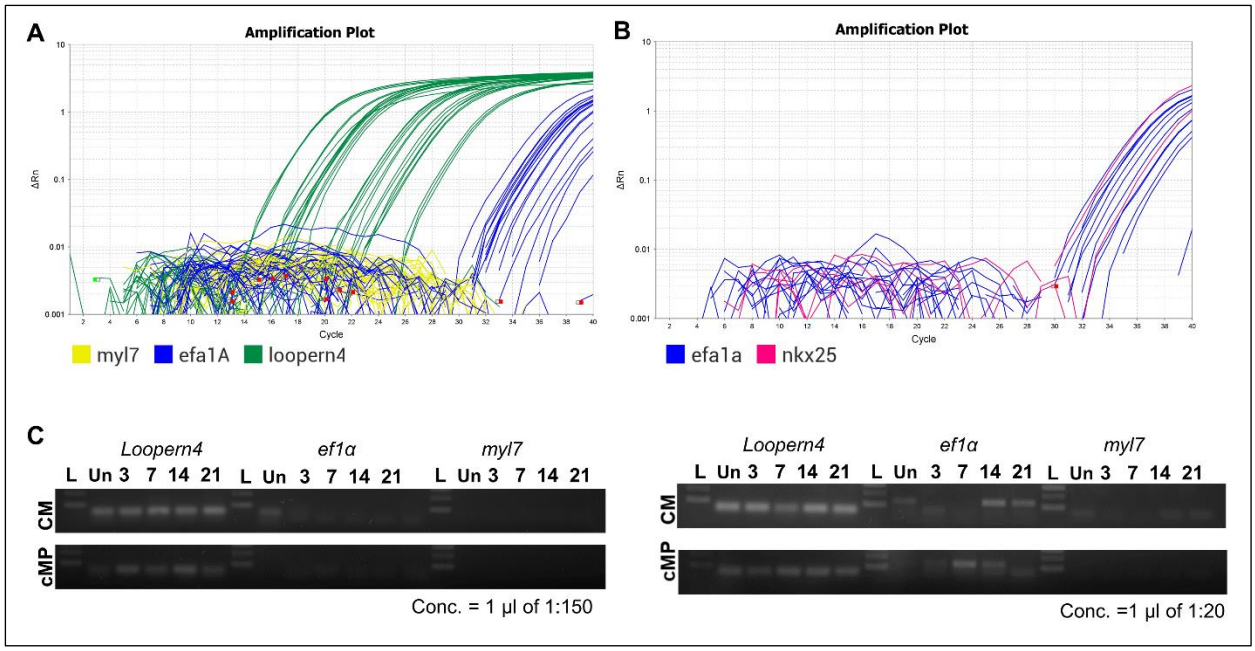

Figure 3.4. Relative quantification (RQ) was performed with amplified cDNA of cardiomyocytes and cardiac macrophages. (A) The amplification plot reveals vast differences in amplification of ***ef1α*** and *loopern4*, which was not observed in the pilot study (*section 3.1.3.1.).* A complete lack of *myl7* expression was observed in all samples (A). The amplification plot for ***ef1α*** and *nkx2.5* reveals similar results (B). (C) RT-PCR analysis also reveals detectable levels of *loopern4*, variable ***ef1α*** and a lack of *myl7* expression in amplified samples. Representative gel electrophoresis results with the lowest (1:150) and highest (1:20) concentrations tested (C).

To address whether the issue lay with the kit or the RNA integrity, all samples were purified further using a QIAquick PCR Purification Kit (28106), designed to purify single- or double-stranded DNA fragments from PCR and other enzymatic reactions, accordingly to the manufacturer's instructions. Sample concentrations were also measured using a Qubit dsDNA HS Assay Kit (Q32851) on an Invitrogen Qubit 3.0 Fluorometer (Thermo Fisher Scientific). In addition, a new 2h amplification of the remaining RNA was performed as in the pilot study and as described in ***section 2.7***. A series of RT-PCR/qPCR analyses were performed with both sample sets (amplified cDNA post-purification and newly amplified cDNA), unfortunately, producing the same inconsistent results. Finally, leftover samples from the 7 dpi time-point were reverse transcribed directly using the Maxima First Strand Kit as used in the first successful qPCR (***section 2.6***). This analysis suggested that the RNA was not degraded as amplification of *ef1α*, *mb* and *myl7* was present at the

expected Ct cycles. These results, further underline the malfunctions of the QuantiTect Whole Transcriptome kit for reproducible RNA amplification and a lack of reliability of resultant cDNA products for use in qPCR, making it unusable for these applications. Due to these technical limitations in amplifying low yield RNA from sorted cells, an alternative strategy to verify cardiomyocyte gene expression in cardiac macrophages was sought.

3.2. RT-qPCR analysis of the expression of five cardiac genes in uninjured and injured zebrafish.

3.2.1. Introduction

Despite limitations in RNA quantities obtained from sorted cells described above, enough material of a suitable quality was obtained for downstream RT-qPCR analysis on a limited number of targets. A panel of five genes of interest (GOI) was selected for RT-qPCR analysis. The chosen genes encode for the proteins which were found to have the highest expression in the proteomic data – Myoglobin (*mb*), Cardiac Regulatory and Essential Light Chain (*myl7* and *cmlc1*), Tropomyosin (*tpm4a*) and Troponin T (*tnnt2a)* (***Figure 1.6B***). In this experiment, the panel of five genes was assessed using cDNA obtained from sorted cells of uninjured and 3 dpi Tg(*mpeg1:mCherry)* adult fish (the only post injury time-point with the suitable RNA quality and quantity). Macrophages (mCherry+) and non-fluorescent cells were sorted from hearts and fins (***Figure 3.5***). The maximum cDNA concentration was used for each time-point; 4 ng/µl from uninjured (Un) fish and 8 ng/µl from samples at 3 dpi. The cycle threshold (C_T) of the target gene in each sample was normalised with the C_T of a reference gene (***ef1α)*** (ΔC_T), then calibrated against the non-fluorescent background cells expression of that gene ($\Delta\Delta C_T$). Furthermore, relative quantification (RQ) according to the Pffafl correlation equation (RQ = E target gene ^ ΔC_T target gene / E ref ^ ΔC_T ref (Pfaffl, 2001)) was calculated.

3.2.3. RT-qPCR confirms the presence of five cardiac genes in cardiac macrophages from uninjured and injured fish

This study confirmed gene expression of all five GOI in cardiac macrophages in healthy (uninjured) (***Figure 3.5A***) and injured fish (***Figure 3.5C***). Amplification of the genes in the samples is presented as the C_T value (***Figure 3.5A-D***). The C_T decreases proportionally to the transcript copy of the targeted gene in each reaction, thus the greater the transcript amount the earlier the C_T value is reached. Samples with C_T <30 are consider as strong positive, C_T = 30 – 35 weak positive and C_T >35 negative. For future fold change analysis samples with C_T >35 Ct were excluded (located above threshold (***Figure 3.5A-D***)). As expected, the reference gene *ef1α* amplified at an early (16 – 21) C_T in all samples (***Figure 3.5A-D***).

In background cells derived from uninjured ventricles, the most abundant gene was *mb* (C_T = 21), consistent with previous findings (Wu *et al.*, 2016), and the least abundant was *tnnt2a* (C_T = 33) (***Figure 3.5A***). Similarly, in cardiac macrophages the most abundant gene was also *mb* (C_T = 25), then *myl7* and *cmlc1* (C_T = 26), *tnnt2a* (C_T = 28), and the least abundant was *tpm4a* (C_T = 29) (***Figure 3.5A***). Similarly to background cells derived from uninjured hearts, 3 dpi ventricles exhibited the highest expression of *mb* (C_T = 23) and the lowest of *tnnt2a* (C_T = 26), but higher expression of *tpm4a* (C_T = 25) (***Figure 3.5C***). Cardiac macrophages derived from hearts at 3 dpi maintained a similar pattern of expression as the background cells, but their expression is lower (3 – 5 < C_T) (***Figure 3.5C***).

Surprisingly, some genes were also expressed in fin cells and fin macrophages. In non-fluorescent cells derived from fins from the same uninjured fish, robust expression of *tpm4a* (C_T = 25) and *mb* (C_T = 29) and weak expression of *cmlc1* and *tnnt2a* ($C_T \geq 31$) was observed (***Figure 3.5B***). Similarly, in fin macrophages robust expression of *tpm4a* (C_T = 28) and weak expression of *mb* and *tnnt2a* ($C_T \geq 32$) was observed (***Figure 3.5B***). In fins from the fish at 3 days post cardiac cryoinjury, similar strong expression of *tpm4a* and *mb* was observed (***Figure 3.5D***). The robust expression of the *tpm4a* isoform was surprising as this has previously been reported to be exclusively expressed in the zebrafish heart (Zhao *et al.*, 2008). No or only very weak expression of *myl7* and *cmlc1* were observed in fin cells pre- or post-injury (***Figure 3.5B,D***).

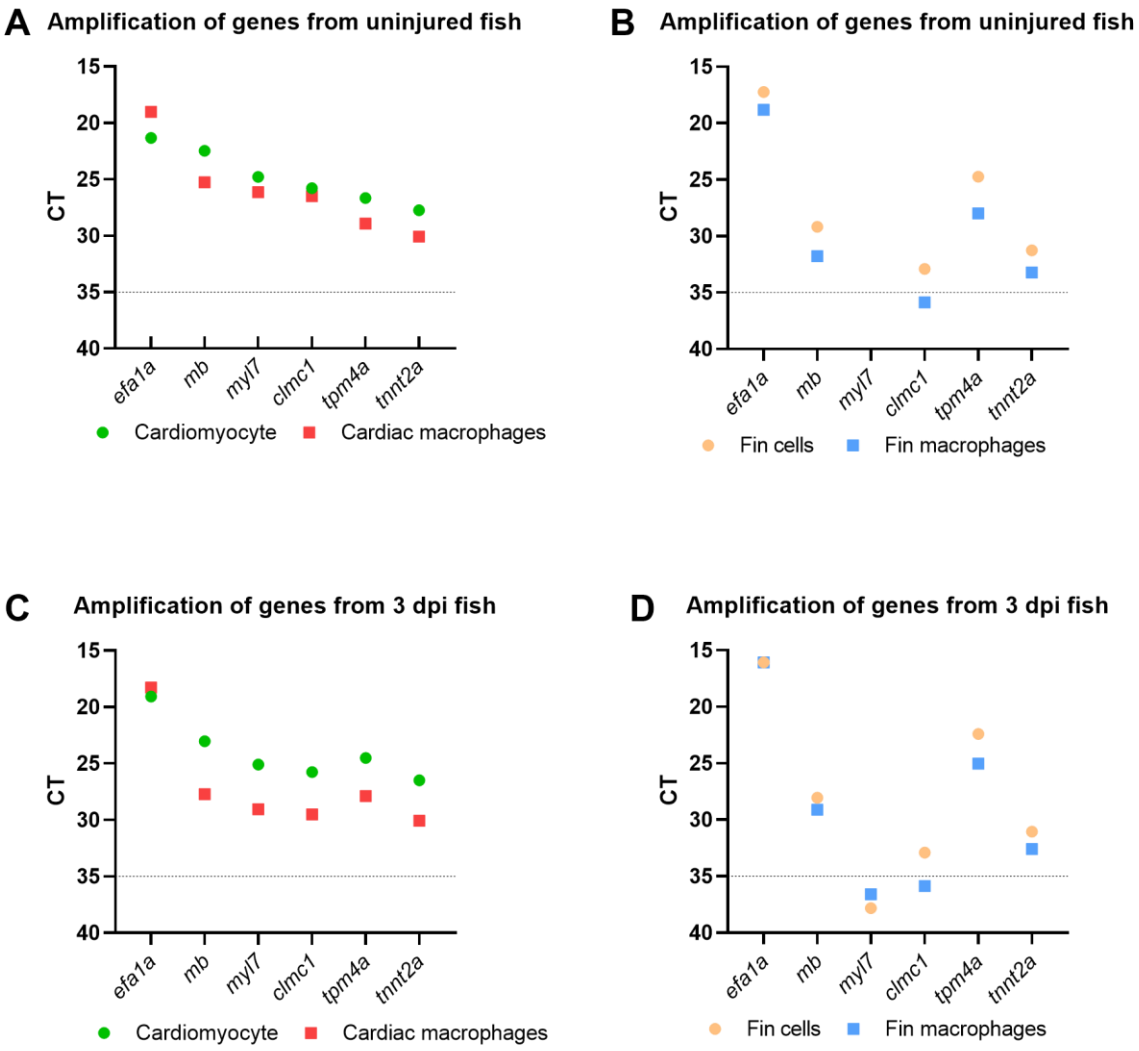

Figure 3.5. Confirmation of gene expression in uninjured and injured tissues. Cardiac gene expression was determined using RT-qPCR. (A-D) Five genes with the highest expression observed in the proteomic data were selected for analysis (*mb*, *myl7*, *cmlc1*, *tpm4a* and *tnnt2a*) along with a reference gene (***ef1α***) from uninjured (Un) (A - B) and injured fish (C - E). C_T values for each gene in background cells (green) and cardiac macrophages (red) of uninjured (A) and 3 dpi fish (C). C_T values for each gene in background fin cells (orange) and fin macrophages (blue) from uninjured (B) and 3 dpi (D) fish. Samples with C_T >35 were excluded from subsequent experiments (A - D).

3.2.4. Relative quantification of gene expression in uninjured and injured tissues.

Relative quantification (RQ) was used to determine the change in gene expression after injury. The RQ values obtained from 3 dpi samples compared to unwounded were transformed to log2 scale and reveal increased and decreased expression for each gene after injury (***Figure 3.6***). This analysis demonstrates decreased expression of all cardiac genes in cardiac background cells after injury (***Figure 3.6***). Similarly, a decrease of the same genes in cardiac macrophages was observed after injury although *tpm4a* was slightly increased (***Figure 3.6***). Conversely, a slight increase in expression of *tpm4a* and *tnnt2a* in background fin cells was observed after injury to the heart, whereas only *tpm4a* was slightly increased in fin macrophages (***Figure 3.6***).

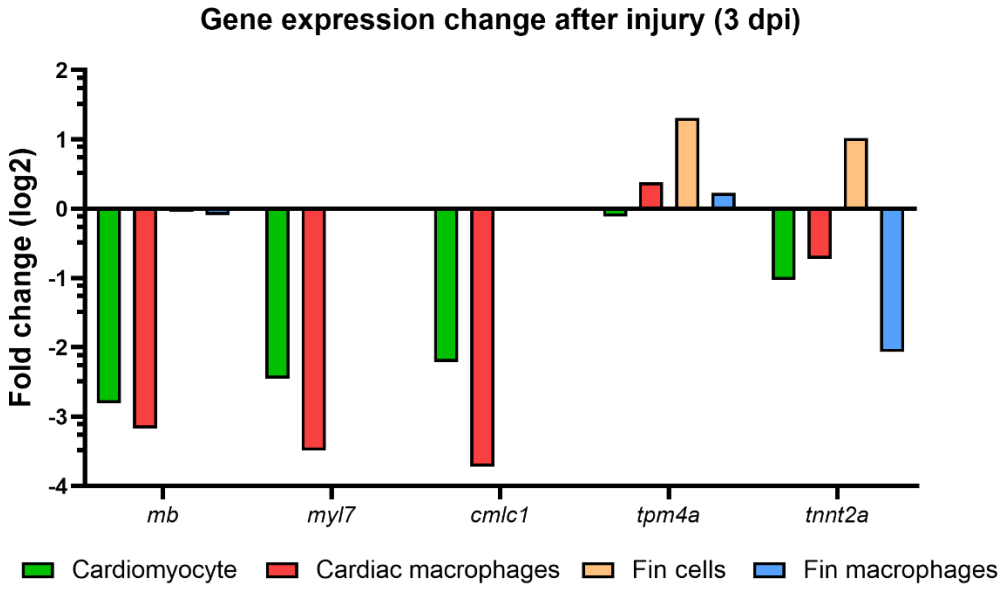

Figure 3.6. Relative quantification (RQ) of five genes after cardiac injury. Downregulation of *mb, myl7, cmlc1* and *tnnt2a* in cardiac background cells and macrophages and upregulation of *tpm4a* in cardiac macrophages after injury was observed. Also, upregulation of *tpm4a* and *tnnt2a* in fin cells was observed. Fold change was transformed to a logarithmic scale (log2) to present up- and down- regulation of genes after injury**.**

3.2.5. Confirmation of cardiac specific gene expression via RT-PCR.

To confirm gene expression across additional time-points post injury the successfully extracted RNA from macrophages (mCherry+) and cardiomyocytes (GFP+) sorted from ventricles of Tg(*myl7*:GFP); Tg(*mpeg1*:mCherry) double transgenic fish outlined in ***section 3***, was used to test the presence of selected genes via RT-PCR. For this experiment samples of 20 ng/µl cDNA from sorted cardiomyocytes and cardiac macrophages were used (***Figure 3.7A***). RT-PCR confirmed the presence of three cardiac specific genes at 3 dpi in cardiac macrophages (cMP) and highlights the significantly lower expression than in cardiomyocytes (CM), where expression was expected to be high (***Figure 3.7B***). *cmlc1* gene expression was not observed in cMP but was in CM. The reference gene ***ef1α*** was included as a positive control to confirm successful RNA extraction and cDNA synthesis (***Figure 3.7B***). RT-PCR was then performed using 5 ng/ul of cDNA purified with RNAClean XP beads confirming expression of *myl7* and *cmlc1* at 7 dpi and suggesting lower expression of *cmlc1* than *myl7* (***Figure 3.7C***), similar to that observed at 3 dpi (***Figure 3.7B***). Additionally, expression of *myl7* and *cmlc1* was assessed at different time points (Un, 3, 14, 21 dpi) in CM and cMP, where RNA quantities allowed (***Figure 3.7D, E***). Expression of ***ef1α*** was observed in all samples tested but only *myl7* was detected in CM and cMP at 14 dpi (***Figure 3.7D, E***). The reduced band strength in cMP compared to CM suggests lower expression of *myl7* in cardiac macrophages, as expected (***Figure 3.7E***). Although the amount of starting material likely limited the amplification in other samples, this experiment highlights the use of RT-PCR to assess gene expression in ultra-low transcript samples and indicates that the highest expression of *myl7* in cardiac macrophages was likely observed at 7 and 14 dpi.

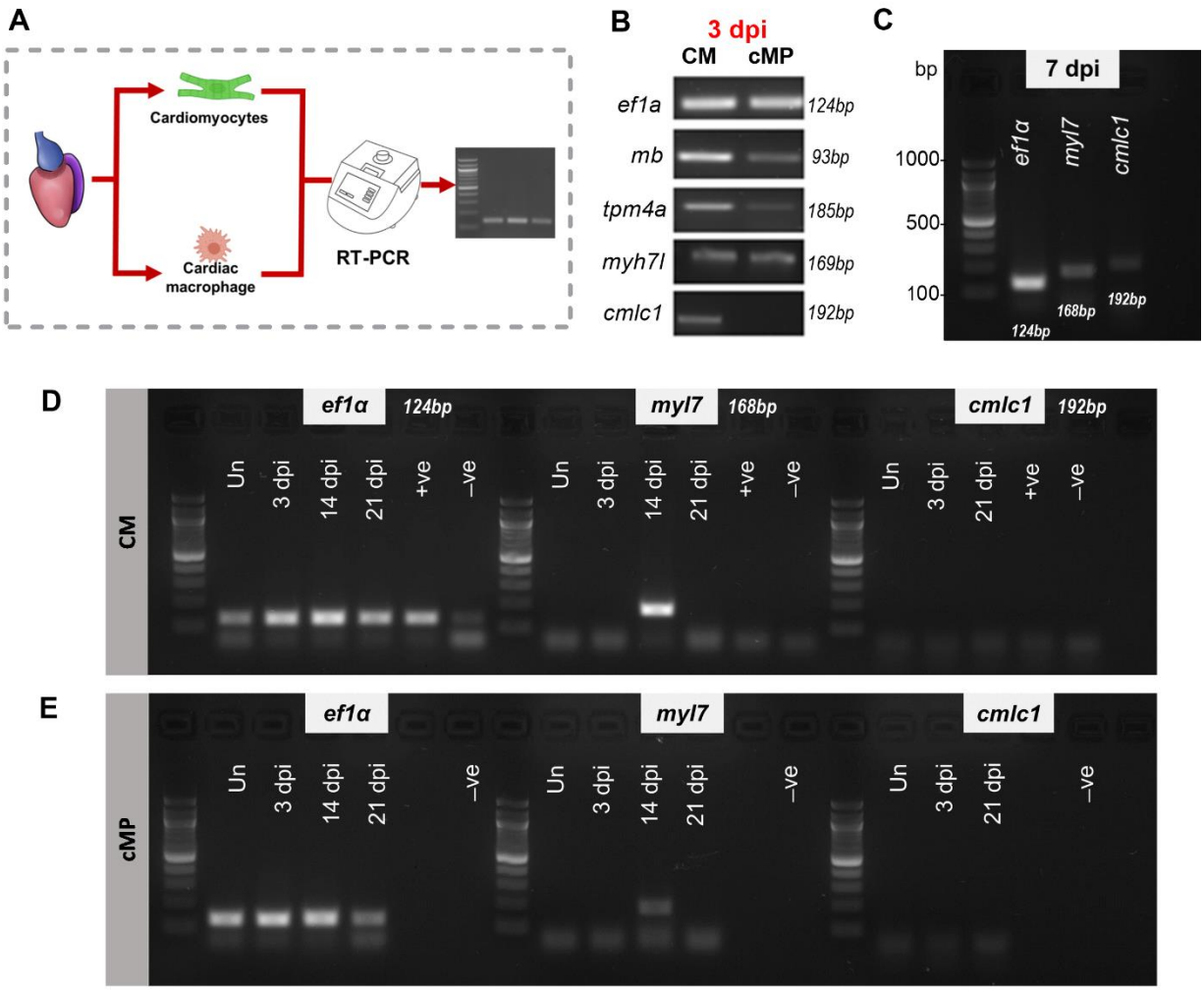

Figure 3.7. Confirmation of cardiac gene expression via RT-PCR. (A) Schematic representation of workflow. (B) RT-PCR performed with 20 ng/ul of RNA extracted with the Micro RNeasy kit confirmed expression of *mb, tpm4a* and *myh7l* in cardiac macrophages at 3 dpi. Lower expression of cardiac genes is observed in sorted cardiac macrophages (cMP) compared to cardiomyocytes (CM). (C) RT-PCR using 5 ng/ul of RNA purified and quantified as described in *sections 3.1.1- 3.1.2* confirms expression of *myl7* and *cmlc1* in cardiac macrophages at 7 dpi. (D, E) RT-PCR or *myl7* and *cmlc1* expression across a time-course after injury confirms expression of *myl7* in cardiac macrophages at 14 dpi (E) at a lower level than *myl7* expression in cardiomyocytes (D). (B-E) Samples were run along with reference gene *ef1a* and 100 bp DNA ladder NEB (N3231S). Positive controls contain cDNA derived from whole hearts, whereas negative controls contain water instead of cDNA template.

Chapter 4. FACS analysis of Tg*(myl7:GFP)*; Tg(*mpeg1:mCherry)* zebrafish reveals *myl7* expressing cardiac macrophages in the adult heart.

4.1. Background

The benefits of genome plasticity and transparency at larval stages has led to the production of many transgenic zebrafish lines which can be used to characterise cellular responses including the immune response. There are two commonly used markers of macrophages in zebrafish, macrophage expressed 1, tandem duplicate 1 (*mpeg1.1)* (Ellett *et al.*, 2011) and colony-stimulating factor 1 receptor (*csf1ra)* (Gray *et al.*, 2011). Further sub-classification of macrophages by expression of the cytokine tumour necrosis factor alpha (*tnfα*), which is primarily synthesised in phagocytes, has been used to differentiate pro-inflammatory (*tnfα*+) and anti-inflammatory (*tnf*α-) populations within zebrafish (Parameswaran and Patial, 2010; Marjoram *et al.*, 2015). Recently, the Richardson lab has shown roles for both populations of macrophages after cardiac injury using Tg(*mpeg1.1:mCherry*); TgBAC(*tnfα:GFP*) double transgenic fish, revealing their functions in scar deposition (*tnfα*+) and subsequent scar removal (*tnfα*-) during regeneration (Bevan *et al.*, 2020).

In the heart, myosin light chain 7 *(myl7,* previously known as *cmlc2)*, is widely utilised as a cardiomyocyte marker in multiple cardiac developmental and functional studies (Geoffrey Burns *et al.*, 2005; de Pater *et al.*, 2009; González-Rosa *et al.*, 2011; Schnabel *et al.*, 2011; Sedletcaia and Evans, 2011; Wu *et al.*, 2016; Scott *et al.*, 2021). For the studies outlined here, Tg(*myl7:GFP*); Tg(*mpeg1.1:mCherry*) double transgenic fish were generated to allow flow activated cell sorting (FACS) of macrophages (mCherry+) and cardiomyocytes (GFP+) and determine if double positive (mCherry+; GFP+) cells could be identified.

Flow cytometry and FACS are widely used optical and fluorescence instrumentations which allow for cell counting and phenotype characterisation of single cells or particles passed through a fluid stream. Both methods are based on the principle of scattered and emitted fluorescent light from the moving “events” (cells or particles)

as they pass through a beam of light. Scattered light detected by forward scatter (FSC) is directly proportional to the size of the particle, whereas light detected by side scatter detectors (SSC) reveals the granularity and complexity of the event (Adan *et al.*, 2017). Similarly, the fluorescence emission proportionally reflects the signal (fluorescently tagged antibody or dye or endogenous fluorescence) used to label cellular components (Büscher, 2019). The intensity of the scattering and emission is converted to voltage and recorded as series of electric pulses (peaks). Combined data from all detectors is represented on histograms or dot plots (Adan *et al.*, 2017). While the same data can be collected by both flow cytometry and FACS, FACS has the capacity to purify and collect different cell populations from a heterogenous sample, based on electromagnetic separation. This allows the separation of cells based on intracellular dyes and incorporated fluorescence reporter proteins (FRP) (Basu *et al.*, 2010; Büscher, 2019). FRPs such as GFP or mCherry are extensively used in many zebrafish transgenic lines where they are instrumental in *in vivo* studies. However, the benefits of FACS, including fluorescence sensitivity and analytical prospects, appear underutilised in zebrafish studies where they are often limited to progenitor and immune cell phenotypic characterisation. In this study, the usefulness of FACS was highlighted as a valuable technique due to its high sensitivity for fluorescent cell markers.

4.2. FACS strategy for analysis of Tg(*myl7:GFP*); Tg(*mpeg1.1:mCherry*) cardiac tissue

To successfully assess single and potentially double cell populations from Tg(*myl7:GFP*); Tg(*mpeg1.1:mCherry*) transgenic fish using FACS, hearts were first collected and dissociated according to ***section 2.3***. Protocols for sorting cardiac macrophages were available in the lab, however cardiomyocytes had not been sorted before, so initial experiments were performed to determine the correct gates to collect the required cell populations (***Figure 4.1***). A three-step gating strategy was used to assess dissociated adult zebrafish hearts (***Figure 4.1***).

Sorting data from non-fluorescent wild type (WT) fish hearts (provided by Bethany Moyse) was used to set up a gating hierarchy in FlowJo (***Figure 4.1A***). First, the FSC-H (x-axis) and SSC (y-axis) of all cell events were assessed to exclude cells with extreme size and granularity. Singlet events were then determined using the

FSC-W (Trigger Pulse Width), revealing the duration of the event pulse, which is longer when two cells pass together and cannot be differentiated, allowing doublets to be excluded. Dead cells could then be excluded from the selected singlets via staining with DRAQ7, which only labels nuclei of dead and permeabilised cells. In the final step, live cells were assessed for mCherry and GFP expression to determine autofluorescent cells *(Step 1,* ***Figure 4.1A***).

Step 2: Gating cell events of single transgenic fish hearts: Before fluorescence specific gates were established, data from both single transgenic lines were analysed according to 'Step 1' to reveal populations of live singlets. Singlets from Tg(*myl7:GFP*) fish expressed high levels of GFP (cardiomyocytes) and no mCherry and can be divided into GFP high (green gate) and GFP low (blue gate) (***Figure 4.1B***). A decline in GFP expression level can be a characteristic of dying cardiomyocytes (Schnabel *et al.*, 2011). However, it has also been reported that GFP low cardiomyocytes are present in the border zone of Tg(*myl7:GFP)* fish at 7 dpi and display signs of dedifferentiation (as described in more details in cardiomyocytes ***section 1.5.2***). Therefore, GFP low cells were eliminated from further analysis to avoid possible contamination from both possibilities. The same approach was taken to establish gates for cardiac macrophages from Tg(*mpeg1.1:mCherry*) fish revealing high mCherry and no GFP expression (***Figure 4.1B***). Following the establishment of the correct gating strategy, this was applied to analyse fluorescent cardiac cell populations from Tg(*myl7:GFP*); Tg(*mpeg1.1:mCherry*) double transgenic fish *(****Figure 4.1C****).*

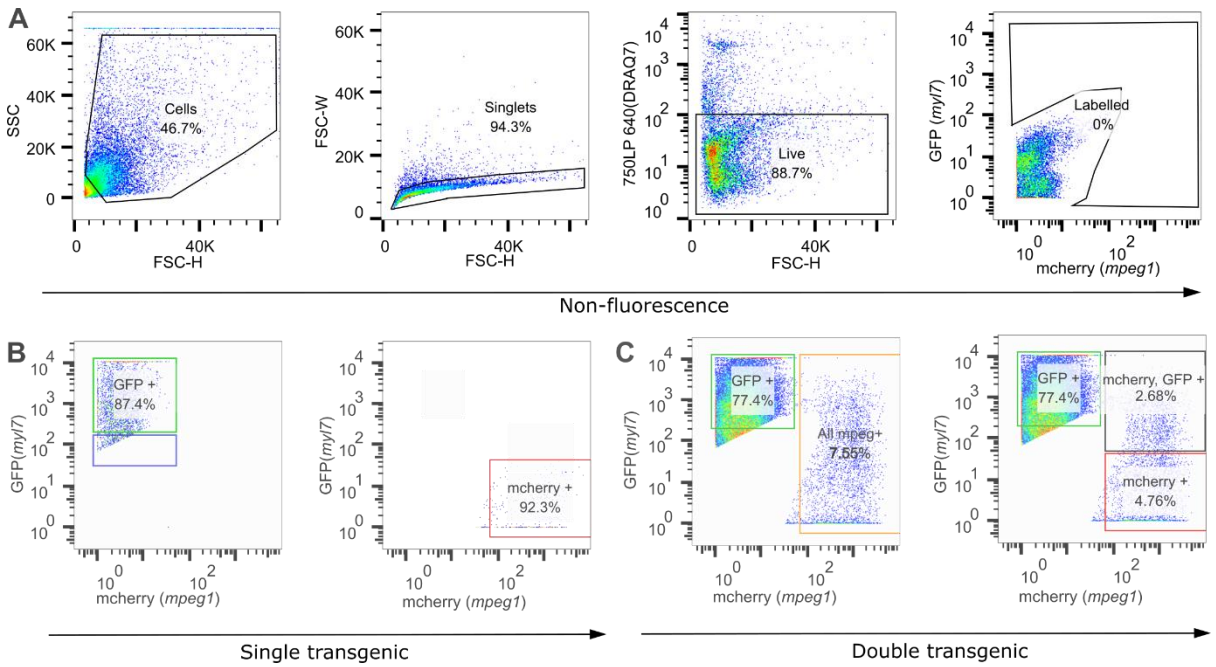

Figure 4.1. Three step gating strategy for analysis of Tg(*myl7:GFP*); Tg(*mpeg1.1:mCherry*) fish. Step 1. Non-fluorescent WT fish were used to establish live singlet cells and background autofluorescence (A). Step 2. This hierarchy was applied and further gates were established for single transgenic Tg(*myl7:GFP*) and Tg(*mpeg1.1:mCherry*) fish. GFP high (green gate) and mCherry (red gate) were established based on population distribution on a GFP versus mCherry fluorescence log scale. The GFP low (blue gate) population was excluded for final analysis. Step 3: This whole established protocol was used to analyse Tg(*myl7:GFP*); Tg(*mpeg1.1:mCherry*) double transgenic fish (C). The distribution of the whole mCherry+ population (C- left plot) and the double positive (mCherry, GFP+) and single positive (mCherry+) (C – right plot) populations are presented. FSC-H – Forward Scatter Height; FSC-W Forward Scatter width.

4.3. FACS reveals a macrophage subset expressing both fluorescent reporters

To investigate a potential double positive population of macrophages (mCherry, GFP+) compared to the total population of macrophages (mCherry+) and cardiomyocytes (GFP+), sorts of pooled heart samples from Tg(*myl7:GFP*); Tg(*mpeg1.1:mCherry*) double transgenic fish were analysed across five different time points – uninjured, 3, 7, 14 and 21 dpi, according to the gating strategy described above (***Figure 4.2A***).

As well as relative numbers, additional cell characteristics including relative size and granularity were determined (***Figure 4.2B***). In this study mCherry+ cardiac macrophages from Tg(*myl7:GFP*); Tg(*mpeg1.1:mCherry*) fish exhibit the expected FACS profile as previously reported for total *mpeg1.1*+ cells at different time points post injury (Moyse and Richardson, 2020) (***Figure 4.2C***). *mpeg1.1*+ macrophages have not previously been described at 21 dpi and, interestingly, this data shows that the granularity of mCherry+ cells increases at this time point (***Figure 4.2C***).

Although Tg*(myl7:GFP)* is commonly used to label zebrafish cardiomyocytes in functional and morphological assessments of the heart and occasionally used for high purity FACS separation for gene and transcriptional studies (Patra *et al.*, 2017; Honkoop *et al.*, 2019), a *myl7:GFP*+ cardiomyocyte FACS profile was not available. This study shows the size and high granularity (complexity) of *myl7:GFP*+ cardiomyocytes in uninjured hearts and at 4 different time points post injury (***Figure 4.2D***). Indeed, the granularity of cardiomyocytes increased further at 3 dpi and 14 dpi (***Figure 4.2D***).

An mCherry+, GFP+ double positive cell population was also identified during FACS, accounting for 0.2 – 2.1% of the total cell count depending on the time point (***Figure 4.2A***). Size (FSC) and complexity (SSC) of mCherry+, GFP+ cells is comparable to mCherry+ macrophages, while distinct from GFP+ cardiomyocytes (***Figure 4.2C-E***). This suggests that mCherry+, GFP+ cells are macrophages expressing *myl7* (***Figure 4.2B-E***). Both macrophage populations display similar granularity at each time point (***Figure 4.2C,E***). An exception from this trend can be seen at 21 dpi, where mCherry+, GFP+ cells appear less granular than single mCherry+ macrophages (***Figure 4.2C,E***). In general, an increase in granularity of macrophages (increase in SSC scatter) is associated with a change in the number of organelles, reflecting their activation and differentiation state (Daigneault *et al.*, 2010). The differentiation state describes the transition from monocyte to tissue macrophages and is also linked to intracellular changes and phagocytosis, leading to an increase in macrophage size as shown in human macrophages (Daigneault *et al.*, 2010).

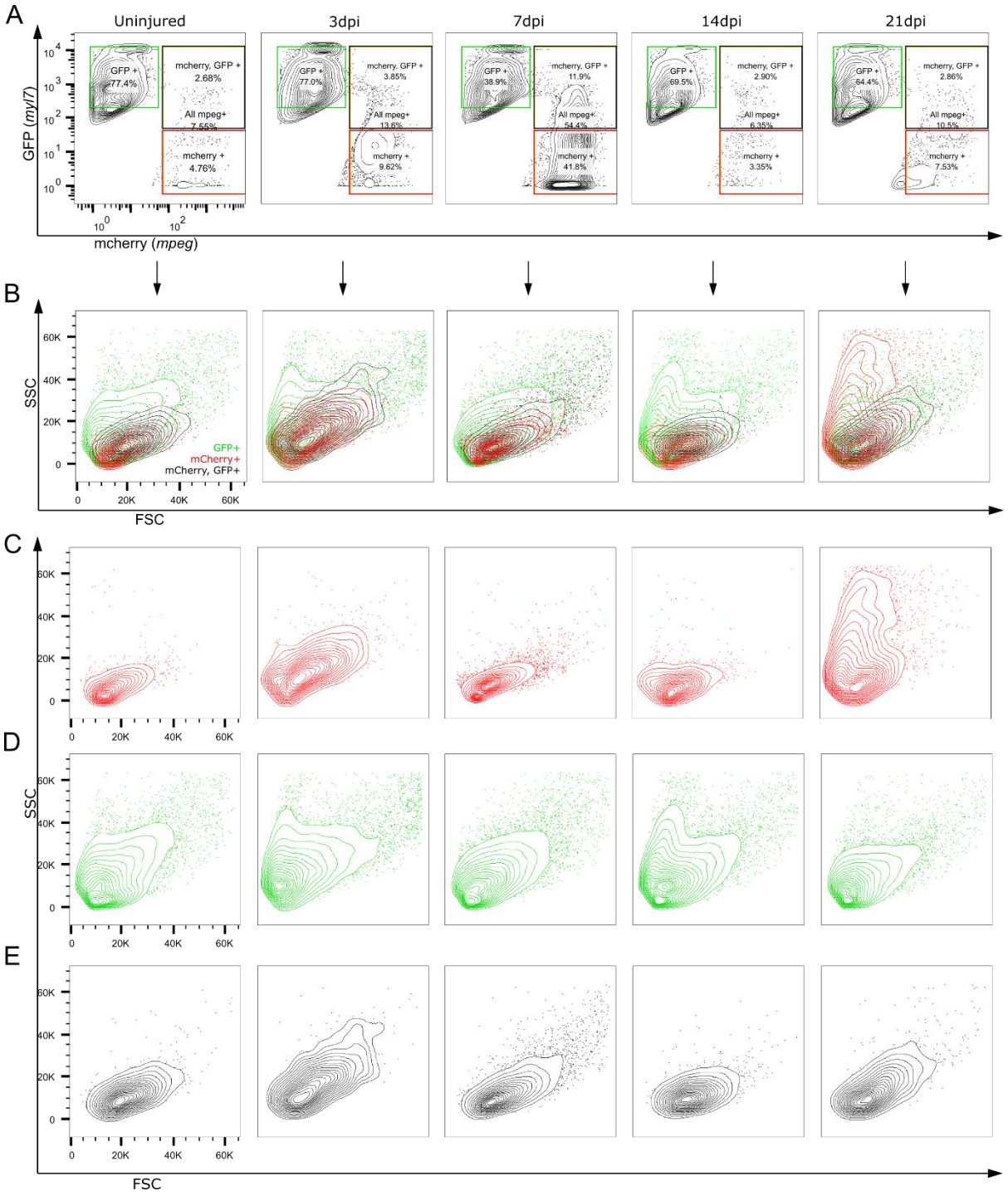

Figure 4.2. FACS analysis of ventricular tissue of Tg(*myl7:GFP*); Tg(*mpeg1.1:mCherry*) prior to and following cryoinjury.Representative plots and relative percentage of fluorescently labelled cells isolated from Tg(*myl7:GFP*); Tg(*mpeg1.1:mCherry*) transgenic fish at the timepoints indicated (A). Corresponding forward and side scatter (F-/SSC) profiles of isolated populations (B): all populations together; (C-E): each population in isolation; mCherry+ macrophages (C), GFP+ cardiomyocytes (D) and mCherry+, GFP+ (E).

4.4. Response of fluorescently labelled cells after injury

4.4.1. FACS reveals changes to cardiomyocytes after injury

As previously discussed, FACS analysis of zebrafish cardiomyocytes has not been described. In this study, large numbers of cardiomyocytes were obtained from Tg*(myl7:GFP)*; Tg(*mpeg1.1:mCherry*) zebrafish hearts (***Figure 4.3A***). For each time-point, 5 – 6 zebrafish hearts were collected. This number was previously determined to be minimal numbers to gather sufficient RNA material from cardiac macrophages. To maintain reproducibility between the samples, fish from the same incross were subjected to the cryoinjury and used as control uninjured fish. Furthermore, the cryoinjury procedure was performed by the same researcher to minimise variability of injury size between the fish. It has been shown via imaging of the heart that cryoinjury results in massive cardiomyocyte death (Chablais *et al.*, 2011; González-Rosa *et al.*, 2011; Schnabel *et al.*, 2011). After injury of Tg*(myl7:GFP)* zebrafish hearts, GFP signal is reduced as early as 1 dpi and at 3 and 7 dpi the wounded area is entirely devoid of GFP signal (Schnabel *et al.*, 2011). The signal starts to recover at the border zone of the injury at these timepoints coinciding with cardiomyocyte proliferation (Schnabel *et al.*, 2011). In line with this previous study, the time course of GFP+ cells after injury indicates massive decline of cardiomyocytes between 3 - 7 dpi before a modest increase at 14 dpi (***Figure 4.3A***). However, cardiomyocytes numbers remain low at 21 dpi when an increase in numbers back to uninjured levels would have been expected (González-Rosa *et al.*, 2011; Schnabel *et al.*, 2011; Bednarek *et al.*, 2015; Bertozzi *et al.*, 2021). This could be due to the sensitivity of cardiomyocytes to a long tissue dissociation protocol and the FACS process, leading to variability in the live cell count.

4.4.2. The mCherry+, GFP+ subset of macrophage contributes to the injury response

Analysis of FACs sorted hearts from Tg*(myl7:GFP)*; Tg(*mpeg1.1:mCherry*) fish also revealed single mCherry+ macrophages which responded to injury in a similar pattern to previous observations by the lab (Bevan *et al.*, 2020; Moyse and Richardson, 2020) (***Figure 4.3B***). *mpeg1*+ macrophages accumulate quickly at the site of the injury at 3 and 7 dpi and their numbers are reduced at 14 dpi (***Figure***

4.3B), representing 2.2% of total cell counts at 3 dpi, 7.3% at 7 dpi and as little as 0.9 % at 14 dpi (***Figure 4.3D***). At all time-points analysed a double positive population (mCherry+, GFP+) was also identified suggesting *myl7* (GFP+) expression in cardiac macrophages of adult zebrafish hearts pre- and post-injury (***Figure 4.2B***). FACS reveals that the mCherry+, GFP+ double positive subset of macrophages accounts for 19.8% - 46.6% of the total mCherry+ population, depending on the time point (***Figure 4.3C***). The highest percentages of GFP+ macrophages were observed in Un, 3 and 14 dpi (36%, 39.9% and 46.6%, respectively) and lower at 7 and 21 dpi (22.2% and 19.8%, respectively) (***Figure 4.3C***). Interestingly, mCherry+, GFP+ macrophages respond to injury in a similar pattern as mCherry+ macrophages, although the massive peak at 7 dpi is not observed (***Figure 4.3B***).

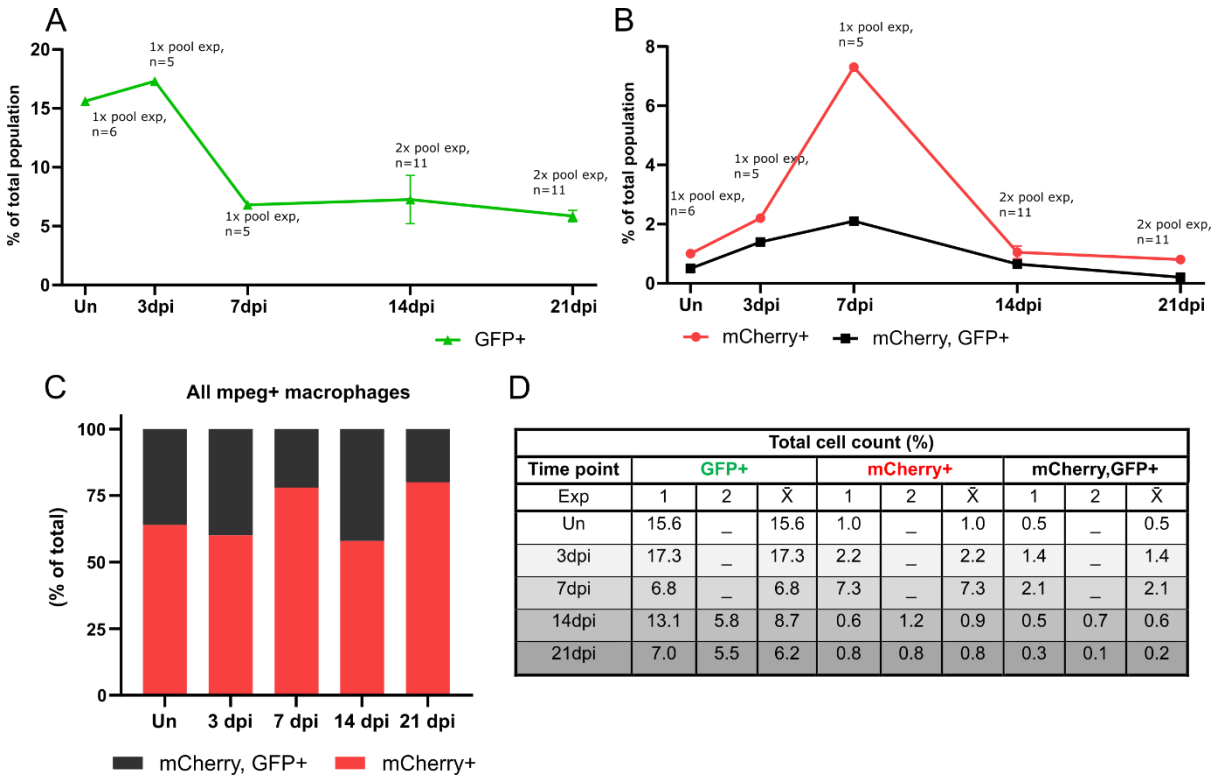

Total cell count (%)									
Time point	GFP+			mCherry+			mCherry,GFP+		
Exp	1	2	X̄	1	2	X̄	1	2	X̄
Un	15.6	_	15.6	1.0	_	1.0	0.5	_	0.5
3dpi	17.3	_	17.3	2.2	_	2.2	1.4	_	1.4
7dpi	6.8	_	6.8	7.3	_	7.3	2.1	_	2.1
14dpi	13.1	5.8	8.7	0.6	1.2	0.9	0.5	0.7	0.6
21dpi	7.0	5.5	6.2	0.8	0.8	0.8	0.3	0.1	0.2

Figure 4.3. Relative percentage of fluorescently labelled cells as a proportion of total cells sorted from ventricular tissues at different time points post-injury.(A) GFP+ cardiomyocytes are drastically reduced between 3 and 7 dpi, then start to recover. (B) mCherry+ numbers increase rapidly until 7 dpi, then decrease to homeostatic level. *myl7*+ macrophages (mCherry+, GFP+) are present in uninjured ventricles and abundant after injury. Both macrophage populations respond similarly to injury but there are reduced numbers of

mCherry+, GFP+, particularly at 7 dpi when compared to mCherry+. (C) The percentage fraction of single (mCherry+) to double (mCherry+, GFP+) macrophages at each time point. (D) Relative percentage number of fluorescently tagged cell population to cell number. Exp – Experiment number, x̄ - geometric mean, Un – uninjured.

4.4.2. Phenotypic characterisation of the mCherry+, GFP+ macrophage subset

Analysing GFP (*myl7*) signal in the total macrophage population (*mpeg1.1+)* versus FSC (***Figure 4.4A***) reveals that the mCherry+, GFP subsets is generally similar in size to the mCherry+ subset although they are slightly larger in unwounded hearts and at 7 and 21 dpi (***Figure 4.4A***). The SSC profile reveals increased complexity of mCherry+, GFP+ macrophages when compared to mCherry+ at all time points analysed except 21 dpi *(**Figure 4.4B**).* In addition, contour plots of both FSC and SSC suggest two populations of *myl7*+ macrophages, GFP high and GFP low, in all time points except 21 dpi (***Figure 4.4.A-B***). This suggests variability of *myl7*+ expression (GFP+) in macrophages.

This study also confirms that two distinct populations can be observed in the macrophage mCherry+ subset (***Figure 4.2.C*** *Un-14 dpi****; Figure 4.4.A-B***) as reported previously (Moyse and Richardson, 2020). These cells likely have a lymphoid origin and appear small and non-granular via FSC and SSC (Moyse and Richardson, 2020).

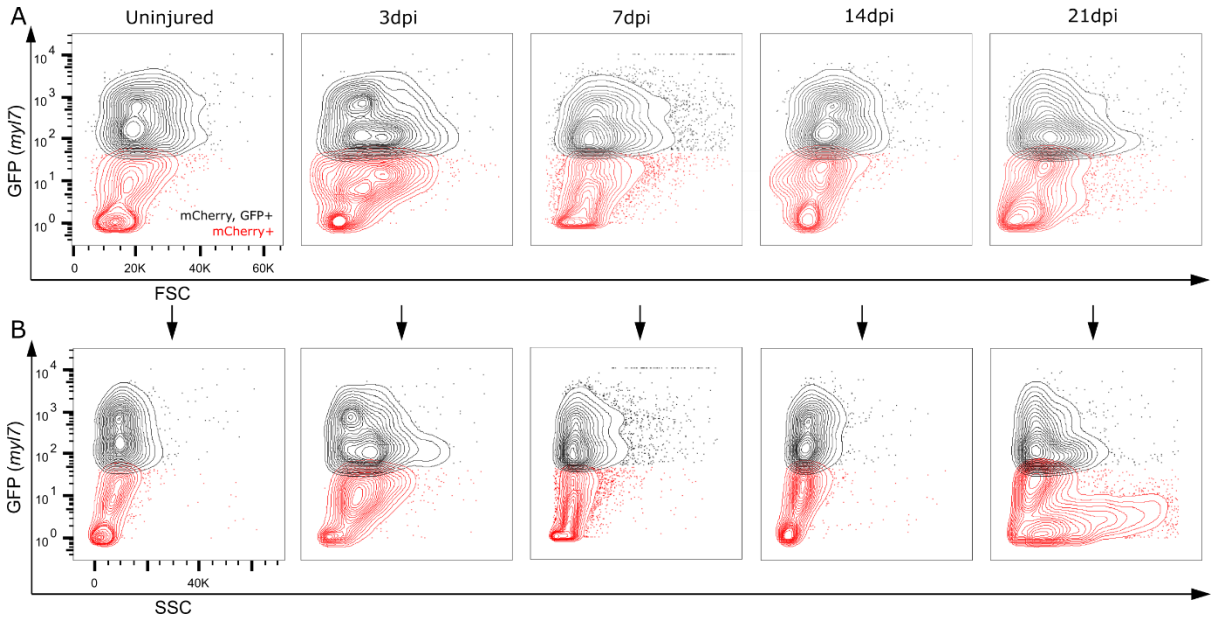

Figure 4.4. Phenotypic characterisation of mCherry+ macrophages from Tg(*myl7:GFP*); Tg(*mpeg1.1:mCherry*) fish via FFC and SSC. (A,B) Two populations of macrophages have been identified: single mCherry+ (red) and double mCherry+, GFP+ (grey) subsets. mCherry+, GFP+ macrophages are slightly bigger in size then mCherry+ cells in uninjured (Un) fish and at 7 and 21 dpi (A) and more granular (apart from at 21 dpi) (B).

4.5. Characterisation of mCherry+, GFP+ macrophages by Imaging Flow Cytometry.

Although FACS was valuable in identifying and the initial characterisation of mCherry+, GFP+ cells (identified as macrophages) from Tg*(myl7:GFP);* Tg*(mpeg1.1:mCherry)* fish, contamination between different populations could not be ruled out. In an effort to characterise the phenotype of mCherry+, GFP+ positive macrophages further, as well as exclude possible cross contamination of populations (e.g. by incomplete dissociation of ventricular tissues or fluorescent cells adhering to each other), ventricles from Tg*(myl7:GFP);* Tg*(mpeg1.1:mCherry)* fish were sent for Imaging Flow Cytometry (IFC) analysis at the University of Exeter. IFC combines the advantages of FACS and fluorescence microscopy, allowing more advanced morphological analysis of thousands of fluorescently labelled cells with various FRPs (Barteneva, Fasler-Kan and Vorobjev, 2012). IFC utilises data-analysis algorithms and real-time imaging so each single cell event can be characterised to a molecular level (Barteneva, Fasler-Kan and Vorobjev, 2012).

For this experiment, ventricles were collected from healthy and 7 dpi Tg*(myl7:GFP);* Tg*(mpeg1.1:mCherry)* fish, together with adequate controls (single Tg(*myl7:GFP*) or Tg(*mpeg1.1:mCherry*) and WT fish). Three ventricles of each were collected, pooled, and dissociated as described in ***section 2.3***. Half of each pooled sample was stained with Zombie NIR™ Fixable Viability kit (423105; Biolegend) according to the manufacturers protocol to differentiate dead cells. All samples were preserved overnight in 1% PFA in PBS. Imaging flow cytometry analysis was carried out using an ImageStreamxMk II (Amnis-Luminex, SA) by Dr Ann Power (University of Exeter). Data analysis was performed later using IDEAS 6.2 EMD (Millipore, SA). Despite all precautions taken, due to the long transit time and assay performance (4 – 24 h to sort all samples), as well as contamination with cell debris, the quality of the prepared cell suspensions was not sufficient to obtain high quality imaging data.

Unfortunately, this prevented further analysis of double positive mCherry+, GFP+ cell populations, but has provided valuable insight into the technical adaptations required for this type of analysis. The acquisition of a ImageStreamxMk II system here in Bristol will greatly facilitate the repeat of this experiment.

Chapter 5. Investigation of *myl7-GFP* signal in cardiac macrophages of Tg(*myl7:GFP*); Tg(*mpeg1.1:mCherry*) ventricles via whole mount image analysis.

5.1. Background

In order to fully utilise the advantages of Tg(*myl7:GFP*); Tg(*mpeg1.1:mCherry*) double transgenic fish, where macrophages are labelled with mCherry and cells expressing *myl7* will be labelled with GFP, high resolution images of fixed hearts were gathered by laser scanning confocal microscopy (LSCM) for image analysis. LSCM allows detection of genetically incorporated fluorescent proteins and other fluorescence reporters, through precise separation of their emission spectra (St Croix, Shand and Watkins, 2005). Point scanning technology reduces out of focus light detection, limiting background noise, which results in the production of high resolution images (across xyz-axes) and collection of robust quantitative data based on signal intensity registration (St Croix, Shand and Watkins, 2005). Image analysis, in particular colocalization, is a widely implemented and powerful tool for elucidating cellular and molecular correlations and has facilitated the dissection of many molecular pathways (Dunn, Kamocka and McDonald, 2011; Paddock and Eliceiri, 2014). Where visual juxtaposition of the fluorescence channels is inadequate for confident determination of co-labelling in the same cell or compartment, statistical colocalization measurements of the co-distribution of two fluorescence signals can be performed (Dunn, Kamocka and McDonald, 2011).

Many software packages are now available for colocalization analyses e.g. ImageJ (Fiji) Coloc2 or JaCop plugins, however, the Tg(*myl7:GFP*); Tg(*mpeg1.1:mCherry*) transgenic line used here is characterised by bright, dispersed GFP+ signal in cardiomyocytes rather than individual, well separated cells, limiting the use of standard colocalization methods. Therefore, for this analysis a custom made Modular Image Analysis (MIA) plugin for Fiji was designed by Dr. Stephen Cross from the Wolfson Bioimaging Centre, University of Bristol, which detects raw GFP signal intensity (green channel) contained in 3D volume projections of macrophages (red channel) generated across Z-stack images. Macrophages are detected through binarization of the original images based on an automatically calculated threshold

using the Otsu algorithm. In addition to determining co-localisation, this plugin allowed the measurement of the volume (µm^3) and circularity (0 – 1 with 1 being a perfect circle) of the detected cardiac macrophages. Unprocessed images of two ventricular regions - the mid ventricle/ unaffected region (UR) and apex/ injury site (IS), of Tg(*myl7:GFP*); Tg(*mpeg1.1:mCherry*) ventricles were analysed (example of the regions analysed across the time points (***Figure 5.1A-F***)) to investigate the distribution and phenotype of the double positive (mCherry+, GFP+) macrophage subset *(described in **section 4.3**)* in greater detail.

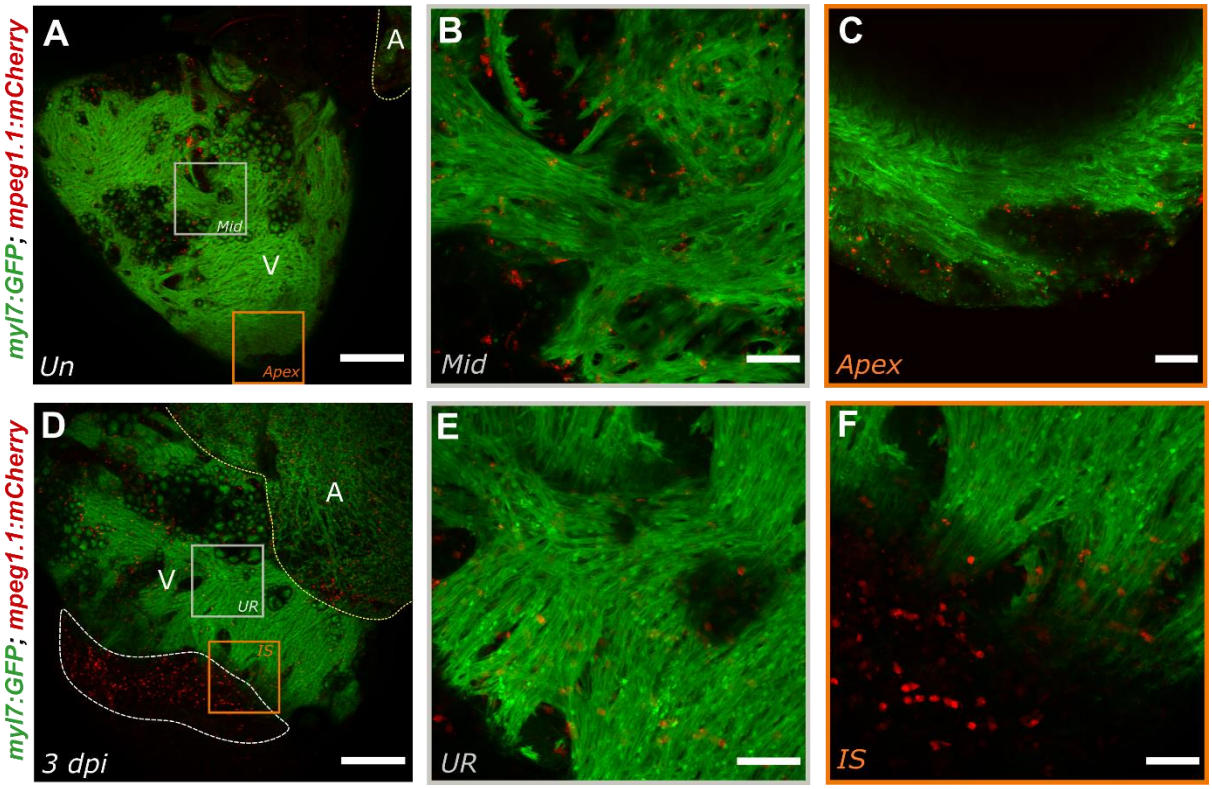

Figure 5.1. Representative ventricular regions of Tg(*myl7:GFP*); Tg(*mpeg1.1:mCherry*) hearts used for image analysis with a Fiji MIA plugin.(A-C) Two distinct regions were selected in the uninjured heart (A) – mid ventricle (B) and apex (C). (D-F) Two corresponding regions from injured hearts (D) were also selected – the unaffected region (UR) (E) and the injury site (IS) (F). Colour coded boxed regions demark the approximate position of each panel (A, D). The yellow dashed line demarks the atrium and the white dashed line demarks the injury site (A, D). A – Atrium, V – Ventricle (A, D). Scale bars: A, D = 250 µm; B, C, E, F = 50 µm**.**

5.2. Selection of *mpeg1.1*-mCherry macrophages for analysis based on their volume

Quantitative data obtained from automated MIA plugin analysis of ventricular regions of two hearts from Uninjured (Un), 3, 7 and 14 dpi Tg(*myl7:GFP*); Tg(*mpeg1.1:mCherry*) fish and two uninjured hearts from TgBAC*(tnfα:GFP)*; Tg(*mpeg1.1:mCherry*) fish (as a background fluorescence control) were analysed. The macrophage threshold was calculated using the Otsu algorithm for binarization (inverse sensitivity = value 1) and cells with a minimum volume of ≥ 70 μm^3, which was selected based on previously obtained data from zebrafish macrophages. This automatically generated a layout of selected cells (macrophages) meeting these chosen criteria and the recorded volume of these layouts were manually assessed to determine acceptable maximum macrophage size. Two unaffected regions (***Figure 5.2A, B***) and an injury site (***Figure 5.2C, D***) from 14 dpi hearts and their corresponding layouts are presented as a representative example of the limitation of the automatic macrophage detection (described in detail below). Small, circular *mpeg1.1:mCherry* cells with a volume of 70 – 150 μm^3 are likely lymphocytes (Moyse and Richardson, 2020) but were included in the analysis (demarked with red arrows in ***Figure 5.2A, B***). Cells with volumes > 999 μm^3 were eliminated from further analysis as they resulted from imprecise segmentation of individual cells which could occur when macrophages were in very close proximity, as often seen at the injury site (demarked with white arrow in ***Figure 5.2C, D***). Finally, data sets collected from uninjured hearts of Tg(*myl7:GFP*); Tg(*mpeg1.1:mCherry*) and TgBAC*(tnfα:GFP)*; Tg(*mpeg1.1:mCherry*) fish, where clustered macrophages were less frequent, were assessed to confirm the *mpeg1.1*+ volume range as 70 - 999μm^3 and cells within this range were considered as an indication of correctly segmented macrophages. Interestingly, the maximum macrophage volume in uninjured hearts is approximately 750 μm^3.

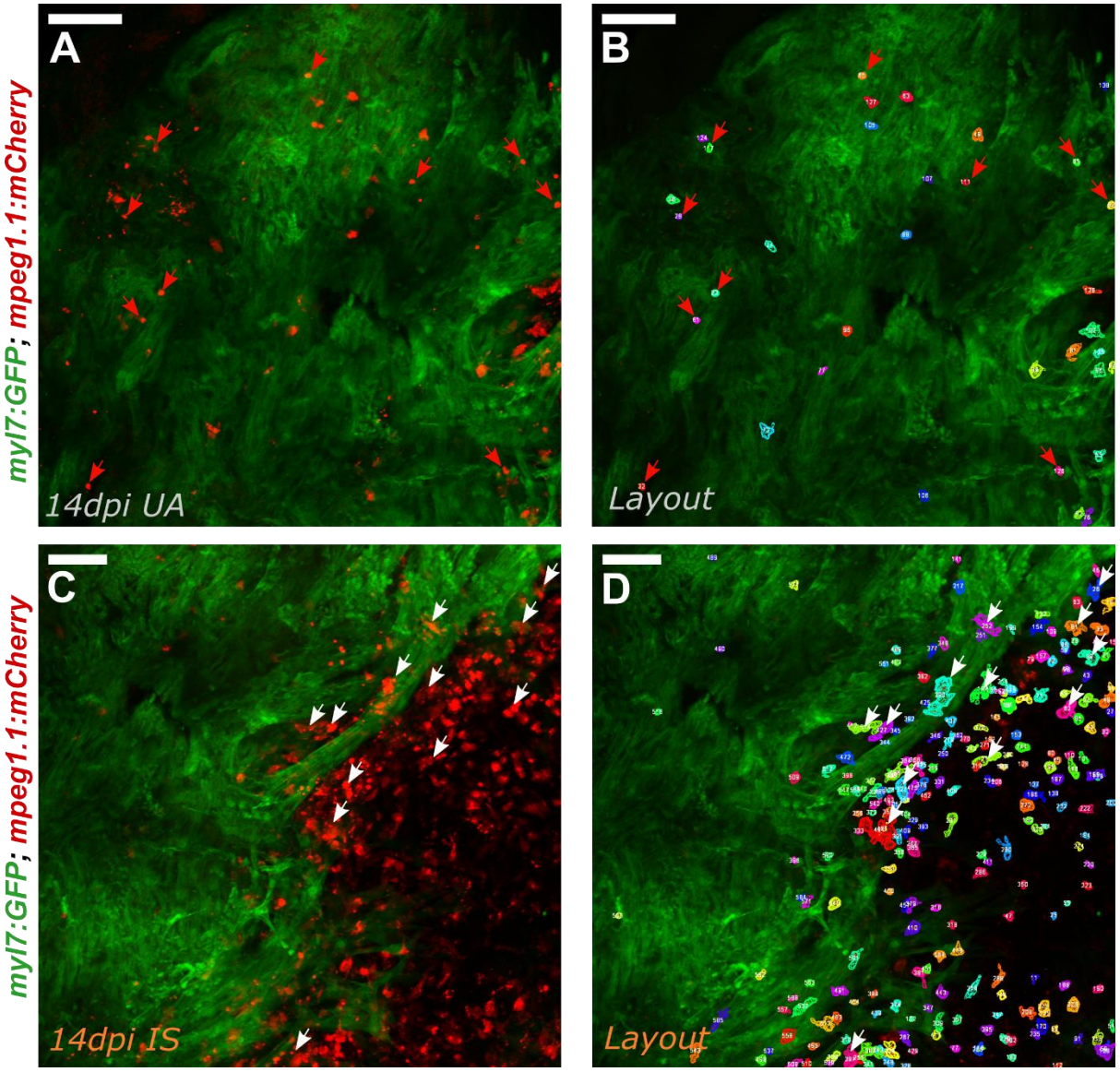

Figure 5.2. Representative ventricular regions with detection layouts from a Tg(*myl7:GFP*); Tg(*mpeg1.1:mCherry*) heart at 14 dpi. (A-D) Two distinct ventricular regions are presented: unaffected region (UA) (A) and its corresponding layout (B) and the injury site (IS) (C) and its corresponding layout (D). Automatically generated layouts and collected volume (μm^3) readings were manually investigated and used to establish an acceptable volume range for macrophages, as some incorrect segmentation occurs when multiple cells are in close proximity. Cells with lower volume (70 -150 μm^3) likely represent *mpeg1.1*+ lymphocytes (red arrows) but were included (A, B). Cells with volume >999 μm^3 were excluded from further analysis due to incorrect segmentation resulting from multiple cells grouped together (white arrows) (C, D). Scale bars: A-D = 50 μm.

5.3. Characterization of *mpeg1.1:mCherry* cells

5.3.1. Phenotype of *mpeg1.1:mCherry*+ cells by shape and volume

Firstly, as the plugin allowed general characteristics of macrophages to be assessed, volume and circularity of these cells in different regions of the heart before and after injury were determined (***Figure 5.3.A, B***). *mpeg1.1*+ macrophages had volumes between 70 – 927 μm^3 within the collected samples, with 50% between 94 – 382.6 μm^3 (Inter-quarter range IQR = 220 μm^3) (***Figure 5.3.A***). Generally, macrophage volume did not differ within regions across time-points, however, a significant difference was observed between cells in the apex region of uninjured fish and the injury site at 7 dpi where macrophages appeared smaller (***Figure 5.3.A***). Comparison of regions within the time-points showed a significant volume change between *mpeg1.1*+ macrophages in the injury site and the unaffected region at 3 and 7 dpi (***Figure 5.3.A***). Interestingly, they were larger in the injury site at 3 dpi and smaller at 7 dpi (***Figure 5.3.A***). The degree of circularity (with a score of 1.0 representing a perfect circle) of the *mpeg1.1*+ macrophages was also measured before and after injury in the two regions of interest (***Figure 5.3.B***). The most variable circularity data was observed between the ventricular regions of uninjured and 7 dpi hearts (***Figure 5.3.B***). *mpeg1.1*+ macrophages were significantly more rounded in the unaffected region of the ventricle at 3 and 7 dpi compared to uninjured hearts (***Figure 5.3.B***) perhaps suggesting the recruitment of monocyte derived, pro-inflammatory macrophages into the injury site. Pro-inflammatory macrophages are more rounded in shape than anti-inflammatory macrophages (McWhorter *et al.*, 2013) and are predominate at 3 – 5 days after MI in mammals (Thackeray and Bengel, 2018), and zebrafish after cryoinjury (Sanz-Morejón *et al.*, 2019; Bevan *et al.*, 2020; Simões *et al.*, 2020). Additionally, significant changes in circularity between regions was observed in uninjured (Un), 7 and 14 dpi hearts. More circular *mpeg1.1*+ macrophages were found at the apex of uninjured ventricles compared to the mid region. Less circular macrophages were observed at the injury site compared to the uninjured region of 7 dpi ventricles, suggesting the presence of more anti-inflammatory macrophages, which are generally more elongated (McWhorter *et al.*, 2013), although injury site cells were more rounded at 14 dpi (***Figure 5.3.B***). However, there was no significant difference between the circularity

of macrophages in this region when compared to the equivalent region of uninjured hearts (***Figure 5.3.B***). Further characterisation of macrophage versus lymphocyte volume would be required to determine the proportion of *mpeg1.1*+ lymphocytes contributing to this data.

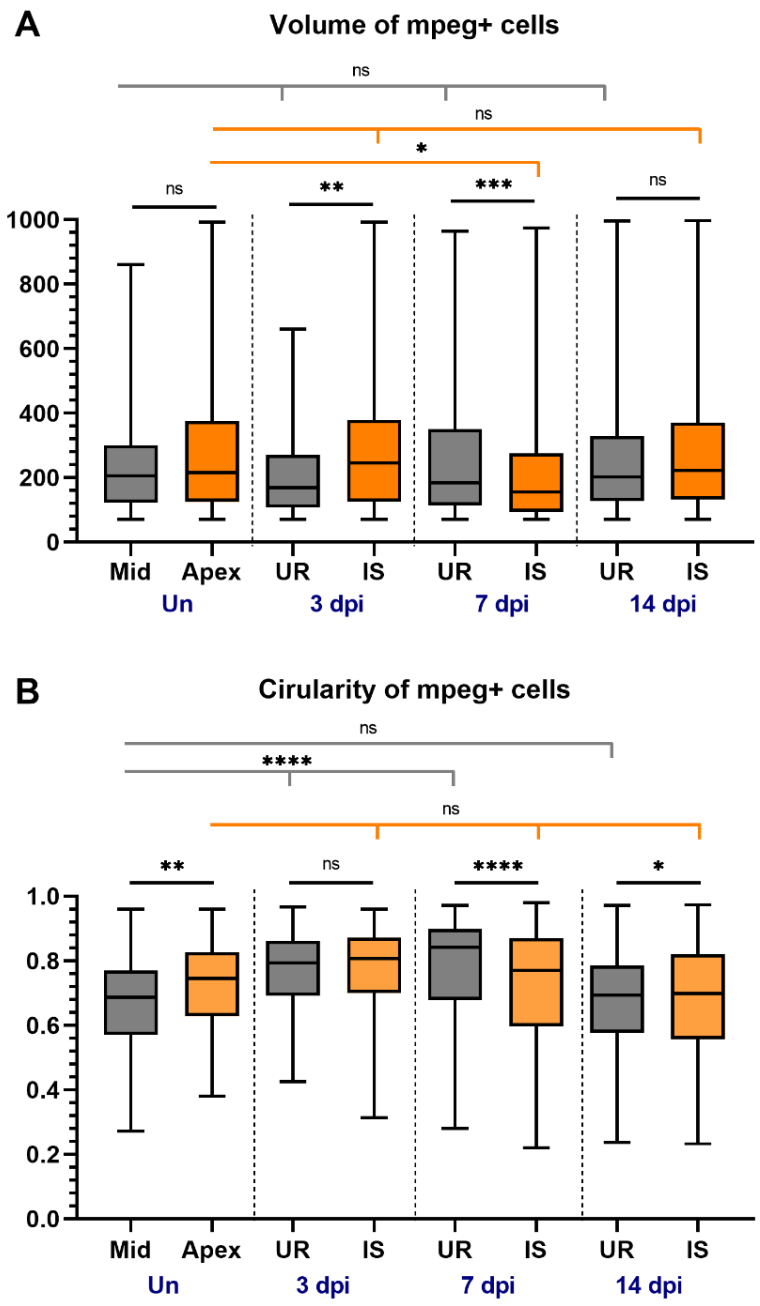

Figure 5.3. Characterization of volume and circularity of *mpeg1.1*+ cells in pre and post injury hearts.Volume (A) and circularity (B) of all *mpeg1.1*+ cells as determined by the Fiji MIA plugin. The overall volume of *mpeg1.1*+ cells ranged from 70 – 927 μm^3 (A). The

circularity of *mpeg1.1*+ cells ranged from 0.22 – 0.98 (B). Box and whisker plots are presented where the horizontal line represents the median and the whiskers show the minimum and maximum values. For statistical analysis, Mann-Whitney tests were used for the difference between the Mid/UR and Apex/IS regions at each time-point. Kruskal-Wallis tests with Dunn's correction for multiple comparisons were used to compare all corresponding regions between uninjured and injured fish. Significance values between injured and injured ventricles mid/unaffected region (in grey) and apex/injury site (in orange) are shown above each time-point. UR – unaffected area; IS – Injury site, Un – Uninjured.

5.3.2. Distribution of mean *myl7* GFP signal in cardiac macrophages before and after injury.

Secondly, distribution of mean GFP signal intensity in *mpeg1.1*+ macrophages in two different ventricular regions of uninjured and injured (n=2) hearts was analysed using the Fiji plugin described above (***Figure 5.4***). GFP signal could be detected in all *mpeg1.1*+ macrophages, however, the intensity varies from cell to cell and between regions. The highest GFP signal is observed in *mpeg1.1*+ cells at 14 dpi in the unaffected region (mGFP = 56.50) and lowest in the 7 dpi Injury site (IS) (mGFP = 13.22) (***Figure 5.4***). Interestingly, the highest mean GFP signal in cardiomyocytes (mGFP = 64.96) was observed at 3 dpi in the unaffected region and lowest (mGFP = 0.142) at 7 dpi at the injury site (measured in approx. 170 μm^2 regions across z-stacks). Comparison of macrophages in the mid/unaffected region and apex/injury site shows no significant difference of the GFP signal intensity in uninjured hearts, whereas a significant difference between these regions was observed at 3, 7 and 14 dpi (***Figure 5.4***). After injury the GFP intensity in *mpeg1.1*+ cells decreased in the unaffected region of the ventricle at 3 and 7 dpi, whereas it was significantly increased at 14 dpi. There was a uniform drop in GFP signal at the injury site at 3, 7 and 14 dpi compared to the apex region of the uninjured heart (***Figure 5.4***).

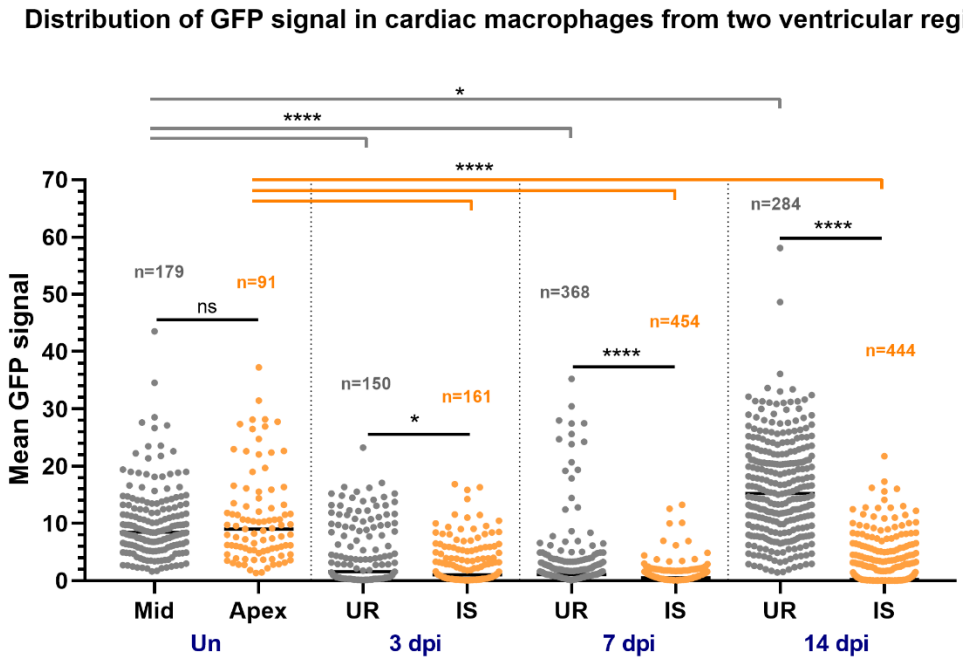

Figure 5.4. Distribution of the GFP signal intensity measured in *mpeg1.1*+ macrophages at two different ventricular regions from uninjured and injured hearts. No significant difference is observed between the regions analysed in uninjured fish but significant changes are observed in both regions after injury. Significantly reduced GFP intensity was observed in the injury site at 3, 7 and 14 dpi compared to corresponding unaffected regions. Two hearts at each timepoint were imaged and the total *mpeg1.1*+ macrophages from each region analysed using the criteria described above. The n number refers to the total macrophages. The line represents the mean value. For statistical analysis, Mann-Whitney tests were used for the difference between the Mid/UR and Apex/IS regions at each time-point. Kruskal-Wallis tests with Dunn's correction for multiple comparisons were used to compare all corresponding regions between uninjured and injured fish. Significance values between injured and injured ventricles mid/unaffected region (in grey) and apex/injury site (in orange) are shown above each time-point.

5.4. Imaging mCherry+, GFP+ cells in the heart

5.4.1. Identification of the mCherry+, GFP+ macrophage subset via imaging

Despite all precautions taken to minimise bleed through of the GFP signal, which is very strongly expressed in surrounding cardiomyocytes, to the mCherry channel, including sequential scanning with 488 (GFP) and 561 (mCherry) excitation lasers

and narrow detection wavelengths, cross-contamination of signal could not be ruled out. In an effort to reduce the likelihood of signal bleed through affecting the results, the mean GFP signal was determined for each group and used as the lower threshold value (internal control for bleed through) (***Figure 5.5A***). All *mpeg1.1*+ macrophages with GFP intensity above the established mean were considered as the mCherry+, GFP+ macrophage subset for this experiment *(located above black box,* ***Figure 5.5A***) and cells with GFP intensity below the mean were considered mCherry+ only (*enclosed in black box,* ***Figure 5.5A***). Before, detailed analysis of mCherry+, GFP+ macrophages was undertaken, the volume and circularity of both macrophage subsets was compared. In general, both macrophage subsets maintain the same circularity (***Figure 5.6A***) and volume (***Figure 5.6B***) within the same region at each time point. However, mCherry+, GFP+ macrophages in the uninjured region at 3 dpi and 7 dpi were significantly less circular than the mCherry+ subset (***Figure 5.6A***). Additionally, mCherry+, GFP+ macrophages in the unaffected region were significantly smaller than mCherry+ cells at 7 dpi but bigger at 14 dpi (***Figure 5.6B***).

5.4.2. Detailed characterisation of the mCherry+, GFP+ macrophage subset

Filtering the data in this way produced similar results to the analysis of total *mpeg1.1*+ macrophages with significant differences between uninjured and injured regions at almost all time-points (expect UR of 3 dpi) and a significant drop in GFP intensity between uninjured and injured regions of the same ventricle at 3 (more significant than prior to cut off), 7 and 14 dpi (***Figure 5.5A***). No significant differences in circularity and volume were found when only the filtered mCherry+, GFP+ macrophage subset was analysed (***Figure 5.5B***). The only exception was a significant increase in macrophage circularity at the injury site at 14 dpi (***Figure 5.5B***).

To determine the proportion of single positive to double positive macrophages, the percentage of each subset in each ventricular region was calculated (***Figure 5.5C***). Similar percentages of mCherry+, GFP+ macrophages were found in the mid region of uninjured hearts and 3 dpi and the apex/IS from uninjured, 3 and 7 dpi hearts (35% ± 1.32) (***Figure 5.5C***). A decreased number of the mCherry+, GFP+ subset was observed in the UR at 7 dpi (19.82) and an increase to 46.48% of this subset in the UR at 14 dpi was observed (***Figure 5.5C***). To determine the total percentage of

mCherry+, GFP+ macrophages at each time point, the regions were combined (***Figure 5.5D***). More mCherry+ cells than mCherry+, GFP+ cells were observed at each time-point with the fewest mCherry+, GFP+ cells being observed at 7 dpi (***Figure 5.5D***). The mCherry+, GFP+ subset constituted 38% of the total macrophage population in uninjured fish, 36% at 3 dpi, 17% at 7 dpi and 38% at 14 dpi (***Figure 5.5E, F***), similar to that reported by FACS (***section 4.4.2****.* and presented in ***Figure 4.3C***).

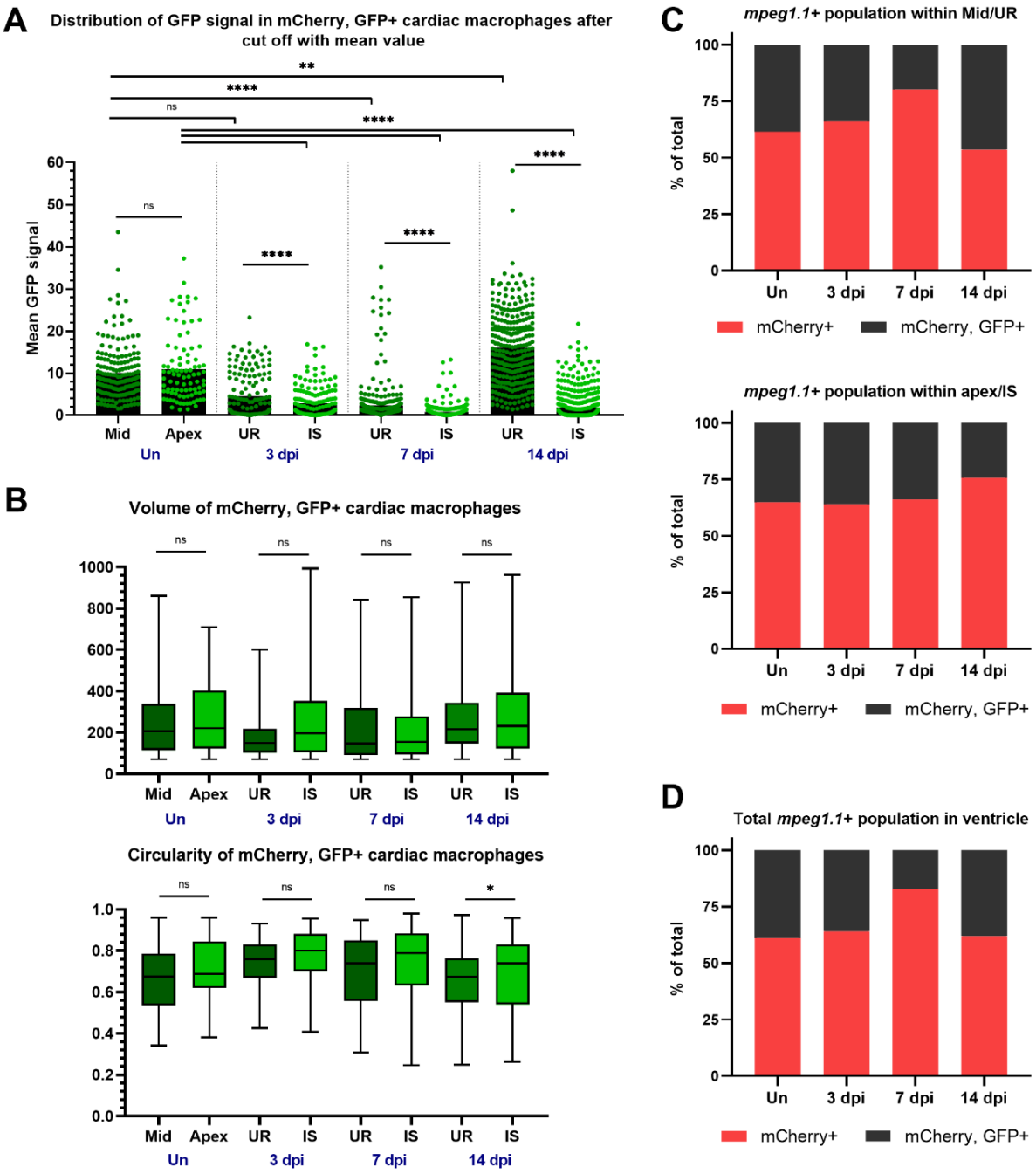

Figure 5.5. Determination of the mCherry+, GFP+ macrophage subset via confocal imaging. (A) The mean GFP intensity value was used as an internal control (same data as shown in Figure 5.4 but significance values correspond to filtered data). Corresponding mean values were used as a lower threshold with cells with a GFP signal > mean (above the black box) considered as the double positive mCherry+, GFP+ macrophage subset, whereas cells with GFP signal ≤ mean were consider as the single positive mCherry+ subset (enclosed in black box) (A). (B) The volume and circularity of these filtered cells was analysed across the regions of the heart. The percentage of mCherry+ to mCherry+, GFP+

macrophages in total *mpeg1.1*+ cells was calculated for each region (C) and ventricle (D) from different time points. For statistical analysis, Mann-Whitney tests were used for the difference between the Mid/UR and Apex/IS regions at each time-point. Kruskal-Wallis tests with Dunn's correction for multiple comparisons were used to compare all corresponding regions between uninjured and injured fish.UR – unaffected area; IS – Injury site, Un – Uninjured.

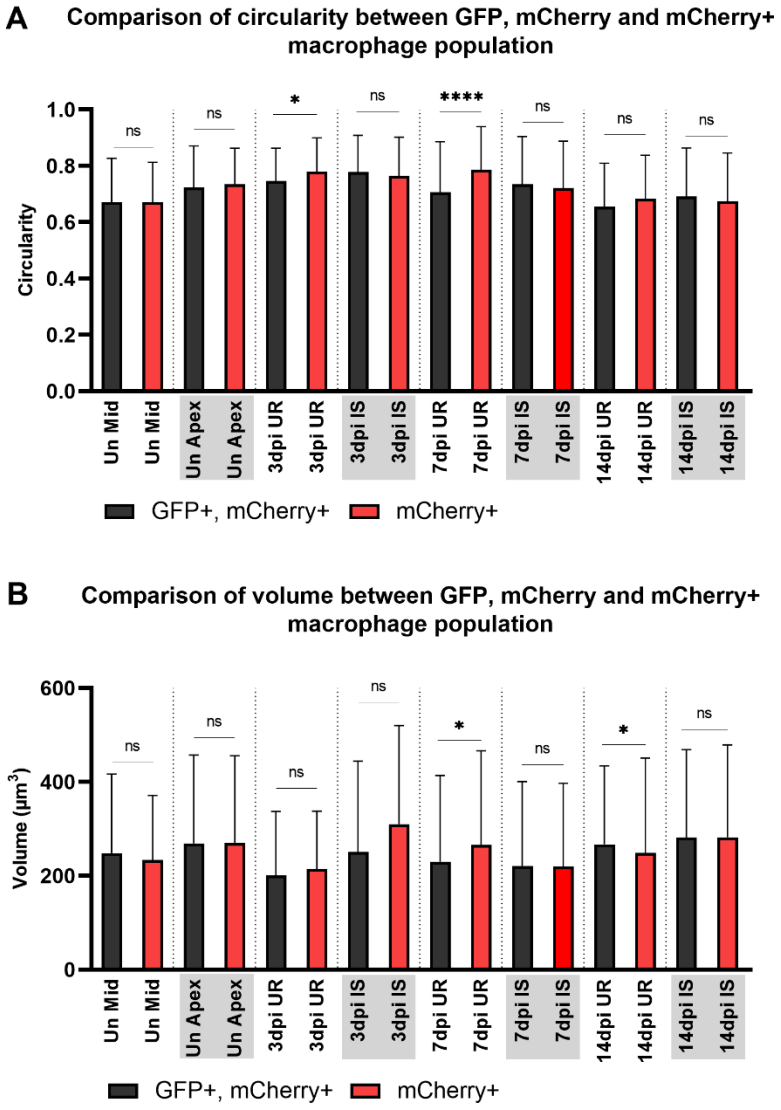

Figure 5.6. **Comparison of phenotype characteristics between mCherry+ and mCherry+, GFP+ macrophages.** Circularity (A) and volume (B) of both macrophages subsets were compared between regions of all time points. (A) Significant differences in circularity between the subsets was only observed in the UR at 3 dpi and 7 dpi. (B) Significant differences in volume were only observed in the UR at 7 dpi and 14 dpi. For statistical analysis, Mann-

Whitney tests were used for the difference between the Mid/UR and Apex/IS regions at each time-point.

To further assess morphology and precise distribution of mCherry+, GFP+ macrophages, examples were chosen and individually tracked *(colour coded data points in **Figure 5.7A-H**)*. The majority of the mCherry+, GFP+ subset are in close contact with cardiomyocytes and/or buried deeply in the ventricular myocardium (***Figure 5.7A-D,E,G***). Interestingly, at later injury time-points (7 and 14 dpi) the mCherry+, GFP+ subset are found in the border region just outside the injury (***Figure 5.7F,H***), where new cardiomyocytes actively proliferate (Jopling *et al.*, 2010; Kikuchi *et al.*, 2010). No mCherry+, GFP+ macrophages were found directly at the site of the injury (***Figure 5.7D,F,H***).

Very low cytoplasmic *myl7* expression (dispersed GFP signal) within macrophages can be observed (***Figure 5.7Ai-ii,Bi,Cii-iii, G,Hii-iii***). RT-qPCR analysis of *myl7* transcript level (***section 3.2.3***) suggests it to be low, perhaps explaining why the expression is hard to visualise, although it can be detected via the image analysis. However, rarely, more pronounced cytoplasmic *myl7* expression was observed (***Figure 5.7,Ei,Fi***). Additionally, small circular GFP+ particles enclosed within macrophages were observed in uninjured hearts *(demarked with white arrow, **Figure 5.7Bii-iii, Di**)*, as well as phagocytic macrophages present at the inflammatory phase (***Figure 5.7Dii***).

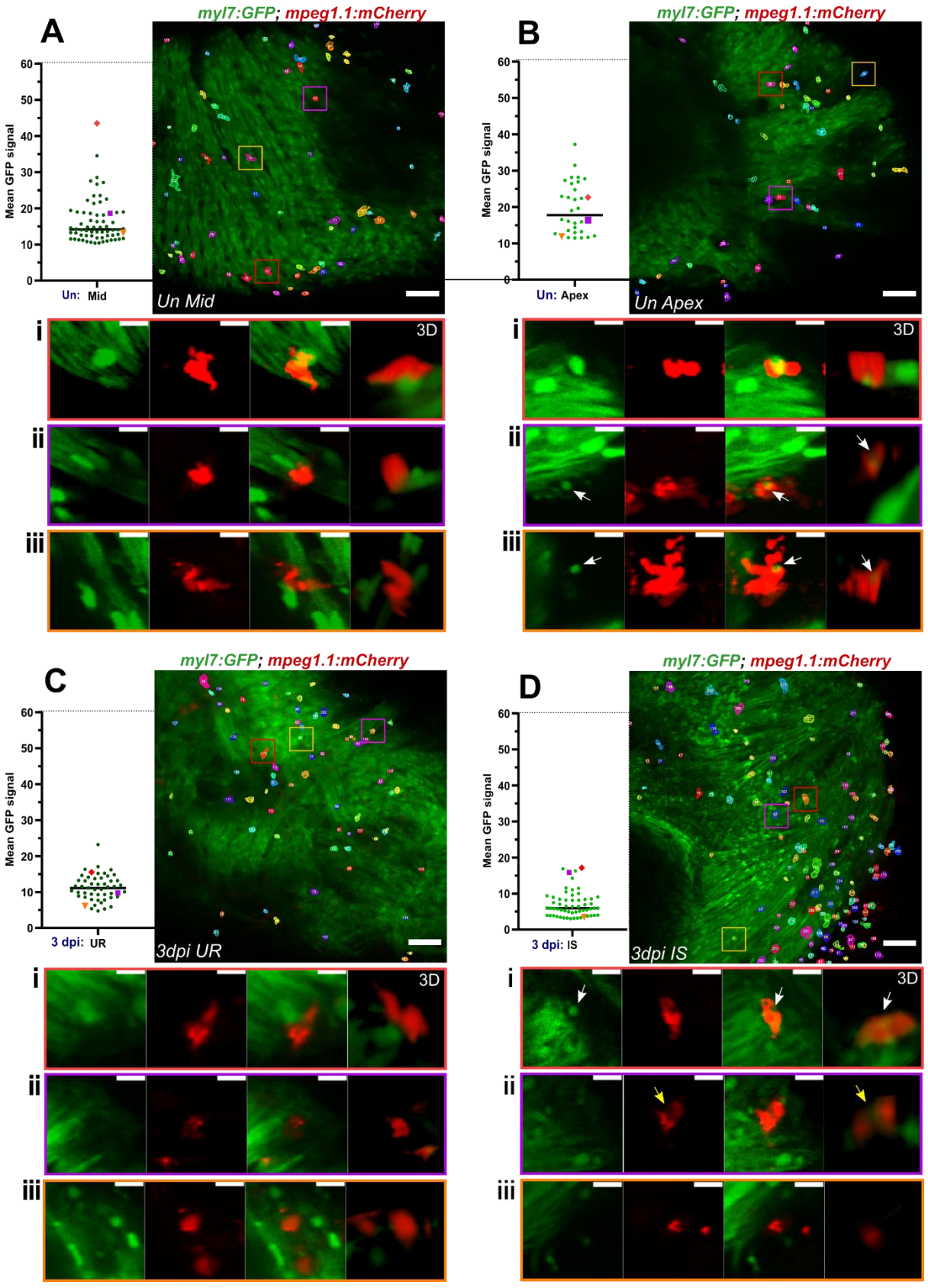
A
myl7:GFP; mpeg1.1:mCherry
Mean GFP signal
Un: Mid
Un Mid
B
myl7:GFP; mpeg1.1:mCherry
Mean GFP signal
Un: Apex
Un Apex
i
ii
iii
3D
C
myl7:GFP; mpeg1.1:mCherry
Mean GFP signal
3 dpi: UR
3dpi UR
D
myl7:GFP; mpeg1.1:mCherry
Mean GFP signal
3 dpi: IS
3dpi IS

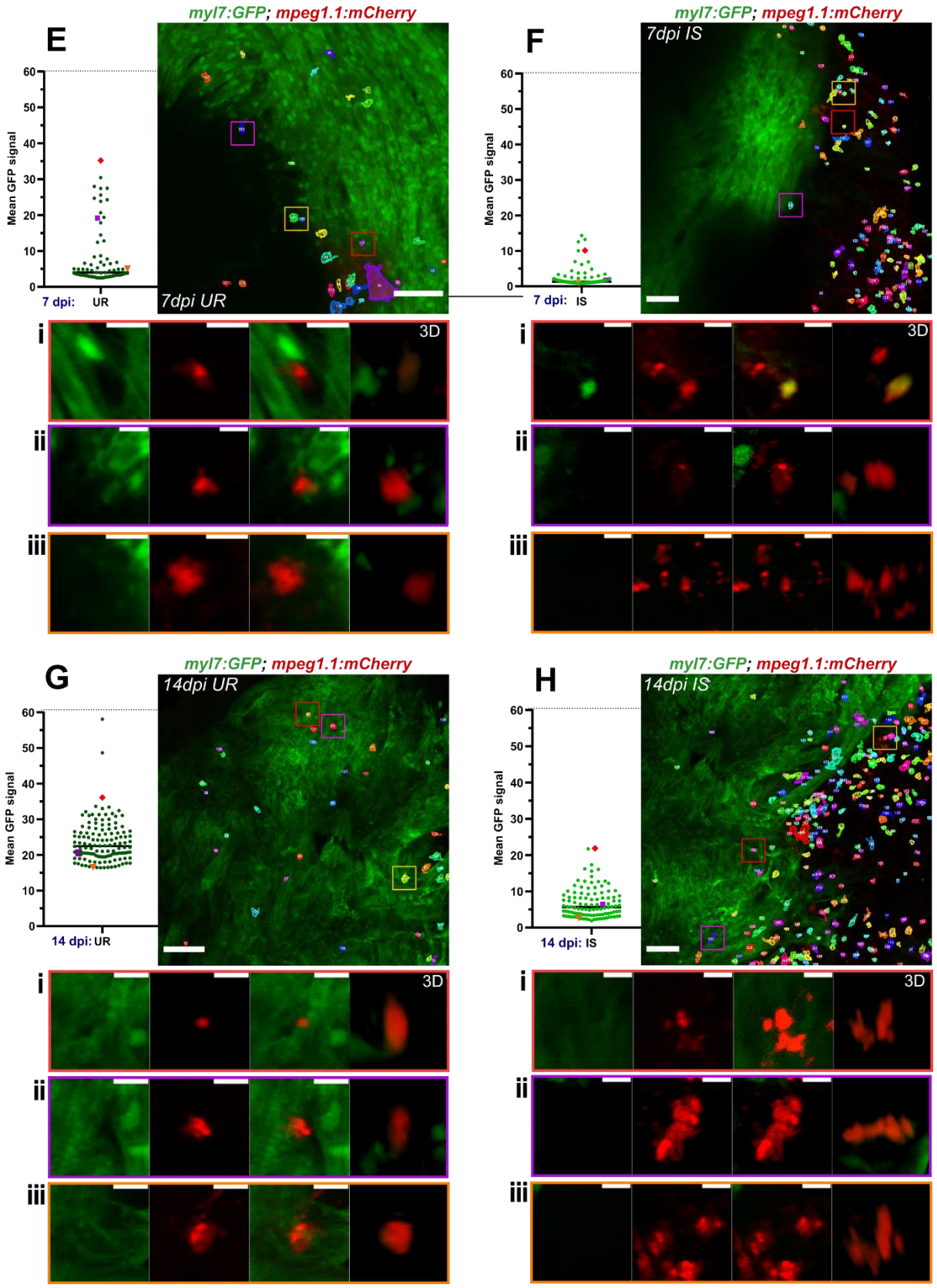

Figure 5.7. Examples of mCherry+, GFP+ macrophages within each region at different time-points. (A-F) The mid ventricle (A) and apex (B) from an uninjured heart, unaffected

region (UR; C) and injury site (IS; D) from 3 dpi, UR (E) and IS (F) from 7 dpi, and UR (E) and IS (F) from a 14 dpi ventricle. Each dot plot shows mCherry+, GFP+ macrophage subset (with GFP signal above mean GFP within the region) filtered as described in *section 5.4.1.* New median value for each experimental group was calculated. In each case the coloured points on the dot plot represent the colour coded *mpeg1.1*+ cells in the low power image (top right) and higher magnification views (bottom). For the high magnification views the GFP channel is shown on the left, then the mCherry channel, then the merge and a 3D projection on the right. Low levels of diffuse GFP expression were observed in cardiac macrophages (A-H). Pronounced cytoplasmic expression was occasionally observed (Ei, Fi). Occasionally, small GFP circular particles were enclosed in macrophages (demarked by white arrow, Bii-iii, Di), as well as phagocytes wrapped around cardiomyocytes remnants (demarked by yellow arrow, Dii).

Chapter 6. Discussion

6.1. Six cardiomyocyte genes are expressed by cardiac macrophages

An MI results in pathophysiological changes in the heart, a reduction in functionality and increased risk of heart failure, which can lead to death in 60% of cases (Frangogiannis, 2015). Unfortunately, the mortality rate after MI increases every year despite advances in treatment regimens (Alabas *et al.*, 2020). Recent studies highlight the significance of the immune response to the outcome of recovery from cardiac injury, especially the time-dependent interplay of diverse populations of macrophages with the post-MI microenvironment at the site of injury, either stimulating repair and scar formation or regeneration and scar resolution (Valentin *et al.*, 2009; Aurora *et al.*, 2014; Lai, Marín-Juez and Stainier, 2019; Sanz-Morejón *et al.*, 2019; Bevan *et al.*, 2020; Simões *et al.*, 2020). Further recent studies have revealed unexpected roles for macrophages in the heart including in cardiac electrical conduction during homeostasis (Hulsmans *et al.*, 2017) and the ability to produce collagen and deposit it at the injury site following damage (Simões *et al.*, 2020). Moreover, these studies have shown that cardiac macrophages in direct contact with cardiomyocytes perform synchronised contraction, improving electrophysiological properties of the heart (Hulsmans *et al.*, 2017).

Previously obtained unbiased proteomic data, which aimed to identify macrophage specific markers expressed during the regenerative response after cryoinjury, revealed surprising expression of a specific set of cardiac contractile proteins in cardiac macrophages (unpublished data). These proteins are all required for correct cardiomyocyte sarcomere assembly (***Figure 1.3***) (Huang, Zhang and Xu, 2009; Yang, Shih and Xu, 2014) or, in the case of myoglobin, oxygen transfer (Vlecken *et al.*, 2009). The work presented in this thesis supports this previously obtained proteomic data (***section 1.6.1, Figure1.6***) by verification of the expression of six cardiac genes (*mb, myl7, cmlc1, tpm4, tnnt2a and myh7l)* via RT-qPCR (***Figure 3.5.C***) and RT-PCR (***Figure 3.7.B***) in cardiac macrophages post injury. Moreover, this data demonstrates that expression of five genes (*mb, myl7, cmlc1, tpm4, tnnt2a*) is not only restricted to the injury response but is also present in macrophages from homeostatic hearts (***Figure 3.5.A***).

Molecular analyses reveals that the amount of each transcript found in cardiac macrophages is extremely low compared to levels in cardiac background cells (including a large proportion of cardiomyocytes) (***Figure 3.5.A,C***). Further to this, analysis revealed alterations in the expression of all of these genes in all cell populations analysed following cardiac injury (***Figure 3.6***). At 3 dpi, all genes except *tpm4a* were downregulated (***Figure 3.6***), which could suggest roles in maintenance of cardiac homeostasis. However, RT-PCR (on limited amounts of RNA) revealed that *cmlc1* and *myl7,* essential and regulatory light chain encoding genes, were also present in later time points after injury (***Figure 3.7B,C,E***). Interestingly, *myl7* and *cmlc1* are similarly expressed in homeostatic hearts but this changes after injury, with lower *cmlc1* expression observed than *myl7* at 7 dpi (***Figure 3.5A,C; Figure 3.7C***). Unfortunately, due to limitations in the amount of mRNA available, a full time course post injury on all selected genes could not be performed.

To further determine possible roles assigned to this specific expression in cardiac macrophages in cardiac repair and regeneration, a functional study using a conditional macrophage specific knock-out (KO) system using Cre loxP (a site-specific recombinase) technology could be utilised (Van Berlo *et al.*, 2014). Such a strategy would be needed because global depletion of cardiac genes results in cardiac malfunction or lethality (Berdougo *et al.*, 2003; Zhao *et al.*, 2008; Sogah *et al.*, 2010). The Cre/LoxP method involves generating a line with a floxed (flanked by loxP sites) region of interest (e.g. the *myl7* transcriptional start site) and another expressing Cre recombinase driven by a tissue-of-interest-specific promoter (e.g. *mpeg1.1)*. These lines can then be combined allowing expression of Cre recombinase only in macrophages and, therefore, recombination and removal of the floxed region, blocking myl7 expression only in these cells (Shi *et al.*, 2018). Comparison of the macrophage response in these Cre loxP fish compared to wildtype will provide better insights into potential roles of this cardiomyocyte gene expression in macrophages in the regenerative response and could underline the importance of the observed expression during homeostasis. It would be particularly interesting to determine changes in key regeneration processes of cardiomyocytes such as sarcomere disassembly and to determine if gene expression returns to baseline (uninjured levels) at 21 dpi or later, when myocardial regeneration is almost

complete (Jopling *et al.*, 2010; Kikuchi *et al.*, 2010; González-Rosa *et al.*, 2011; Chablais and Jaźwińska, 2012a; Bertozzi *et al.*, 2021).

6.2. Expression of some genes of interest is observed in additional cell types

Interestingly, low expression of *mb, tpm4a* and *tnnt2a* was observed in background cells and macrophages from fin tissue extracted from uninjured fish and from fish following cryoinjury (***Figure 3.5B,D***). Negligible expression of *cmlc1* in fin background cells was also observed. According to a previous study in zebrafish, *mb* is not exclusively expressed in cardiac and skeletal muscle, with low levels found in smooth muscle and in non-muscle tissues around the body eg. gills, hepatocytes, neurones, epidermal cell and endothelial cells (Cossins *et al.*, 2009; Vlecken *et al.*, 2009; Jaspers *et al.*, 2014). This may explain the *mb* expression observed in fin background cells, however, expression in macrophages has not been reported previously. The detection of *tpm4a* (transcript variant (tv) 1), supposedly a cardiac specific isoform of tropomyosin essential for heart function (Zhao *et al.*, 2008), was unexpected. A longer isoform (*tpm4a- tv2*) has previously been found in skeletal muscle, vasculature and other cell types (Zhao *et al.*, 2008; Dube *et al.*, 2017), however, the specificity of the primers designed for *tpm4a (tv1)* were checked via BLAST during primer design and melting curve analysis and presence of a single band in RT-PCR analysis confirm this specificity *(**Figure 3.7C***). Further work will be required to determine the importance of this expression in cells away from the heart.

6.3. Technical challenges of analysing small amounts of RNA

The work presented here indicates that conventional RT-PCR and RT-qPCR are sensitive enough to detect very low transcript levels and investigate gene expression changes after injury from very small cell populations, however, challenges remain in obtaining an appropriate amount of mRNA. The quality and quantity of even ultra-low amounts of mRNA can be significantly improved by implementation of correct protocols, and the work I have presented here outlines a detailed workflow to achieve this from sorted zebrafish cell populations *(described in **section 3.1-3.1.2**).* Furthermore, I have tested amplification kits which could potentially increase the amount of cDNA that can be obtained from small amounts of starting material

(described in ***section 3.1.3****).* Unfortunately, the results obtained from the QuantiTect Whole Transcriptome kit were inconsistent, which could lead to biased results. These findings suggest that this technology is still underdeveloped and further technique optimisation will be required before amplification of low yield RNA samples will be reliable for downstream applications such as RT-qPCR. These limitations in mRNA yield limited the panel of the genes and time points I could investigate so future work will be required to address this. The RT-qPCR gene expression analysis should be repeated for all genes of interest and across multiple time points, although this will require a large amount of adult zebrafish to obtain enough starting material. Additionally, to exclude possible contamination of cardiac macrophages with cardiomyocytes (and vice versa), potentially due to incomplete tissue dissociation, additional tissue specific genes (e.g. *nkx2.5* and *mef2a* (cardiomyocytes) and *mfap4* and *csf1ra* (macrophages); not identified in the original proteomics) should be included as cross contamination controls.

6.4. FACS of Tg*(myl7:GFP)*; Tg(*mpeg1.1:mCherry*) transgenic fish reveals double positive cells that respond to injury

Benefiting from the Tg*(myl7:GFP)*; Tg(*mpeg1.1:mCherry*) double transgenic line, I could further investigate *myl7* expression in cardiac macrophages in response to the injury via a combination of FACS and confocal microscopy. FACS revealed a double positive (mCherry+, GFP+) subtype of cardiac macrophages in uninjured hearts and following cardiac injury (***Figure 4.2A, Figure 4.1B-C, Figure 4.4***.). Their presence in uninjured hearts and at 3-14 dpi supports my findings of *myl7* expression in cardiac macrophages via RT-q/PCR (***Figure 3.5A,C*** and ***Figure 3.7B,C,E***). The *myl7* expressing macrophage subset did not differ significantly in size and granularity from *mpeg1.1*+ only macrophages (mCherry+) apart from at 21 dpi where the mCherry+ cells surprisingly appeared larger and more granular/activated (***Figure 4.2C,E***). Similarly, analysis of confocal images of the heart showed limited differences in volume and circularity of *myl7* expressing macrophages to *mpeg1.1*+ only, although some differences, predominantly in the unaffected region at 7 dpi, were found (discussed more below; ***Figure 5.6***). FACS reveals *myl7*+ cardiac macrophages contribute approx. 20 – 48 % of the total *mpeg1.1*+ macrophage population depending on the time-point (***Figure 4.3C***). The *myl7*+ macrophages respond to the

injury in a similar manner to *mCherry*+ cardiac macrophages, however, the peak at 7 dpi is reduced compared to non-*myl7* expressing macrophages (***Figure 4.3B***). This corresponds to the time point where pro-inflammatory macrophage numbers decrease and more anti-inflammatory (pro-reparative) macrophages become predominate (Thackeray and Bengel, 2018; Bevan *et al.*, 2020). However, the classification of macrophage subtypes may be more complex as *wt1b*$^{+}$ pro-regenerative macrophages have been shown to peak earlier at 4 dpi, when they constitute 50-70% of the total macrophage population, with their numbers reducing at 21 dpi to 44% (Sanz-Morejón *et al.*, 2019). The relative number of mCherry+, GFP+ (*myl7*+) macrophages increases to the highest proportion of total macrophages at uW, 3 and 14 dpi (36 – 46%) whereas they are reduced at 3 and 21 dpi (~20%). This pattern is somewhat different, therefore, to that observed for the *wt1b*$^{+}$ pro-regenerative population, although time-points between 4 – 21 dpi were not investigated in this study (***Figure 4.3C***). This might indicate that the *myl7*+ macrophage subset might be independent from *wt1b*$^{+}$ pro-regenerative macrophages. This data together suggests from the heterogeneous cardiac macrophage population, both pro-inflammatory and anti-inflammatory macrophages could be responsible for *myl7* expression, to a different degree (potentially favouring those with a pro-inflammatory phenotype), although further investigation with additional markers of macrophage phenotype (expression of *tnfa* and *wt1b*, respectively) would be required to confirm this.

Interestingly, initial cell death after cryoinjury is mostly reduced by 7 dpi (Chablais *et al.*, 2011) reducing the likelihood that double positive cells are due to residual GFP from engulfed cardiomyocytes present in the phagosomes of cardiac macrophages. Double positive cells identified at 3 dpi, however, could include some active phagocytes. GFP is rapidly quenched in acidic conditions (pH ~4.5 - 6) (Shinoda, Shannon and Nagai, 2018) and during phagocytosis phagosome acidity drops to ~ 5.0 pH within 10-30 min (Canton *et al.*, 2014), thus the GFP+ signal from engulfed cardiomyocytes should be at least partially degraded by this point, reducing the possibility of capturing active phagocytosis. Therefore, the double positive subset of cardiac macrophages could indicate endogenous expression of *myl7*. However, some indication of GFP within phagosomes was identified during analysis of confocal images and will be discussed more below.

6.5. Imaging analysis confirms cardiomyocyte gene expression in cardiac macrophages and reveals their distribution in the heart

The FACS analysis suggested *myl7* expressing macrophages could be identified in the ventricle of Tg*(myl7:GFP)*; Tg(*mpeg1.1:mCherry*) fish, however, it could not reveal the distribution of this subset of cells in the heart or the appearance of the GFP signal within the cells. Therefore, an image analysis strategy was developed using data acquired from confocal microscopy of fixed hearts at different time points post injury. This allowed the investigation of large numbers of *mpeg1.1*+ macrophages in two ventricular areas, the apex/injury site and the mid zone of ventricle/unaffected region. Together with Dr Stephen Cross from the Wolfson Bioimaging Facility, I was able to develop an automated Fiji plugin which allowed more rapid analysis of multiple cells with less bias. Using this imaging pipeline, I was able to investigate GFP+ distribution in cardiac macrophages (***Figure 5.4***). Significant differences in GFP level between ventricular regions was observed after injury (***Figure 5.4***).

Similar GFP levels were observed in macrophages in both areas analysed in uninjured fish whereas lower GFP was observed in macrophages at the injury site where there were no underling cardiomyocytes (***Figure 5.4***). This suggests that some of the GFP signal observed in macrophages in close proximity to cardiomyocytes (e.g. in uninjured regions) could result from bleed through of the GFP signal to the mCherry channel despite image acquisition parameters chosen to limit this possibility (***section 2.10***). To further limit the likelihood of bleed through between fluorescent channels I used the mean GFP value for each region as an internal control with only cells with GFP intensity above this value being taken forward for further analysis (***section 3.4****;* ***Figure 5.5A***). Even following this refinement, a significant reduction in GFP level in macrophages at the injury site was observed at 3, 7 and 14 dpi (***Figure 5.5A***). Although cardiomyocyte renewal is occurring by 14 dpi (Schnabel *et al.*, 2011) the injury area still appeared devoid of GFP signal at this stage (***Figure 5.7H***).

Interestingly, significant differences in GFP levels in the uninjured region were observed after injury (***Figure 5.5A***). There was a significant decrease in GFP level in macrophages in the uninjured region at 7 dpi but a significant increase at 14 dpi

when compared to the same region in uninjured fish (***Figure 5.5A***). This is despite these regions all exhibiting strong GFP signal in surrounding cardiomyocytes at all time points analysed (***Figure 5.7***). Analysis of the size and shape of cardiac macrophages in these regions indicates no significant differences between the mCherry+, GFP+ subset and remaining macrophages (***Figure 5.6***). In comparison, pro-regenerative mCherry+, *wt1b*$^{+}$ macrophages differ in morphology to the single *mpeg1*+ population (Sanz-Morejón *et al.*, 2019). Although both populations maintain typical myeloid shape, cytoplasmic area and irregular nuclear shape, the *wt1b*+ population are slightly larger and have greater cytoplasmic to nuclear ratio (Sanz-Morejón *et al.*, 2019). As the *myl7*+ macrophages described here maintain a more similar morphology to single positive mCherry+ macrophages, perhaps they represent a more pro-inflammatory rather than anti-inflammatory population. The relative percentage of mCherry+, GFP+ macrophages differs across the regions analysed (***Figure 5.5C***), but their total relative amount in the whole ventricle at different time points were similar to that observed by FACS (***Figure 4.3C***; ***Figure 5.5D***).

6.6. Potential explanations for GFP signal in cardiac macrophages

The automated detection of GFP+ macrophages in 3D allowed the tracking of individual cells and the ability to assess their GFP level *in situ*. Macrophages with a higher level of GFP are usually located in the uninjured myocardium and tend to accumulate in the border zone of the injury rather than directly at the injury site (***Figure 5.7A-H***), suggesting they may play a role in the recovery of cardiomyocytes. Although the observed GFP signal in cardiac macrophages was very low, often difficult to visualise and potentially still affected by bleed through between channels, careful assessment of both channels in 3D allowed the identification of three distinct processes which could explain *myl7* presence in cardiac macrophages: phagocytosis (demarked with yellow arrows, ***Figure 5.7Dii***), extracellular vesicle transport (demarked with white arrow, ***Figure 5.7Bii-iii, Di***) and endogenous expression of *myl7* (***Figure 5.7Ei,Fi***).

Clearance of dead cells and cellular debris by macrophages following injury is an indispensable process for successful tissue repair. Thus, this data can not completely exclude the possibility of active phagocytosis of GFP+ cardiomyocytes by

mCherry+ macrophages present in the injured ventricle, especially during the early inflammatory phase when phagocytic cells were observed (***Figure 5.7Dii***). In order to eliminate phagocytic macrophages from the image analysis, a fluorescent dye such as Lyso Tracker could be used to label acidic organelles like lysosomes within dissociated live cells prior to FACS (Warnes, 2015) and/or in whole mount fixed heart samples prior to confocal imaging (Song *et al.*, 2008), respectively.

Intriguingly**,** I also identified extracellular vesicle (EV) like particles enclosed in macrophages in the apex region of uninjured and 3 dpi fish (demarked with white arrows, ***Figure 5.7Bii-iii, Di***). No vesicle-like structures were observed in macrophages at later time points. EVs are membranous structures derived from cells which allow intercellular communication via molecule trafficking (i.e. lipid, protein and mRNA) (Van Niel, D'Angelo and Raposo, 2018) and studies have shown their importance in cardiac remodelling (Berezin and Berezin, 2020). Recently published work from our lab has shown that cardiomyocyte-derived EVs are present in the pericardial space of larval zebrafish (Scott *et al.*, 2021). Moreover, active transfer of cardiomyocyte and endothelial cell-derived EVs to cardiac resident macrophages in the homeostatic state was observed (Scott *et al.*, 2021). Therefore, this suggest that a fraction of the mCherry+, GFP+ macrophages in uninjured and 3 dpi hearts might contain EVs with cardiomyocyte-derived cargo. This previous study from our lab utilised transgenic lines with membrane tethered fluorophores (incorporated into the EV membrane produced by labelled cells) whereas the *myl7* line used in this study exhibits cytoplasmic GFP labelling. This may suggest that only larger EVs (containing more GFP) were detected here, potentially limiting the EV crosstalk between these cell types that could be observed.

Interestingly, I also observed cytoplasmic distribution of *myl7* in cardiac macrophages (***Figure 5.7Ei,Fi***), supporting the RT-PCR and FACS analysis described in this thesis, however, further studies to determine why macrophages are expressing these muscle/cardiomyocyte contractile proteins will still be required. Perhaps mRNA transcript and/or proteins forming cardiac contractile units are transcribed in cardiac macrophages and then transferred to cardiomyocytes, similar to what has been described for miRNA in the infarcted heart (Zheng, Gong and Chen, 2021), to provide 'spare parts' to the myocardium.

Imaging flow cytometry, where each recorded object is also imaged, of *myl7* expression would assist in establishing precise cellular localisation of the fluorophore (e.g. in vesicles, phagosomes or cytoplasm), as well as further ruling out contamination of signal between cells (*described in* ***section 4.5***). This could result from incomplete dissociation of cardiac tissues, as tissue resident macrophages are buried deeply in the myocardium. Alternatively, cytological analyses of FACS sorted populations followed by high resolution microscopy could identify morphology-phenotype correlation of *myl7* expressing macrophages and also exclude possible contamination (Li *et al.*, 2017). Perhaps, more advanced techniques such as RNAscope for *in situ* gene expression studies, either alone or in combination with traditional immunofluorescent (IF) staining, applied on optically cleared zebrafish hearts (Morrison, McKinney and Kulesa, 2017) could be a solution for the two major encountered limitations of this study (low mRNA quantities and overlapping spectra between channels). Tissue clearing is a chemical method of lipid, pigment and calcium removal to achieve transparency of the tissue (Ueda *et al.*, 2020), which results in minimized light scattering and absorption from adjacent cells allowing deeper penetration of the tissue, preserves nucleic acids and protein, thus allowing high quality 3D imaging of whole hearts (Ariel, 2017). RNA scope is multiplex assay, allowing precise spatial detection of up to three distinct fluorescently tagged mRNA transcripts in individual cells and allows transcript number quantification (Gross-Thebing, Paksa and Raz, 2014). Simultaneous detection of mRNA and protein via IF is also possible (Gross-Thebing, Paksa and Raz, 2014; Morrison, McKinney and Kulesa, 2017).

Recently, myoglobin bound iron released during skeletal muscle injury has been found in infiltrating macrophages up to 10 dpi (Corna *et al.*, 2016). It was suggested that the engulfed myoglobin acts as a temporary iron storage, preventing its oxidation, before it is transferred by the macrophages to regenerating fibres (Corna *et al.*, 2016). Perhaps a similar mechanism is observed in the injured heart muscle after cryoinjury. Apart from this study in skeletal muscle (Corna *et al.*, 2016), no previous study has reported endogenous expression of muscle proteins in macrophages. It has previously been shown that cardiac tissue resident macrophages in the mouse AV node and ventricle are enriched for cardiomyocyte genes associated with cardiac electrical conduction. Those cells in direct contact

with cardiomyocytes contribute to electrical conduction and maintain the synchronised heart beat (Hulsmans *et al.*, 2017). This study demonstrates that macrophages have unexpected roles in supporting cardiac function and so, perhaps, these macrophages can also contain a primitive sarcomeric structure to aid this unexpected function.

Similar to our finding in cardiac macrophages, endothelial cells have also been identified to express organ specific molecular signatures of parenchymal cells in the brain, lungs and heart (Jambusaria *et al.*, 2020). Interestingly, some of the highest expressed genes in mouse cardiac endothelial cells (ECs) found in this study (*Myh6, Mb*, *Actin* (*acta1a*), *Tnnt2* and *Tpm4*) are orthologues of the sarcomeric genes identified in our proteomic data. A second study, which focused only on cardiac ECs, confirmed these previous findings and extended the genes found to include *Tnnc1*, *Myl7* and *Myl4* (*cmlc1*) (Yucel *et al.*, 2020). Both of these studies observed expression of genes restricted to cardiac myofibril and metabolic genes (Jambusaria *et al.*, 2020; Yucel *et al.*, 2020). Furthermore, these studies determined that ECs and cardiomyocytes have open chromatin at myofibril genes with access to promotors and enhancers suggesting that active transcription of these genes is occurring in ECs (Yucel *et al.*, 2020). It was suggested that the ECs could undertake functions of the underlying parenchyma, but the exact consequences of this active transcription were not revealed. Following on from this work, I investigated Tabula Muris, an online atlas of transcriptomes obtained from 20 organs and tissues of mice (Schaum *et al.*, 2018). In this comprehensive study, single cell-transcriptomes of seven FACS sorted cardiac cell population were investigated (available in public data base: http://tabula-muris.ds.czbiohub.org/). Low transcript numbers of 8 orthologous genes (but not *myh7l*) encoding contractile proteins were found in cardiac leukocytes, however precise leukocyte populations were not distinguished (***Figure 6.1***). The expression level was similar to that observed from ECs (***Figure 6.1***). Interestingly, Tabula Muris and Yucel *et al.* indicates that single ECs do not contain all sarcomeric transcripts together suggesting that these cells cannot form a contractile unit. Determining if this is true in cardiac macrophages would help to determine if the expression of these genes can have a contractile function or if the individual components are more likely to be transferred to cardiomyocytes (perhaps via EVs).

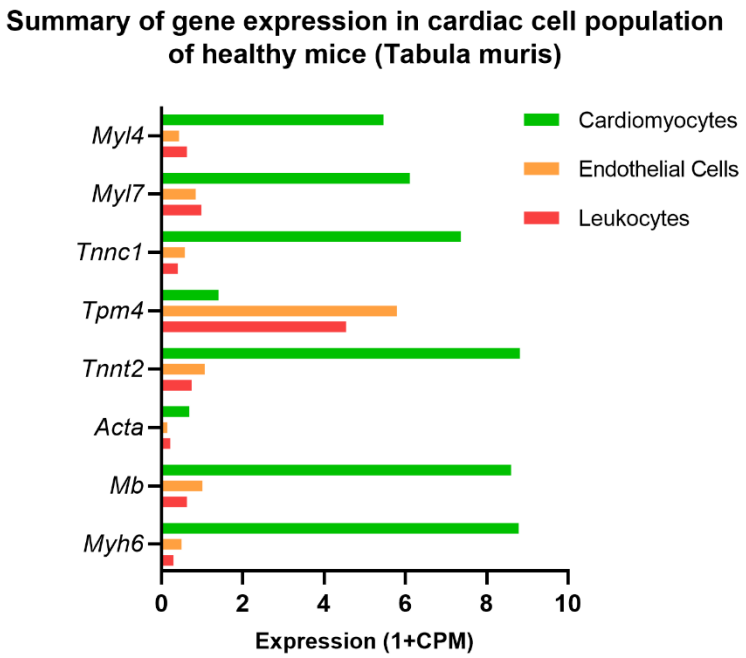

Figure 6.1. Summary of orthologous gene expression in three cardiac cell populations obtained from Tabula Muris. Eight orthologous genes to those identified in zebrafish proteomic data were also expressed in endothelial cells and leukocytes derived from healthy mouse hearts. Similar levels of expression of genes is observed between leukocytes and endothelial cells, which are lower than expression in cardiomyocytes. Expression is presented as 1+CPM, 1+ transcript copy per million.

6.7. Summary

In summary, I have confirmed that mRNA transcripts of six functional cardiac genes can be detected in cardiac macrophages following injury and five of these are also present in macrophages in healthy hearts. RQ analysis revealed a reduction of gene expression post injury suggesting roles in the homeostatic heart. Furthermore, using a combination of fluorescence imaging techniques, I have investigated *myl7* expression in cardiac macrophages during repair and regeneration. This analysis demonstrates that *myl7*+ macrophages respond to injury in a similar pattern to *myl7*- macrophages and this subset accounts for 20 – 48 % of total cardiac macrophage numbers. Although I could not determine precise levels of *myl7* expression via whole mount imaging, automated image analysis allowed the distribution of cardiac macrophages to be determined and identified three possible processes (phagocytosis, vesicle transport and endogenous expression) to explain the mRNA

transcript/protein presence in cardiac macrophages. Additionally, the data presented here suggests that both pro- and anti-inflammatory macrophages could contribute to these phenomena, corresponding with the initial unbiased proteomic results.

Cardiac repair and regeneration is a complex process, which involves interplay between all cardiac cell populations. Macrophage roles in cardiac homeostasis and post MI have been highlighted by many studies. Further work is required to understand and establish the role of cardiac mRNA/protein expression in cardiac macrophages during homeostasis and the significance of this expression in cardiac repair and regeneration. This could be achieved by answering a few important questions: *How does the expression of these genes change after injury?* Relative gene quantification in cardiac macrophages across all important cardiac repair and regeneration phases should be investigated. RT-qPCR has proven to be sensitive for detection low transcript levels in this study. However, such a robust gene expression analysis would require increased mRNA quantities, which was the main limitation of this study. *Which macrophage subsets are expressing this gene and where are they located?* My data has gone some way to answering this question but further analysis of different genes of interest would confirm these findings and further address the sub-cellular localisation of the resultant proteins. *What is the functional consequence of this gene expression in cardiac macrophages?* Zebrafish are amenable to genetic manipulation allowing strategies to be devised to block expression of these genes only in cardiac macrophages and determine the consequence on normal heart function and/or in the response to injury.

Bibliography

Adams, G. (2020) ‘A beginner’s guide to RT-PCR, qPCR and RT-qPCR’, *Biochemist*. doi: 10.1042/bio20200034.

Adan, A. *et al.* (2017) ‘Flow cytometry: basic principles and applications’, *Critical Reviews in Biotechnology*. doi: 10.3109/07388551.2015.1128876.

Adler, C. P. *et al.* (1996) ‘Variability of cardiomyocyte DNA content, ploidy level and nuclear number in mammalian hearts’, *Virchows Archiv*. doi: 10.1007/BF00192438.

Ahuja, P., Sdek, P. and MacLellan, W. R. (2007) ‘Cardiac myocyte cell cycle control in development, disease, and regeneration’, *Physiological Reviews*. doi: 10.1152/physrev.00032.2006.

Alabas, O. A. *et al.* (2020) ‘Statistics on mortality following acute myocardial infarction in 842 897 Europeans’, *Cardiovascular Research*. doi: 10.1093/cvr/cvz197.

Van Amerongen, M. J. *et al.* (2007) ‘Macrophage depletion impairs wound healing and increases left ventricular remodeling after myocardial injury in mice’, *American Journal of Pathology*. doi: 10.2353/ajpath.2007.060547.

Ariel, P. (2017) ‘A beginner’s guide to tissue clearing’, *International Journal of Biochemistry and Cell Biology*. doi: 10.1016/j.biocel.2016.12.009.

Aurora, A. B. *et al.* (2014) ‘Macrophages are required for neonatal heart regeneration’, *Journal of Clinical Investigation*. doi: 10.1172/JCI72181.

Azevedo, P. S. *et al.* (2016) ‘Cardiac Remodeling: Concepts, Clinical Impact, Pathophysiological Mechanisms and Pharmacologic Treatment’, *Arquivos brasileiros de cardiologia*. doi: 10.5935/abc.20160005.

Bakkers, J. (2011) ‘Zebrafish as a model to study cardiac development and human cardiac disease’, *Cardiovascular Research*. doi: 10.1093/cvr/cvr098.

Barteneva, N. S., Fasler-Kan, E. and Vorobjev, I. A. (2012) ‘Imaging Flow Cytometry: Coping with Heterogeneity in Biological Systems’, *Journal of Histochemistry and Cytochemistry*. doi: 10.1369/0022155412453052.

Basu, S. *et al.* (2010) ‘Purification of specific cell population by fluorescence activated cell sorting (FACS)’, *Journal of Visualized Experiments*. doi: 10.3791/1546.

Bednarek, D. *et al.* (2015) ‘Telomerase Is Essential for Zebrafish Heart Regeneration’, *Cell Reports*. doi: 10.1016/j.celrep.2015.07.064.

Beffagna, G. (2019) ‘Zebrafish as a Smart Model to Understand Regeneration After Heart Injury: How Fish Could Help Humans’, *Frontiers in Cardiovascular Medicine*. doi: 10.3389/fcvm.2019.00107.

Benard, E. L. *et al.* (2015) ‘Macrophage-expressed perforins Mpeg1 and Mpeg1.2 have an anti-bacterial function in zebrafish’, *Journal of Innate Immunity*. doi: 10.1159/000366103.

Berdougo, E. *et al.* (2003) ‘Mutation of weak atrium/atrial myosin heavy chain disrupts atrial function and influences ventricular morphogenesis in zebrafish’, *Development*. doi: 10.1242/dev.00838.

Berezin, A. E. and Berezin, A. A. (2020) ‘Extracellular Endothelial Cell-Derived Vesicles: Emerging Role in Cardiac and Vascular Remodeling in Heart Failure’, *Frontiers in Cardiovascular Medicine*. doi: 10.3389/fcvm.2020.00047.

Bergmann, O. *et al.* (2009) ‘Evidence for cardiomyocyte renewal in humans’, *Science*. doi: 10.1126/science.1164680.

Bergmann, O. *et al.* (2015) ‘Dynamics of Cell Generation and Turnover in the Human Heart’, *Cell*. doi: 10.1016/j.cell.2015.05.026.

Van Berlo, J. H. *et al.* (2014) ‘C-kit+ cells minimally contribute cardiomyocytes to the heart’, *Nature*. doi: 10.1038/nature13309.

Bersell, K. *et al.* (2009) ‘Neuregulin1/ErbB4 Signaling Induces Cardiomyocyte Proliferation and Repair of Heart Injury’, *Cell*. doi: 10.1016/j.cell.2009.04.060.

Bertozzi, A. *et al.* (2021) ‘Is zebrafish heart regeneration “complete”? Lineage-restricted cardiomyocytes proliferate to pre-injury numbers but some fail to differentiate in fibrotic hearts’, *Developmental Biology*. doi: 10.1016/j.ydbio.2020.12.004.

Bevan, L. *et al.* (2020) ‘Specific macrophage populations promote both cardiac scar deposition and subsequent resolution in adult zebrafish’, *Cardiovascular Research*. doi: 10.1093/CVR/CVZ221.

Bise, T. *et al.* (2020) ‘Multiple cryoinjuries modulate the efficiency of zebrafish heart regeneration’, *Scientific Reports*. doi: 10.1038/s41598-020-68200-1.

Brodsky, V. Y., Chernyaev, A. L. and Vasilyeva, I. A. (1992) ‘Variability of the cardiomyocyte ploidy in normal human hearts’, *Virchows Archiv B Cell Pathology Including Molecular Pathology*. doi: 10.1007/BF02890430.

Büscher, M. (2019) ‘Flow Cytometry Instrumentation – An Overview’, *Current Protocols in Cytometry*. doi: 10.1002/cpcy.52.

Cano-Martínez, A. *et al.* (2010) ‘Functional and structural regeneration in the axolotl heart (Ambystoma mexicanum) after partial ventricular amputation’, *Archivos de Cardiologia de Mexico*.

Canton, J. *et al.* (2014) ‘Contrasting phagosome pH regulation and maturation in human M1 and M2 macrophages’, *Molecular Biology of the Cell*. doi: 10.1091/mbc.E14-05-0967.

Chablais, F. *et al.* (2011) ‘The zebrafish heart regenerates after cryoinjury-induced myocardial infarction’, *BMC Developmental Biology*. doi: 10.1186/1471-213X-11-21.

Chablais, F. and Jaźwińska, A. (2012a) ‘Induction of myocardial infarction in adult zebrafish using cryoinjury’, *Journal of Visualized Experiments*. doi: 10.3791/3666.

Chablais, F. and Jaźwińska, A. (2012b) ‘The regenerative capacity of the zebrafish heart is dependent on TGFβ signaling’, *Development*. doi: 10.1242/dev.078543.

Corna, G. *et al.* (2016) ‘The Repair of Skeletal Muscle Requires Iron Recycling through Macrophage Ferroportin’, *The Journal of Immunology*. doi: 10.4049/jimmunol.1501417.

Cossins, A. R. *et al.* (2009) ‘Diverse cell-specific expression of myoglobin isoforms in brain, kidney, gill and liver of the hypoxia-tolerant carp and zebrafish’, *Journal of Experimental Biology*. doi: 10.1242/jeb.026286.

Daigneault, M. *et al.* (2010) ‘The identification of markers of macrophage differentiation in PMA-stimulated THP-1 cells and monocyte-derived macrophages’, *PLoS ONE*. doi: 10.1371/journal.pone.0008668.

Darehzereshki, A. *et al.* (2015) ‘Differential regenerative capacity of neonatal mouse hearts after cryoinjury’, *Developmental Biology*. doi: 10.1016/j.ydbio.2014.12.018.

Dee, C. T. *et al.* (2016) ‘CD4-Transgenic Zebrafish Reveal Tissue-Resident Th2- and Regulatory T Cell–like Populations and Diverse Mononuclear Phagocytes’, *The Journal of Immunology*. doi: 10.4049/jimmunol.1600959.

Desjardins, C. and Naya, F. (2016) ‘The Function of the MEF2 Family of Transcription Factors in Cardiac Development, Cardiogenomics, and Direct Reprogramming’, *Journal of Cardiovascular Development and Disease*. doi: 10.3390/jcdd3030026.

Dick, S. A. *et al.* (2019) ‘Self-renewing resident cardiac macrophages limit adverse remodeling following myocardial infarction’, *Nature Immunology*. doi: 10.1038/s41590-018-0272-2.

Dittrich, A. and Lauridsen, H. (2019) ‘Myocardial infarction and the immune response - Scarring or regeneration? A comparative look at mammals and popular regenerating animal models’, *Journal of Immunology and Regenerative Medicine*. doi: 10.1016/j.regen.2019.100016.

Dube, D. K. *et al.* (2017) ‘Identification, characterization, and expression of sarcomeric tropomyosin isoforms in zebrafish’, *Cytoskeleton*. doi: 10.1002/cm.21352.

Dunn, K. W., Kamocka, M. M. and McDonald, J. H. (2011) ‘A practical guide to evaluating colocalization in biological microscopy’, *American Journal of Physiology - Cell Physiology*. doi: 10.1152/ajpcell.00462.2010.

Ellett, F. *et al.* (2011) ‘mpeg1 promoter transgenes direct macrophage-lineage expression in zebrafish’, *Blood*. doi: 10.1182/blood-2010-10-314120.

Epelman, S. *et al.* (2014) ‘Embryonic and adult-derived resident cardiac

macrophages are maintained through distinct mechanisms at steady state and during inflammation', *Immunity*. doi: 10.1016/j.immuni.2013.11.019.

Frangogiannis, N. G. (2015) 'Pathophysiology of myocardial infarction', *Comprehensive Physiology*. doi: 10.1002/cphy.c150006.

Frodermann, V. and Nahrendorf, M. (2018) 'Macrophages and cardiovascular health', *Physiological Reviews*. doi: 10.1152/physrev.00068.2017.

Gan, P., Patterson, M. and Sucov, H. M. (2020) 'Cardiomyocyte Polyploidy and Implications for Heart Regeneration', *Annual Review of Physiology*. doi: 10.1146/annurev-physiol-021119-034618.

Gentek, R., Molawi, K. and Sieweke, M. H. (2014) 'Tissue macrophage identity and self-renewal', *Immunological Reviews*. doi: 10.1111/imr.12224.

Geoffrey Burns, C. *et al.* (2005) 'High-Throughput Assay for Small Molecules That Modulate Zebrafish Embryonic Heart Rate', *Nature Chemical Biology*. doi: 10.1038/nchembio732.

George, V., Colombo, S. and Targoff, K. L. (2015) 'An early requirement for nkx2.5 ensures the first and second heart field ventricular identity and cardiac function into adulthood', *Developmental Biology*. doi: 10.1016/j.ydbio.2014.12.019.

Giardoglou, P. and Beis, D. (2019) 'On zebrafish disease models and matters of the heart', *Biomedicines*. doi: 10.3390/biomedicines7010015.

Gistelinck, C. *et al.* (2016) 'Zebrafish Collagen Type I: Molecular and Biochemical Characterization of the Major Structural Protein in Bone and Skin', *Scientific Reports*. doi: 10.1038/srep21540.

González-Rosa, J. M. *et al.* (2011) 'Extensive scar formation and regression during heart regeneration after cryoinjury in zebrafish', *Development*. doi: 10.1242/dev.060897.

González-Rosa, J. M. *et al.* (2018) 'Myocardial Polyploidization Creates a Barrier to Heart Regeneration in Zebrafish', *Developmental Cell*. doi: 10.1016/j.devcel.2018.01.021.

González-Rosa, J. M. and Mercader, N. (2012) ‘Cryoinjury as a myocardial infarction model for the study of cardiac regeneration in the zebrafish’, *Nature Protocols*. doi: 10.1038/nprot.2012.025.

González-Rosa, J. M., Peralta, M. and Mercader, N. (2012) ‘Pan-epicardial lineage tracing reveals that epicardium derived cells give rise to myofibroblasts and perivascular cells during zebrafish heart regeneration’, *Developmental Biology*. doi: 10.1016/j.ydbio.2012.07.007.

Goren, I. *et al.* (2009) ‘A transgenic mouse model of inducible macrophage depletion: Effects of diphtheria toxin-driven lysozyme m-specific cell lineage ablation on wound inflammatory, angiogenic, and contractive processes’, *American Journal of Pathology*. doi: 10.2353/ajpath.2009.081002.

Gray, C. *et al.* (2011) ‘Simultaneous intravital imaging of macrophage and neutrophil behaviour during inflammation using a novel transgenic zebrafish’, *Thrombosis and Haemostasis*. doi: 10.1160/TH10-08-0525.

Gross-Thebing, T., Paksa, A. and Raz, E. (2014) ‘Simultaneous high-resolution detection of multiple transcripts combined with localization of proteins in whole-mount embryos’, *BMC Biology*. doi: 10.1186/s12915-014-0055-7.

Heidt, T. *et al.* (2014) ‘Differential contribution of monocytes to heart macrophages in steady-state and after myocardial infarction’, *Circulation Research*. doi: 10.1161/CIRCRESAHA.115.303567.

Hein, S. J. *et al.* (2015) ‘Advanced echocardiography in adult zebrafish reveals delayed recovery of heart function after myocardial cryoinjury’, *PLoS ONE*. doi: 10.1371/journal.pone.0122665.

Hesse, M. *et al.* (2021) ‘Proximity to injury, but neither number of nuclei nor ploidy define pathological adaptation and plasticity in cardiomyocytes’, *Journal of Molecular and Cellular Cardiology*. doi: 10.1016/j.yjmcc.2020.11.012.

Honkoop, H. *et al.* (2019) ‘Single-cell analysis uncovers that metabolic reprogramming by ErbB2 signaling is essential for cardiomyocyte proliferation in the regenerating heart’, *eLife*. doi: 10.7554/eLife.50163.

Howe, K. *et al.* (2013) ‘The zebrafish reference genome sequence and its relationship to the human genome’, *Nature*. doi: 10.1038/nature12111.

Hu, N. *et al.* (2000) ‘Structure and function of the developing zebrafish heart’, *Anatomical Record*. doi: 10.1002/1097-0185(20001001)260:2<148::AID-AR50>3.0.CO;2-X.

Huang, W., Zhang, R. and Xu, X. (2009) ‘Myofibrillogenesis in the developing zebrafish heart: A functional study of tnnt2’, *Developmental Biology*. doi: 10.1016/j.ydbio.2009.04.039.

Hulsmans, M. *et al.* (2017) ‘Macrophages Facilitate Electrical Conduction in the Heart’, *Cell*. doi: 10.1016/j.cell.2017.03.050.

Ibanez, B. *et al.* (2018) ‘2017 ESC Guidelines for the management of acute myocardial infarction in patients presenting with ST-segment elevation’, *European Heart Journal*. doi: 10.1093/eurheartj/ehx393.

Jambusaria, A. *et al.* (2020) ‘Endothelial heterogeneity across distinct vascular beds during homeostasis and inflammation’, *eLife*. doi: 10.7554/eLife.51413.

Jaspers, R. T. *et al.* (2014) ‘Increased oxidative metabolism and myoglobin expression in zebrafish muscle during chronic hypoxia’, *Biology Open*. doi: 10.1242/bio.20149167.

Jopling, C. *et al.* (2010) ‘Zebrafish heart regeneration occurs by cardiomyocyte dedifferentiation and proliferation’, *Nature*. doi: 10.1038/nature08899.

Jung, K. *et al.* (2013) ‘Endoscopic time-lapse imaging of immune cells in infarcted mouse hearts’, *Circulation Research*. doi: 10.1161/CIRCRESAHA.111.300484.

Kain, V. *et al.* (2015) ‘Resolvin D1 activates the inflammation resolving response at splenic and ventricular site following myocardial infarction leading to improved ventricular function’, *Journal of Molecular and Cellular Cardiology*. doi: 10.1016/j.yjmcc.2015.04.003.

Kain, V., Prabhu, S. D. and Halade, G. V. (2014) ‘Inflammation revisited: inflammation versus resolution of inflammation following myocardial infarction’, *Basic*

Research in Cardiology. doi: 10.1007/s00395-014-0444-7.

Khodayari, S. *et al.* (2019) 'Inflammatory microenvironment of acute myocardial infarction prevents regeneration of heart with stem cells therapy', *Cellular Physiology and Biochemistry*. doi: 10.33594/000000180.

Kikuchi, K. *et al.* (2010) 'Primary contribution to zebrafish heart regeneration by gata4+ cardiomyocytes', *Nature*. doi: 10.1038/nature08804.

Kikuchi, K. *et al.* (2011) 'Retinoic Acid Production by Endocardium and Epicardium Is an Injury Response Essential for Zebrafish Heart Regeneration', *Developmental Cell*. doi: 10.1016/j.devcel.2011.01.010.

Koetsier, G. and Cantor, E. (2019) 'A Practical Guide to Analyzing Nucleic Acid Concentration and Purity with Microvolume Spectrophotometers', *New England Biolabs*, 1(1), pp. 1–8. Available at: https://www.neb.com/-/media/catalog/application-notes/mvs_analysis_of_na_concentration_and_purity.pdf?rev=be7c8e19f4d34e558527496ea51623dc (Accessed: 24 July 2021).

Koster, R. and Sassen, W. A. (2015) 'A molecular toolbox for genetic manipulation of zebrafish', *Advances in Genomics and Genetics*. doi: 10.2147/agg.s57585.

Kosuge, M. *et al.* (2006) 'Differences between men and women in terms of clinical features of ST-segment elevation acute myocardial infarction', *Circulation Journal*. doi: 10.1253/circj.70.222.

Krenning, G., Zeisberg, E. M. and Kalluri, R. (2010) 'The origin of fibroblasts and mechanism of cardiac fibrosis', *Journal of Cellular Physiology*. doi: 10.1002/jcp.22322.

Laflamme, M. A. and Murry, C. E. (2005) 'Regenerating the heart', *Nature Biotechnology*. doi: 10.1038/nbt1117.

Lai, S. L. *et al.* (2017) 'Reciprocal analyses in zebrafish and medaka reveal that harnessing the immune response promotes cardiac regeneration', *eLife*. doi: 10.7554/eLife.25605.

Lai, S. L., Marín-Juez, R. and Stainier, D. Y. R. (2019) 'Immune responses in cardiac

repair and regeneration: a comparative point of view', *Cellular and Molecular Life Sciences*. doi: 10.1007/s00018-018-2995-5.

Lavine, K. J. *et al.* (2014) 'Distinct macrophage lineages contribute to disparate patterns of cardiac recovery and remodeling in the neonatal and adult heart', *Proceedings of the National Academy of Sciences of the United States of America*. doi: 10.1073/pnas.1406508111.

Lepilina, A. *et al.* (2006) 'A Dynamic Epicardial Injury Response Supports Progenitor Cell Activity during Zebrafish Heart Regeneration', *Cell*. doi: 10.1016/j.cell.2006.08.052.

Li, J. and Eberwine, J. (2018) 'The successes and future prospects of the linear antisense RNA amplification methodology', *Nature Protocols*. doi: 10.1038/nprot.2018.011.

Li, Z. *et al.* (2017) 'Utilization of cytocentrifugation slides in flow cytometry laboratory: a tool for correlation of morphology and immunonophenotype', *Journal of Hematopathology*. doi: 10.1007/s12308-017-0299-6.

Liew, L. C., Ho, B. X. and Soh, B. S. (2020) 'Mending a broken heart: Current strategies and limitations of cell-based therapy', *Stem Cell Research and Therapy*. doi: 10.1186/s13287-020-01648-0.

Loontiens, S. *et al.* (2019) 'Purification of high-quality RNA from a small number of fluorescence activated cell sorted zebrafish cells for RNA sequencing purposes', *BMC Genomics*. doi: 10.1186/s12864-019-5608-2.

Lu, L. *et al.* (2015) 'Myocardial Infarction: Symptoms and Treatments', *Cell Biochemistry and Biophysics*. doi: 10.1007/s12013-015-0553-4.

Mack, E., Neubauer, A. and Brendel, C. (2007) 'Comparison of RNA yield from small cell populations sorted by flow cytometry applying different isolation procedures', *Cytometry Part A*. doi: 10.1002/cyto.a.20391.

Mahmoud, A. I. *et al.* (2014) 'Surgical models for cardiac regeneration in neonatal mice', *Nature Protocols*. doi: 10.1038/nprot.2014.021.

Mann, D. L. (1999) ‘Mechanisms and models in heart failure: A combinatorial approach’, *Circulation*. doi: 10.1161/01.CIR.100.9.999.

Marín-Juez, R. *et al.* (2016) ‘Fast revascularization of the injured area is essential to support zebrafish heart regeneration’, *Proceedings of the National Academy of Sciences of the United States of America*. doi: 10.1073/pnas.1605431113.

Marjoram, L. *et al.* (2015) ‘Epigenetic control of intestinal barrier function and inflammation in zebrafish’, *Proceedings of the National Academy of Sciences of the United States of America*. doi: 10.1073/pnas.1424089112.

McCurley, A. T. and Callard, G. V. (2008) ‘Characterization of housekeeping genes in zebrafish: Male-female differences and effects of tissue type, developmental stage and chemical treatment’, *BMC Molecular Biology*. doi: 10.1186/1471-2199-9-102.

McWhorter, F. Y. *et al.* (2013) ‘Modulation of macrophage phenotype by cell shape’, *Proceedings of the National Academy of Sciences of the United States of America*. doi: 10.1073/pnas.1308887110.

Moriarty, M. A. *et al.* (2012) ‘Loss of plakophilin 2 disrupts heart development in zebrafish’, *International Journal of Developmental Biology*. doi: 10.1387/ijdb.113390mm.

Morrison, J. A., McKinney, M. C. and Kulesa, P. M. (2017) ‘Resolving in vivo gene expression during collective cell migration using an integrated RNAscope, immunohistochemistry and tissue clearing method’, *Mechanisms of Development*. doi: 10.1016/j.mod.2017.06.004.

Moyse, B. R. and Richardson, R. J. (2020) ‘ A Population of Injury-Responsive Lymphoid Cells Expresses mpeg1.1 in the Adult Zebrafish Heart ’, *ImmunoHorizons*. doi: 10.4049/immunohorizons.2000063.

Münch, J. *et al.* (2017) ‘Notch signalling restricts inflammation and Serpine1 expression in the dynamic endocardium of the regenerating zebrafish heart’, *Development (Cambridge)*. doi: 10.1242/dev.143362.

Murray, P. J. and Wynn, T. A. (2011) ‘Protective and pathogenic functions of

macrophage subsets', *Nature Reviews Immunology*. doi: 10.1038/nri3073.

Nahrendorf, M. *et al.* (2007) 'The healing myocardium sequentially mobilizes two monocyte subsets with divergent and complementary functions', *Journal of Experimental Medicine*. doi: 10.1084/jem.20070885.

Nemtsas, P. *et al.* (2010) 'Adult zebrafish heart as a model for human heart? An electrophysiological study', *Journal of Molecular and Cellular Cardiology*. doi: 10.1016/j.yjmcc.2009.08.034.

Nguyen-Chi, M. *et al.* (2015) 'Identification of polarized macrophage subsets in zebrafish', *eLife*. doi: 10.7554/eLife.07288.

Van Niel, G., D'Angelo, G. and Raposo, G. (2018) 'Shedding light on the cell biology of extracellular vesicles', *Nature Reviews Molecular Cell Biology*. doi: 10.1038/nrm.2017.125.

Notari, M. *et al.* (2018) 'The local microenvironment limits the regenerative potential of the mouse neonatal heart', *Science Advances*. doi: 10.1126/sciadv.aao5553.

O'Rourke, S. A., Dunne, A. and Monaghan, M. G. (2019) 'The Role of Macrophages in the Infarcted Myocardium: Orchestrators of ECM Remodeling', *Frontiers in Cardiovascular Medicine*. doi: 10.3389/fcvm.2019.00101.

OBERPRILLER, J. O. *et al.* (1995) 'Stimulation of Proliferative Events in the Adult Amphibian Cardiac Myocyte', *Annals of the New York Academy of Sciences*. doi: 10.1111/j.1749-6632.1995.tb17404.x.

van Opbergen, C. J. M. *et al.* (2018) 'Cardiac Ca 2+ signalling in zebrafish: Translation of findings to man', *Progress in Biophysics and Molecular Biology*. doi: 10.1016/j.pbiomolbio.2018.05.002.

Paddock, S. W. and Eliceiri, K. W. (2014) 'Laser scanning confocal microscopy: History, applications, and related optical sectioning techniques', *Methods in Molecular Biology*. doi: 10.1007/978-1-60761-847-8_2.

Parameswaran, N. and Patial, S. (2010) 'Tumor Necrosis Factor-α Signaling in Macrophages Narayanan', *Advances in Global Change Research*.

de Pater, E. *et al.* (2009) ‘Distinct phases of cardiomyocyte differentiation regulate growth of the zebrafish heart’, *Development*. doi: 10.1242/dev.030924.

Patra, C. *et al.* (2017) ‘The zebrafish ventricle: A hub of cardiac endothelial cells for in vitro cell behavior studies’, *Scientific Reports*. doi: 10.1038/s41598-017-02461-1.

Patterson, M. *et al.* (2017) ‘Frequency of mononuclear diploid cardiomyocytes underlies natural variation in heart regeneration’, *Nature Genetics*. doi: 10.1038/ng.3929.

Pfaffl, M. W. (2001) ‘A new mathematical model for relative quantification in real-time RT-PCR’, *Nucleic Acids Research*. doi: 10.1093/nar/29.9.e45.

Pinto, A. R. *et al.* (2016) ‘Revisiting cardiac cellular composition’, *Circulation Research*. doi: 10.1161/CIRCRESAHA.115.307778.

Poon, K. L. *et al.* (2016) ‘Development of the cardiac conduction system in zebrafish’, *Gene Expression Patterns*. doi: 10.1016/j.gep.2016.08.003.

Porrello, E. R. *et al.* (2011) ‘Transient regenerative potential of the neonatal mouse heart’, *Science*. doi: 10.1126/science.1200708.

Porrello, E. R. *et al.* (2013) ‘Regulation of neonatal and adult mammalian heart regeneration by the miR-15 family’, *Proceedings of the National Academy of Sciences of the United States of America*. doi: 10.1073/pnas.1208863110.

Poss, K. D., Wilson, L. G. and Keating, M. T. (2002) ‘Heart regeneration in zebrafish’, *Science*. doi: 10.1126/science.1077857.

Prabhu, S. D. and Frangogiannis, N. G. (2016) ‘The biological basis for cardiac repair after myocardial infarction’, *Circulation Research*. doi: 10.1161/CIRCRESAHA.116.303577.

De Preux Charles, A. S. *et al.* (2016) ‘Distinct effects of inflammation on preconditioning and regeneration of the adult zebrafish heart’, *Open Biology*. doi: 10.1098/rsob.160102.

Rassier, D. E. (2017) ‘Sarcomere mechanics in striated muscles: From molecules to

sarcomeres to cells', *American Journal of Physiology - Cell Physiology*. doi: 10.1152/ajpcell.00050.2017.

Raya, A. *et al.* (2003) 'Activation of Notch signaling pathway precedes heart regeneration in zebrafish', *Proceedings of the National Academy of Sciences of the United States of America*. doi: 10.1073/pnas.1834204100.

Renard, M. *et al.* (2018) 'Expressed repetitive elements are broadly applicable reference targets for normalization of reverse transcription-qPCR data in mice', *Scientific Reports*. doi: 10.1038/s41598-018-25389-6.

Richardson, W. J. *et al.* (2015) 'Physiological implications of myocardial scar structure', *Comprehensive Physiology*. doi: 10.1002/cphy.c140067.

Roesner, A., Hankeln, T. and Burmester, T. (2006) 'Hypoxia induces a complex response of globin expression in zebrafish (Danio rerio)', *Journal of Experimental Biology*. doi: 10.1242/jeb.02243.

Rooijen, N. Van and Sanders, A. (1994) 'Liposome mediated depletion of macrophages: mechanism of action, preparation of liposomes and applications', *Journal of Immunological Methods*. doi: 10.1016/0022-1759(94)90012-4.

Ryan, R., Moyse, B. R. and Richardson, R. J. (2020) 'Zebrafish cardiac regeneration—looking beyond cardiomyocytes to a complex microenvironment', *Histochemistry and Cell Biology*. doi: 10.1007/s00418-020-01913-6.

Sallin, P. *et al.* (2015) 'A dual epimorphic and compensatory mode of heart regeneration in zebrafish', *Developmental Biology*. doi: 10.1016/j.ydbio.2014.12.002.

Sánchez-Iranzo, H. *et al.* (2018) 'Transient fibrosis resolves via fibroblast inactivation in the regenerating zebrafish heart', *Proceedings of the National Academy of Sciences of the United States of America*. doi: 10.1073/pnas.1716713115.

Sander, V. *et al.* (2013) 'Isolation and in vitroculture of primary cardiomyocytes from adult zebrafish hearts', *Nature Protocols*. doi: 10.1038/nprot.2013.041.

Sanz-Morejón, A. *et al.* (2019) 'Wilms Tumor 1b Expression Defines a Pro-regenerative Macrophage Subtype and Is Required for Organ Regeneration in the

Zebrafish', *Cell Reports*. doi: 10.1016/j.celrep.2019.06.091.

Saxena, A. *et al.* (2013) 'IL-1 Induces Proinflammatory Leukocyte Infiltration and Regulates Fibroblast Phenotype in the Infarcted Myocardium', *The Journal of Immunology*. doi: 10.4049/jimmunol.1300725.

Schaum, N. *et al.* (2018) 'Single-cell transcriptomics of 20 mouse organs creates a Tabula Muris', *Nature 2018 562:7727*. Nature Publishing Group, 562(7727), pp. 367–372. doi: 10.1038/s41586-018-0590-4.

Schindelin, J. *et al.* (2012) 'Fiji: An open-source platform for biological-image analysis', *Nature Methods*. doi: 10.1038/nmeth.2019.

Schmidt-Weber, C. B. *et al.* (1996) 'Apoptotic cell death in activated monocytes following incorporation of clodronate-liposomes', *Journal of Leukocyte Biology*. doi: 10.1002/jlb.60.2.230.

Schnabel, K. *et al.* (2011) 'Regeneration of cryoinjury induced necrotic heart lesions in zebrafish is associated with epicardial activation and cardiomyocyte proliferation', *PLoS ONE*. doi: 10.1371/journal.pone.0018503.

Schroeder, A. *et al.* (2006) 'The RIN: An RNA integrity number for assigning integrity values to RNA measurements', *BMC Molecular Biology*. doi: 10.1186/1471-2199-7-3.

Scott, A. *et al.* (2021) 'In Vivo Characterization of Endogenous Cardiovascular Extracellular Vesicles in Larval and Adult Zebrafish', *Arteriosclerosis, Thrombosis, and Vascular Biology*. doi: 10.1161/atvbaha.121.316539.

Sedletcaia, A. and Evans, T. (2011) 'Heart chamber size in zebrafish is regulated redundantly by duplicated tbx2 genes', *Developmental Dynamics*. doi: 10.1002/dvdy.22622.

Sedmera, D. *et al.* (2003) 'Functional and morphological evidence for a ventricular conduction system in zebrafish and Xenopus hearts', *American Journal of Physiology - Heart and Circulatory Physiology*. doi: 10.1152/ajpheart.00870.2002.

Senyo, S. E. *et al.* (2013) 'Mammalian heart renewal by pre-existing

cardiomyocytes', *Nature*. doi: 10.1038/nature11682.

Shanker, S. *et al.* (2015) 'Evaluation of commercially available RNA amplification kits for RNA sequencing using very low input amounts of total RNA', *Journal of Biomolecular Techniques*. doi: 10.7171/jbt.15-2601-001.

Shi, J. *et al.* (2018) 'Cre driver mice targeting macrophages', in *Methods in Molecular Biology*. doi: 10.1007/978-1-4939-7837-3_24.

Shih, Y. H. *et al.* (2015) 'Cardiac Transcriptome and Dilated Cardiomyopathy Genes in Zebrafish', *Circulation: Cardiovascular Genetics*. doi: 10.1161/CIRCGENETICS.114.000702.

Shinoda, H., Shannon, M. and Nagai, T. (2018) 'Fluorescent proteins for investigating biological events in acidic environments', *International Journal of Molecular Sciences*. doi: 10.3390/ijms19061548.

Shiraishi, M. *et al.* (2016) 'Alternatively activated macrophages determine repair of the infarcted adult murine heart', *Journal of Clinical Investigation*. doi: 10.1172/JCI85782.

Simões, F. C. *et al.* (2020) 'Macrophages directly contribute collagen to scar formation during zebrafish heart regeneration and mouse heart repair', *Nature Communications*. doi: 10.1038/s41467-019-14263-2.

Sogah, V. M. *et al.* (2010) 'Distinct troponin C isoform requirements in cardiac and skeletal muscle', *Developmental Dynamics*. doi: 10.1002/dvdy.22445.

Song, J. W. *et al.* (2008) 'Lysosomal activity associated with developmental axon pruning', *Journal of Neuroscience*. doi: 10.1523/JNEUROSCI.0720-08.2008.

Soonpaa, M. H. *et al.* (1996) 'Cardiomyocyte DNA synthesis and binucleation during murine development', *American Journal of Physiology - Heart and Circulatory Physiology*. doi: 10.1152/ajpheart.1996.271.5.h2183.

Spath, N. B., Mills, N. L. and Cruden, N. L. (2016) 'Novel cardioprotective and regenerative therapies in acute myocardial infarction: A review of recent and ongoing clinical trials', *Future Cardiology*. doi: 10.2217/fca-2016-0044.

Squire, J. M. (2016) ‘Muscle contraction: Sliding filament history, sarcomere dynamics and the two Huxleys’, *Global Cardiology Science and Practice*. doi: 10.21542/gcsp.2016.11.

St Croix, C. M., Shand, S. H. and Watkins, S. C. (2005) ‘Confocal microscopy: comparisons, applications, and problems.’, *BioTechniques*. doi: 10.2144/000112089.

Strungs, E. G. *et al.* (2013) ‘Cryoinjury models of the adult and neonatal mouse heart for studies of scarring and regeneration’, *Methods in Molecular Biology*. doi: 10.1007/978-1-62703-505-7_20.

Sultana, N. *et al.* (2015) ‘Resident c-kit + cells in the heart are not cardiac stem cells’, *Nature Communications*. doi: 10.1038/ncomms9701.

Talman, V. and Ruskoaho, H. (2016) ‘Cardiac fibrosis in myocardial infarction—from repair and remodeling to regeneration’, *Cell and Tissue Research*. doi: 10.1007/s00441-016-2431-9.

Tang, R. *et al.* (2007) ‘Validation of zebrafish (Danio rerio) reference genes for quantitative real-time RT-PCR normalization’, *Acta Biochimica et Biophysica Sinica*. doi: 10.1111/j.1745-7270.2007.00283.x.

Targoff, K. L. *et al.* (2013) ‘Nkx genes are essential for maintenance of ventricular identity’, *Development (Cambridge)*. doi: 10.1242/dev.095562.

Targoff, K. L., Schell, T. and Yelon, D. (2008) ‘Nkx genes regulate heart tube extension and exert differential effects on ventricular and atrial cell number’, *Developmental Biology*. doi: 10.1016/j.ydbio.2008.07.037.

Taylor, S. *et al.* (2010) ‘A practical approach to RT-qPCR-Publishing data that conform to the MIQE guidelines’, *Methods*. doi: 10.1016/j.ymeth.2010.01.005.

Thackeray, J. T. and Bengel, F. M. (2018) ‘Molecular Imaging of Myocardial Inflammation With Positron Emission Tomography Post-Ischemia: A Determinant of Subsequent Remodeling or Recovery’, *JACC: Cardiovascular Imaging*. doi: 10.1016/j.jcmg.2018.05.026.

Tsai, C. T. *et al.* (2011) ‘In-vitro recording of adult zebrafish heart electrocardiogram -

A platform for pharmacological testing', *Clinica Chimica Acta*. doi: 10.1016/j.cca.2011.07.002.

Turner, N. A. *et al.* (2009) 'Interleukin-1α stimulates proinflammatory cytokine expression in human cardiac myofibroblasts', *American Journal of Physiology - Heart and Circulatory Physiology*, 297(3). doi: 10.1152/ajpheart.00372.2009.

Turner, N. A. (2016) 'Inflammatory and fibrotic responses of cardiac fibroblasts to myocardial damage associated molecular patterns (DAMPs)', *Journal of Molecular and Cellular Cardiology*. doi: 10.1016/j.yjmcc.2015.11.002.

Ueda, H. R. *et al.* (2020) 'Tissue clearing and its applications in neuroscience', *Nature Reviews Neuroscience*. doi: 10.1038/s41583-019-0250-1.

Valentin, J. E. *et al.* (2009) 'Macrophage participation in the degradation and remodeling of extracellular matrix scaffolds', *Tissue Engineering - Part A*. doi: 10.1089/ten.tea.2008.0419.

Vandesompele, J. *et al.* (2002) 'Accurate normalization of real-time quantitative RT-PCR data by geometric averaging of multiple internal control genes.', *Genome biology*. doi: 10.1186/gb-2002-3-7-research0034.

Vanhauwaert, S. *et al.* (2014) 'Expressed repeat elements improve RT-qPCR normalization across a wide range of zebrafish gene expression studies', *PLoS ONE*. doi: 10.1371/journal.pone.0109091.

Villani, A. *et al.* (2019) 'Clearance by Microglia Depends on Packaging of Phagosomes into a Unique Cellular Compartment', *Developmental Cell*. doi: 10.1016/j.devcel.2019.02.014.

Vlecken, D. H. *et al.* (2009) 'A critical role for myoglobin in zebrafish development', *International Journal of Developmental Biology*. doi: 10.1387/ijdb.082651dv.

Walton, E. M. *et al.* (2015) 'The macrophage-specific promoter mfap4 allows live, long-term analysis of macrophage behavior during mycobacterial infection in zebrafish', *PLoS ONE*. doi: 10.1371/journal.pone.0138949.

Wang, J. *et al.* (2011) 'The regenerative capacity of zebrafish reverses cardiac

failure caused by genetic cardiomyocyte depletion', *Development*. doi: 10.1242/dev.068601.

Wang, J. *et al.* (2019) 'Evaluation of ultra-low input RNA sequencing for the study of human T cell transcriptome', *Scientific Reports*. doi: 10.1038/s41598-019-44902-z.

Wang, Y. X. *et al.* (2005) 'Requirements of myocyte-specific enhancer factor 2A in zebrafish cardiac contractility', *FEBS Letters*. doi: 10.1016/j.febslet.2005.07.068.

Warnes, G. (2015) 'Flow cytometric assays for the study of autophagy', *Methods*. doi: 10.1016/j.ymeth.2015.03.027.

Witman, N. *et al.* (2011) 'Recapitulation of developmental cardiogenesis governs the morphological and functional regeneration of adult newt hearts following injury', *Developmental Biology*. doi: 10.1016/j.ydbio.2011.03.021.

World Health Organization (WHO) (2016) *Cardiovascular diseases (CVDs) factsheet*. Available at: https://www.who.int/nmh/publications/fact_sheet_cardiovascular_en.pdf (Accessed: 26 September 2021).

Wu, C. C. *et al.* (2016) 'Spatially Resolved Genome-wide Transcriptional Profiling Identifies BMP Signaling as Essential Regulator of Zebrafish Cardiomyocyte Regeneration', *Developmental Cell*. doi: 10.1016/j.devcel.2015.12.010.

Yan, X. *et al.* (2013) 'Temporal dynamics of cardiac immune cell accumulation following acute myocardial infarction', *Journal of Molecular and Cellular Cardiology*. doi: 10.1016/j.yjmcc.2013.04.023.

Yang, J., Shih, Y. huan and Xu, X. (2014) 'Understanding cardiac sarcomere assembly with zebrafish genetics', *Anatomical Record*. doi: 10.1002/ar.22975.

Ye, L. *et al.* (2018) 'Early regenerative capacity in the porcine heart', *Circulation*. doi: 10.1161/CIRCULATIONAHA.117.031542.

Yona, S. *et al.* (2013) 'Fate Mapping Reveals Origins and Dynamics of Monocytes and Tissue Macrophages under Homeostasis', *Immunity*. doi: 10.1016/j.immuni.2012.12.001.

Yucel, N. *et al.* (2020) ‘Cardiac endothelial cells maintain open chromatin and expression of cardiomyocyte myofibrillar genes’, *eLife*. doi: 10.7554/eLife.55730.

Zajdel, R. W. *et al.* (2013) ‘Expression of tropomyosin in relation to myofibrillogenesis in axolotl hearts’, *Regenerative Medicine Research*. doi: 10.1186/2050-490x-1-8.

Zebrowski, D. C. and Engel, F. B. (2013) ‘The cardiomyocyte cell cycle in hypertrophy, tissue homeostasis, and regeneration’, *Reviews of Physiology, Biochemistry and Pharmacology*. doi: 10.1007/112_2013_12.

Zhao, L. *et al.* (2008) ‘Heart-specific isoform of tropomyosin4 is essential for heartbeat in zebrafish embryos’, *Cardiovascular Research*. doi: 10.1093/cvr/cvn177.

Zheng, S., Gong, M. and Chen, J. (2021) ‘Erratum: Extracellular vesicles enriched with miR-150 released by macrophages regulates the TP53-IGF-1 axis to alleviate myocardial infarction (Am J Physiol Heart Circ (2021) 320 (H969-H979) DOI: 10.1152/ajpheart.00304.2020)’, *American Journal of Physiology - Heart and Circulatory Physiology*. doi: 10.1152/AJPHEART.00304.2020_RET.

Zhou, P. and Pu, W. T. (2016) ‘Recounting cardiac cellular composition’, *Circulation Research*. doi: 10.1161/CIRCRESAHA.116.308139.

Zlatanova, I., Pinto, C. and Silvestre, J. S. (2016) ‘Immune Modulation of Cardiac Repair and Regeneration: The Art of Mending Broken Hearts’, *Frontiers in Cardiovascular Medicine*. doi: 10.3389/fcvm.2016.00040.